DESIGN AND MATERIALS APPLICATIONS OF QUADRUPLY HYDROGEN-BONDING MODULES

BY

DARRELL W. KUYKENDALL

DISSERTATION

Submitted in partial fulfillment of the requirements
for the degree of Doctor of Philosophy in Chemistry
in the Graduate College of the
University of Illinois at Urbana-Champaign, 2010

Urbana, Illinois

Doctoral Committee:

Professor Steven C. Zimmerman, Chair
Professor Anne M. Baranger
Professor Peter Beak
Professor Deborah E. Leckband

Abstract

PART I. DESIGN AND SYNTHESIS OF HIGH-AFFNITY, HIGH-FIDELITY QUADRUPLY HYDROGEN BONDING MODULES

PART II. MATERIALS APPLICATIONS OF THE DeUG·DAN HETEROCOMPLEX

Darrell W. Kuykendall
Department of Chemistry
University of Illinois at Urbana-Champaign, 2010
Professor Steven C. Zimmerman, Advisor

Part I

Despite the remarkable advances made in recent years toward the development of hydrogen bonding modules, there still exists a recognized need to expand the "supramolecular toolkit" with synthetically accessible, high-affinity, high-fidelity modules that are readily incorporated into materials. Part I of this dissertation describes the design and synthesis of a high-affinity, high-fidelity quadruply hydrogen bonding heterocomplex. A novel urea of 7-deazaguanine (DeUG) was designed as a synthetically versatile and chemically robust analogue of Park and Zimmerman's urea of guanosine (UG), and as complement to 2,7-diamido-1,8-naphthyridine (DAN). Analytically pure DeUG, which can be easily incorporated into materials, can be readily prepared on multigram scale in six steps and an overall yield of ca. 35% without the need to resort to column chromatography for purification at any stage. ^{1}H NMR dilution studies and van't Hoff analysis revealed that DeUG only moderately self-associates (K_{dimer} = 610 M^{-1}). Moreover, because DeUG is preorganized into the complementary hydrogen bonding motif to DAN, DeUG displays exceptionally high-affinity with DAN (K_{assoc} = 2 × 10^{8} M^{-1}) in organic solvents. The low propensity of DeUG to dimerize, coupled with the high

stability of the DeUG·DAN heterocomplex, results in a heterocomplex with excellent fidelity.

Part II

Hydrogen bonding homocomplexes and heterocomplexes have enjoyed enormous success toward the creation of novel materials with unprecedented properties. However, many challenges and unique opportunities remain. Part II of this dissertation describes materials applications of the DeUG·DAN heterocomplex. Chapter 3 details the development and application of a photoresponsive DAN (pDAN). Through covalent incorporation of anthracene moieties, which are capable of reversible, photochemical dimerization, into DAN, it is possible to modulate the DeUG·DAN binding event. This, in turn, allowed for the reversible formation of supramolecular network polymers as demonstrated by the reversible transition from gel to solution phases.

In Chapter 4, the application of the DeUG·DAN heterocomplex in the arena of surface chemistry is described. Several types of siliceous surfaces and nanoparticles, and polymer beads were covalently modified to bear DeUG. These surfaces were characterized by a number of complementary surface analysis techniques, such as AFM, SIMS and XPS. Self-assembly of DAN and DAN-functionalized polymers on these materials was demonstrated. Additionally, the application of these functionalized surfaces and polymers as interfacial adhesion promoters is described.

For my family...past, present and future...

Acknowledgments

I wish to sincerely thank my graduate research advisor, Professor Steven C. Zimmerman, for the many years of support and guidance provided during my graduate studies. I would also like to thank the current members of my doctoral committee Professor Anne M. Baranger, Professor Peter Beak, Professor Deborah E. Leckband and past members Professor Mary S. Gin and Professor Jeffrey S. Moore for their insight and support. Additionally, I wish to thank my undergraduate research advisor, Professor Carl R. Kemnitz, for his exemplary mentorship during my undergraduate studies and Professor Kenward Vaughan for quirky inspiration and encouragement.

I would also like to thank all past and present members of the Zimmerman group with whom I have had the distinct privilege of working and, specifically, the supramolecular subgroup: Cyrus A. Anderson, Dr. Hugo C. Ong, Dr. J. Kwansima Quansah, Dr. Taiho Park and Professor Eric M. Todd. You have challenged and inspired me. I would also like to thank the undergraduate and graduate student teaching assistants with whom I had the pleasure of working while teaching Chemistry 233. You were a dedicated bunch and I am grateful for all that you did.

I wish to express my deepest appreciation to my family—my wife, Sonya Kuykendall, and our beautiful daughter, Anna—for being so supportive throughout my graduate studies and believing in me. I could not have done it without you and I am indebted to you both.

Table of Contents

Part I: Design and Synthesis of High-Affinity, High-Fidelity Quadruply Hydrogen Bonding Modules

Portions of the work presented in Part I were adapted from a previous publication: Kuykendall, D. W.; Anderson, C. A.; Zimmerman, S. C. *Org. Lett.* **2009**, *11*, 61-64.

Chapter 1

Introduction

1.1 Supramolecular Chemistry

The concept of the "supermolecule" (*übermoleküle*) can be traced at least as far back as 1937 when Wolf used the term to describe hydrogen bonded dimers of acetic acid.[1] In recent decades, supramolecular chemistry[2]—that is, the spontaneous self-assembly of complex, yet well-defined, macromolecular architectures through specific, reversible, noncovalent interactions—has gained widespread popularity due, in part, to its potential in facilitating a "bottom-up" approach in the design and creation of functional materials.[3,4] Nature, the paradigmatic master of such processes, has been a limitless source of inspiration to scientists in this regard.

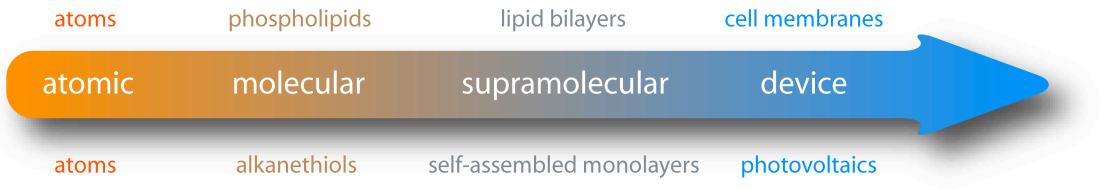

Figure 1. A structural continuum of matter emphasizing the correlation between nature and the bottom-up approach to functional device creation.

Nature uses relatively simple building blocks to create extraordinarily complex architectures. For example, under the right conditions, phospholipids will spontaneously assemble into a lipid bilayer. At next level of complexity, a cell membrane emerges—replete with additional molecules such as surface receptors and membrane channels, which impart a truly amazing level of functionality to the structure.

In an attempt to mimic nature's exquisite control over the creation of functional materials from simple building blocks, scientists have developed a variety of assembly techniques. Self-assembled monolayers (SAMs) have been widely used in this regard. For example, the well-known proclivity of alkanethiols to form SAMs on gold surfaces[5] been implemented toward the creation of functional devices such as photovoltaics.[6] Clearly, supramolecular chemistry holds the potential to completely revolutionize the design, fabrication and engineering of materials. Currently, that potential is limited only by the imagination, dedication and ingenuity of those seeking to advance this promising field.

1.2 Hydrogen Bonding

The hydrogen bond represents a vitally important type of noncovalent interaction and is largely responsible for several essential natural phenomena—from the peculiar properties of water to the molecular recognition between base pairs in DNA. Although relatively weak (ca. 1-5 kcal mol^{-1}), the hydrogen bond is typically stronger than van der Waals interactions (ca. 1-2 kcal mol^{-1}), yet far weaker than covalent or ionic bonds.[7]

As exemplified by the DNA base pairs, the strength of hydrogen bonding interactions can be magnified by creating arrays of contiguous hydrogen bond donors (D) and hydrogen bond acceptors (A). The length of the array, combined with the arrangement of donors and acceptors, allows for the formation of motifs that facilitate specificity between complementary arrays. As shown in Figure 2, this specificity is evident in the canonical forms of the DNA base pairs.

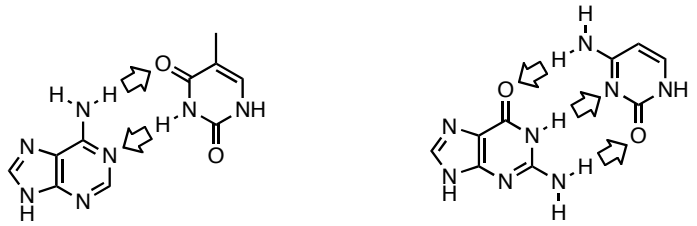

Figure 2. Canonical forms of the DNA base pairs.

Designed supramolecular interactions continue to play a central role in the development of novel and functional nanoscale devices and materials. Partly inspired by DNA base-pairing, as well as the strength, directionality and, thus, predictability of hydrogen bonding interactions, many efforts to expand the "supramolecular toolkit" have focused on heterocyclic compounds that form hydrogen bonded homocomplexes or heterocomplexes.[8]

1.3 Conclusion

The objective of the following chapters is to present the development of a high-affinity, high-fidelity quadruply hydrogen bonding heterocomplex and its materials applications explored thus far. Chapter 2 describes the design criteria, modeling, synthesis and characterization of the hydrogen bonding units. Chapter 3 begins the foray into materials applications with the development of a means to modulate complexation between the units and its application toward reversible formation of supramolecular network polymers. Chapter 4 details the application of the units in the general area of surface chemistry, with examples of self-assembly and adhesion promotion at interfaces.

Chapter 2

Development of New Quadruply Hydrogen Bonding Modules

2.1 Background

High-fidelity complexation between molecular recognition units based upon contiguous arrays of multiple hydrogen bond donors (D) and acceptors (A) is an increasingly common element of self-assembly processes and supramolecular architectures. Control of the tautomeric form and preorganization can be critical to achieving high levels of fidelity between complementary hydrogen bonding modules. Modules with persistent tautomeric forms are more likely to afford high fidelity recognition, whereas preorganized modules provide higher complex stability.[8f,8h] Despite the ongoing advances in this field, there still exists a recognized need to develop synthetically accessible, high-affinity, high-fidelity (orthogonal) hydrogen bonding modules that are readily linked to surfaces, nanoparticles, polymers and other compounds and materials.[9,10]

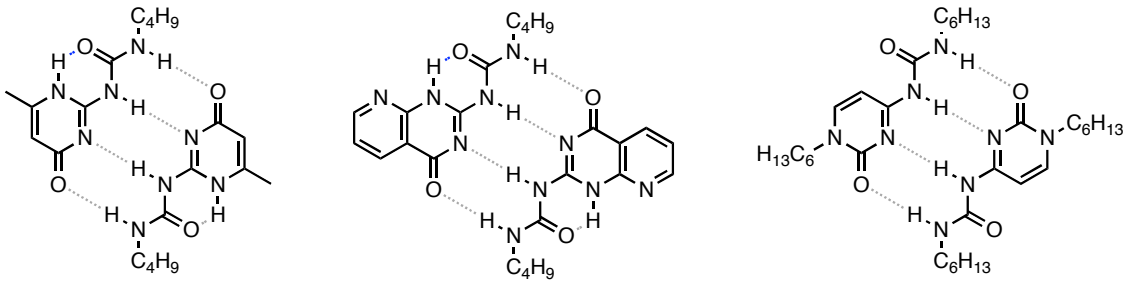

1·1, K_{dimer} = 6 x 10^7 M^{-1} ($CDCl_3$)

2·2, K_{dimer} = 9 x 10^7 M^{-1} ($CDCl_3$)

3·3, $K_{dimer} \geq 9 \times 10^6$ M^{-1} (C_6D_6)

Figure 3. Selected examples of high-affinity, self-complementary quadruple hydrogen bonding modules and their dimerization constants.

Among quadruply hydrogen bonded systems, the ureidopyrimidinone (UPy, **1**) unit is especially noteworthy because of its synthetic ease and high stability, and now widespread use.[11] Additional examples include Corbin and Zimmerman's deazapterin (DeAP, **2**)[12] and the more recently reported urea of cytosine (**3**).[13] Each of these units was shown to strongly self-associate via their AADD forms (Figure 3). However, the accessibility of the ADDA forms (**1'** and **2'**) allows both UPy and DeAP to bind strongly to 2,7-diamido-1,8-naphthyridines (DAN) such as **4** also, thus decreasing their fidelity (Figure 4).[14] Further complicating the picture is the observation that the K_{assoc} for the UPy·DeAP heterocomplex via their AADD motifs is on the order of 10^8 M^{-1}.[15]

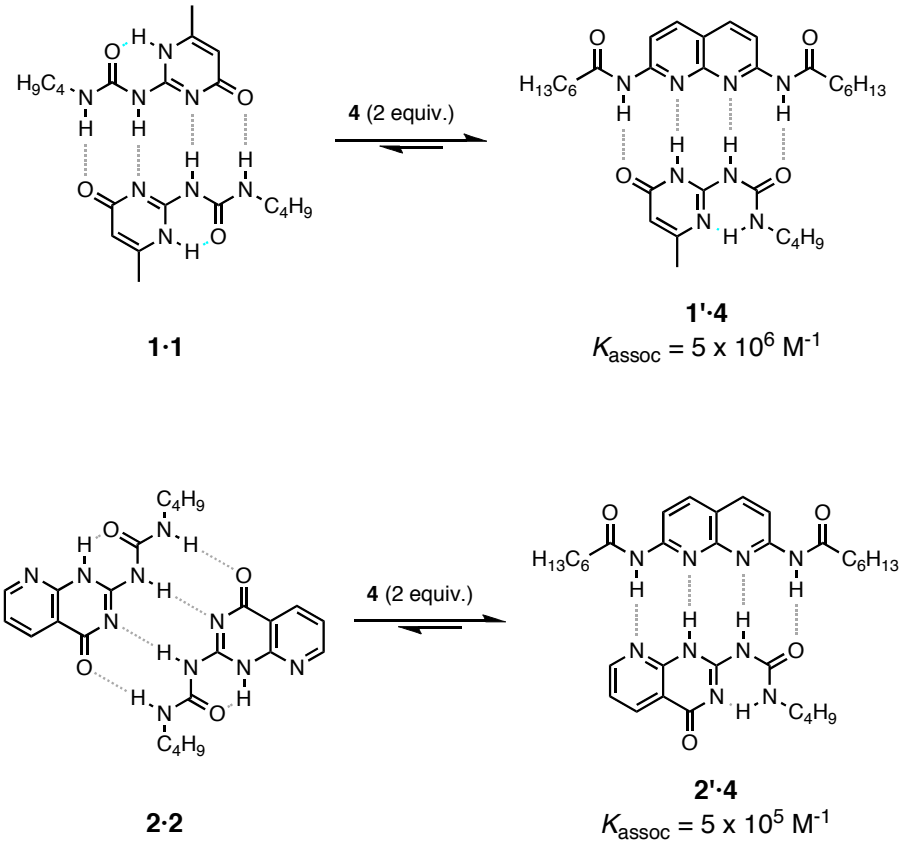

Figure 4. Heterocomplexation of UPy (**1**) and DeAP (**2**) with DAN (**4**) and their association constants in $CDCl_3$.

In simple applications using only one of these units to generate a single type of assembly, these competing interactions are not an issue. However, in recognition driven self-assembly processes involving multiple hydrogen bonding modules and/or different types of compounds and materials, this can lead to undesired architectures via competing, complex equilibria.

Recent work in the Zimmerman laboratory has led to the development of a urea of guanosine (UG, **5**) that displays high fidelity recognition of DAN **4** (Figure 5a).[16,17] It was envisioned that, by virtue of their persistent tautomeric form, nucleobase analogues would make attractive candidates for use in molecular recognition systems by affording higher fidelity recognition. Indeed, UG has been shown to only weakly dimerize (K_{assoc} = 200-300 M^{-1}), indicating that the desired tautomeric persistence had been realized (Figure 5b).

(a)

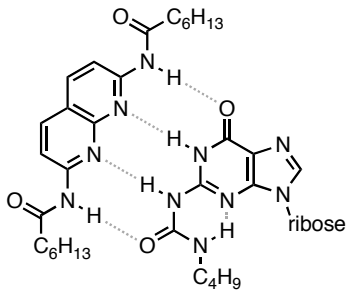

4·5
K_{assoc} = 5 x 10^7 M^{-1}

(b)

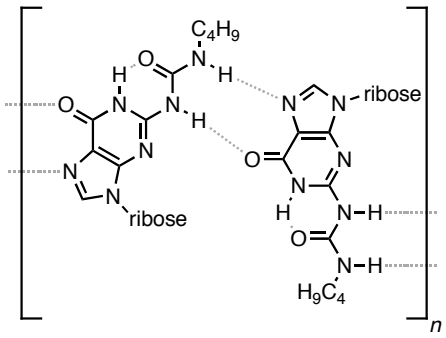

5'·5'
K_{oligo} ≈ 200-300 M^{-1}

Figure 5. (a) Structure and association constant for the **4·5** heterocomplex in $CDCl_3$. (b) A proposed mode oligomerization for **5** via the *N*1H-*anti* ureido conformer.

Although the fidelity of the UG·DAN heterocomplex is quite high, decreasing the stability of the UG homocomplex while, at the same time, increasing the propensity for heterocomplexation should improve the fidelity.[18] Additionally, because the *anti*-ureido conformer **5'** has been shown to be preferred for UG, the energy cost associated with switching to the preorganized *syn*-ureido conformer **5** translates into an equivalent decrease in the free energy of heterocomplexation. Thus, control over the urea conformation could provide an opportunity to modestly increase the binding affinity.

2.2 7-Deazaguanine Urea (DeUG) Analogues

2.2.1 Design Principles and Modeling

The overarching goal with respect to the redesign of our guanosine-derived urea (UG, **5**), which forms highly stable quadruply hydrogen bonded complexes with diamidonaphthyridines, is to create a synthetically versatile and chemically robust analogue. Toward this end, we identified three major criteria. First, it was anticipated that replacement of *N*7 with a CH group would preclude the formation of the types dimers or oligomers that require Hoogsteen-urea contacts (e.g., **5'·5'**) such as those proposed for UG (*vide supra*, Figure 5). Second, to enhance the chemical stability and, thus, processibility of supramolecular polymers and other materials containing these modules, the labile ribose unit of UG, which serves as the point of materials attachment, was to be replaced with a more chemically robust group that could also serve as a means to modulate solubility and a secondary point for further synthetic elaboration. Lastly, introduction of a primary synthetic handle (preferably at *C*8 so as to be nearly orthogonal

to the binding face) for ease of incorporation into materials completes the redesign. These design criteria are summarized in Figure 6.

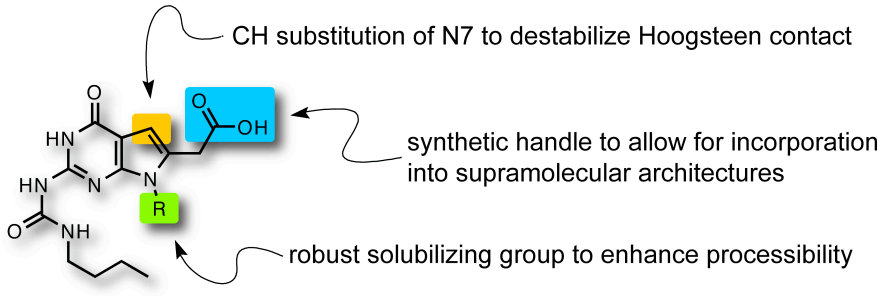

Figure 6. Proposed structural modifications leading to the DeUG module.

Density functional theory (DFT) calculations were performed on five conformers/ tautomers of a simplified DeUG analogue to assess their relative energies (Figure 7). Before considering the results of these calculations, it would be prudent to mention that they represent "gas-phase" energies[19] of single species. As such they do not offer any meaningful insight into the proposed mode of preorganization, nor do they account for solvent effects, which can play a significant role. Nonetheless, these calculations do offer a significant first approximation of which species can be expected to dominate at equilibrium.

Of the five forms considered here, the *N*1-H-*anti* ureido form (**6**, Figure 7) was calculated to be the lowest in energy, with the desired *N*1-H-*syn* ureido **6'** form being quite accessible at only ca. 0.56 kcal mol^{-1} higher in energy. The calculated energy of the

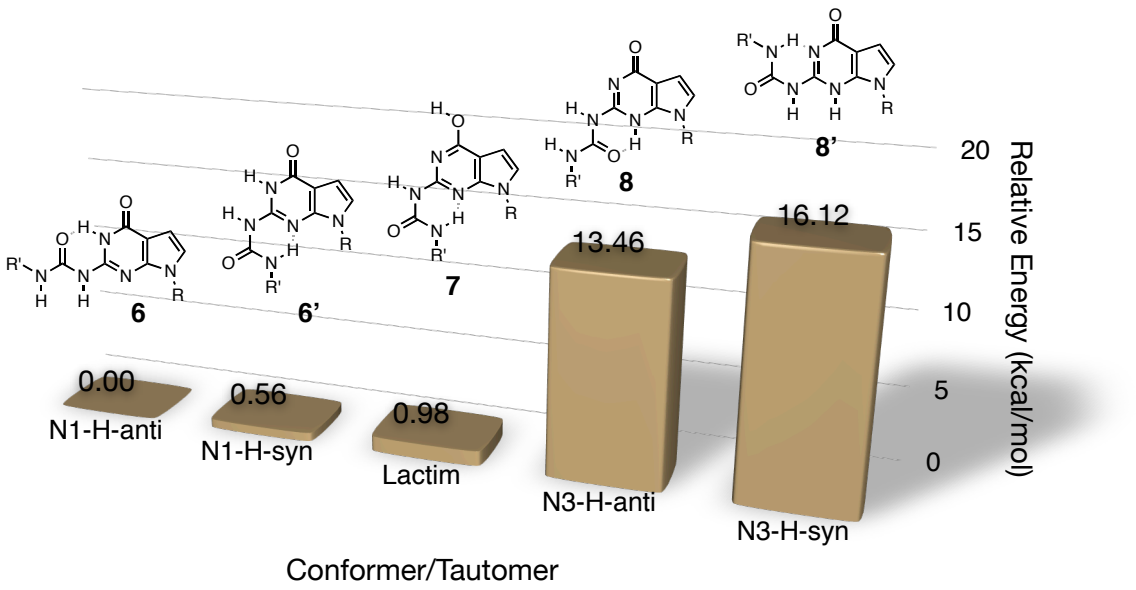

Figure 7. Relative energies of five conformers/tautomers of a simplified DeUG analogue (R = R' = methyl) by B3LYP/6-31G(d)//B3LYP/6-311+G(d,p).

*N*3-H-*syn* ureido form, which by analogy to UPy **1** and DeAP **2** would be expected to strongly dimerize, is ca. 13.5 kcal mol^{-1} higher than the *N*1-H-*anti* ureido form. The apparent accessibility of the lactim species **7**, which was calculated to be only ca. 0.42 kcal mol^{-1} above the desired *N*1-H-*syn* ureido form and can self-associate via its DADA motif, was not regarded as sufficient reason to question the expected tautomeric persistence for at least three reasons: (1) previous work in our laboratory had shown that 7-deazaguanine exhibits the tautomerically persistent *N*1-H form in chloroform,[20] (2) the calculated differences in energies for all five species are very similar to those calculated for the analogous UG forms[17] and (3) under standard conditions, the lactim tautomer of UG was not observed by ^{1}H NMR.[21]

Furthermore, it was reasoned that the lack of availability of Hoogsteen-urea contact forms might favor the *N*1-H-*syn* ureido conformer **6'** because it facilitates the formation of doubly hydrogen bonded dimers which are enhanced by secondary interactions,[22] whereas the *N*1-H-*anti* ureido conformer **6** can form bifurcated hydrogen bonded dimers only (Figure 8).

The above line of reasoning was supported by our initial *ab initio* calculations, which showed that the *N*1-H-*syn* dimer is ca. 6.3 kcal mol^{-1} lower in energy than the corresponding *N*1-H-*anti* dimer. Additionally, a preference for the *N*1-H-*syn* ureido conformer would impart a preorganizational advantage to DeUG analogues and, thus, should result in higher-affinity complexation with the diamidonaphthyridines. It is, however, reasonable to expect an increase the self-association constant for the same reason.

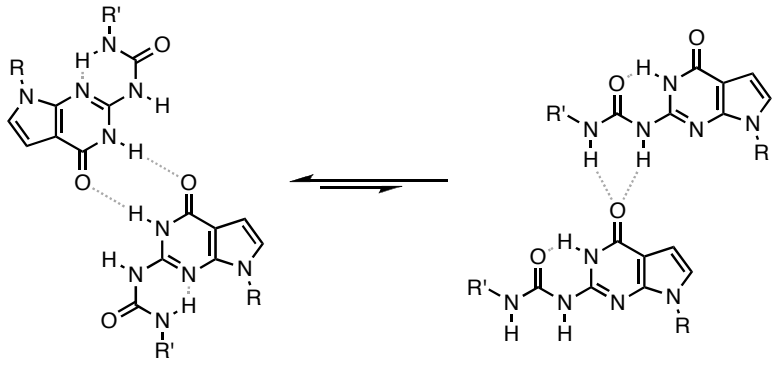

Figure 8. Two probable modes of dimerization for DeUG via the *N*1H tautomer (R = R' = methyl) and their B3LYP/6-31G(d) relative energies.

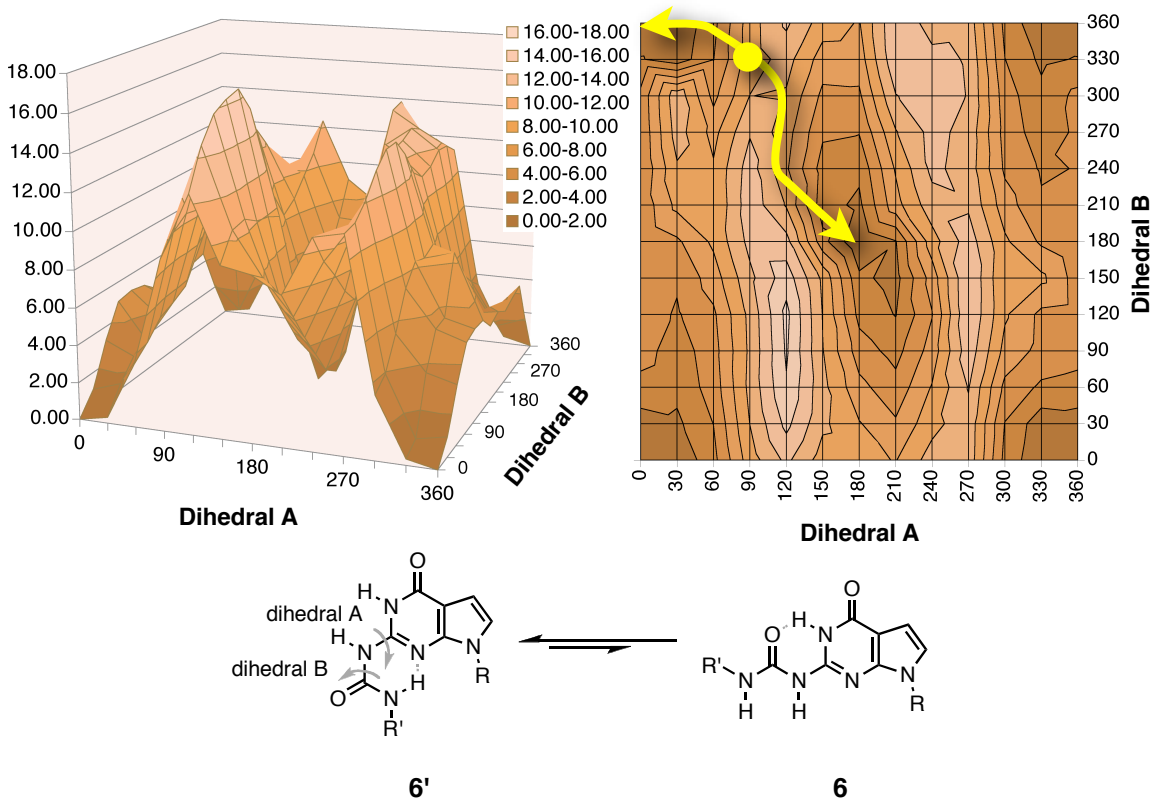

Figure 9. Semi-empirical (PM3) energy surface for a simplified DeUG (R = R' = methyl) *N*1-H-*syn/anti* conformational switch.

At this point in time, it was unclear what effect these competing factors might have on the fidelity of the DeUG·DAN heterocomplex when compared to that of UG·DAN—that is, will the anticipated increase in association constant for the DeUG·DAN heterocomplex be of sufficient magnitude to compensate for the expected increase in DeUG self-association and, thus, result in higher fidelity?

Semi-empirical (PM3) molecular modeling of the conformational dynamics predicted that the barrier to interconversion between **6** and **6'** is ca. 10 kcal mol^{-1}, which is in agreement with the qualitative results by ^{1}H NMR as reported by Ong (Figure 9).[18] The energy surface was calculated in increments of 30° for each dihedral involved in the

interconversion between **6** and **6'**. As highlighted by the trace in Figure 9, the lowest energy pathway roughly corresponds to initial rotation about the exocyclic guanidine *C*-*N* bond (dihedral A) to the extent of ca. 60°. Concerted rotation about both dihedrals by ca. 60° then occurs. This is followed by another 60° rotation about the proximal urea *C*-*N* bond (dihedral B). Another round of concerted rotation about both dihedrals by an additional 60° results in the *N*1-H-*syn* conformer, which, by PM3 methods, was predicted to be 0.10 kcal mol^{-1} higher in energy than the *N*1-H-*anti* conformer. The maximum barrier along this pathway was calculated to be ca. 9.8 kcal mol^{-1}, which is marked by a dot along the path highlighted in Figure 9.

2.2.2 Synthetic Approaches to DeUG Analogues

Retrosynthetic analysis and literature precedent both suggest 2-amino-4,6-dichloropyrimidine **9** as the logical precursor to diaminopyrimidinones such as **11**, which is the key intermediate toward the synthesis of DeUG analogues (Scheme 1). Commercially available **9** readily undergoes monosubstitution with cyclohexanemethyl amine in moderate to good yield. Indeed, this was the scheme used in our laboratory at the outset of this project and it served our needs at the time. However, with plans for future scale-up, an alternative synthesis was sought as a result of the relatively high cost of **9**, the capricious hydrolysis of **10** and overall poor yields (ca. 26% over two steps) early in the synthetic sequence.

Scheme 1

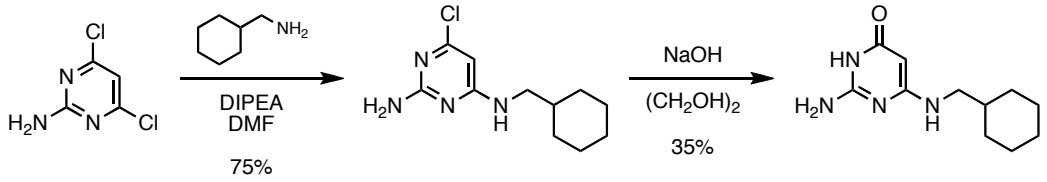

9 **10** **11**

The preparation of DeUG analogues was instead begun with the chlorination of commercially available and much less expensive **12** using phosphorus oxychloride with slow addition of *N*,*N*-dimethylaniline, following a slight modification to the procedure reported by Appleton, affording, on average, 91% of **9**. Other, more environmentally benign bases, such as triethylamine, can also be used for this transformation, albeit with minor reductions in yield.[23] Hydrolysis of **9** in refluxing, aqueous NaOH, following the procedure of Carrell and Burgdorf,[24] gave chloropyrimidinone **13** in excellent to quantitative yield after neutralization with glacial acetic acid. Although both **9** and **13** are commercially available, they are easily and less expensively prepared as described. Moreover, beginning from advanced intermediate **13** offers only a small (ca. 5%) improvement in overall yield at significant cost.

The conversion of **13** to **14** was anticipated to be difficult due to scarcity of literature procedures[25] and the fact that **9** underwent monosubstitution only (*vide supra*, Scheme 1). Nevertheless, the task of carrying out this transformation was undertaken. After surveying many different reaction conditions, much to our delight, it was discovered that the conversion proceeded smoothly via treatment with

cyclohexanemethyl amine in refluxing *n*-butanol and triethylamine (Scheme 2). Three other primary alkyl amines gave similar results.

Scheme 2

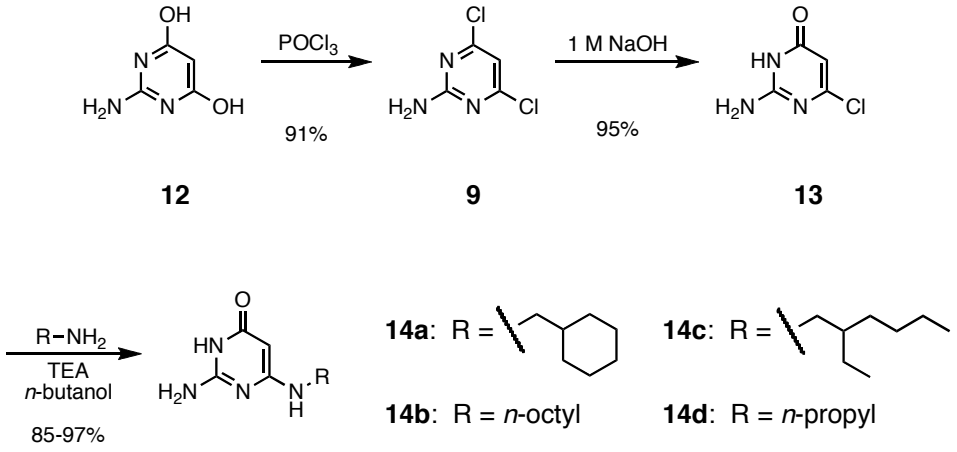

In a procedure similar to that reported by Gangjee and coworkers,[26] the formation of 7-deazaguanine acetic acid ethyl ester **15** was accomplished in modest to good yield via cyclocondensation of **14a** and ethyl 4-chloroacetoacetate (slow addition) in DMF/H_2O with sodium acetate (Scheme 3). The major side product was found to be diethyl 2,5-dioxo-1,4-cyclohexanedicarboxylate (diethyl succinyl succinate, DESS, **16**), which is presumably formed by self-condensation of ethyl 4-chloroacetoacetate. Slow addition of the *β*-keto ester only modestly decreased the amount of DESS formed. Attempts at further suppressing this side reaction proved unsuccessful and had only a minor impact on the yield of **15**.

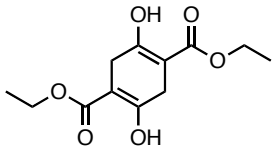

16

Figure 10. Diethyl succinyl succinate (DESS).

Scheme 3

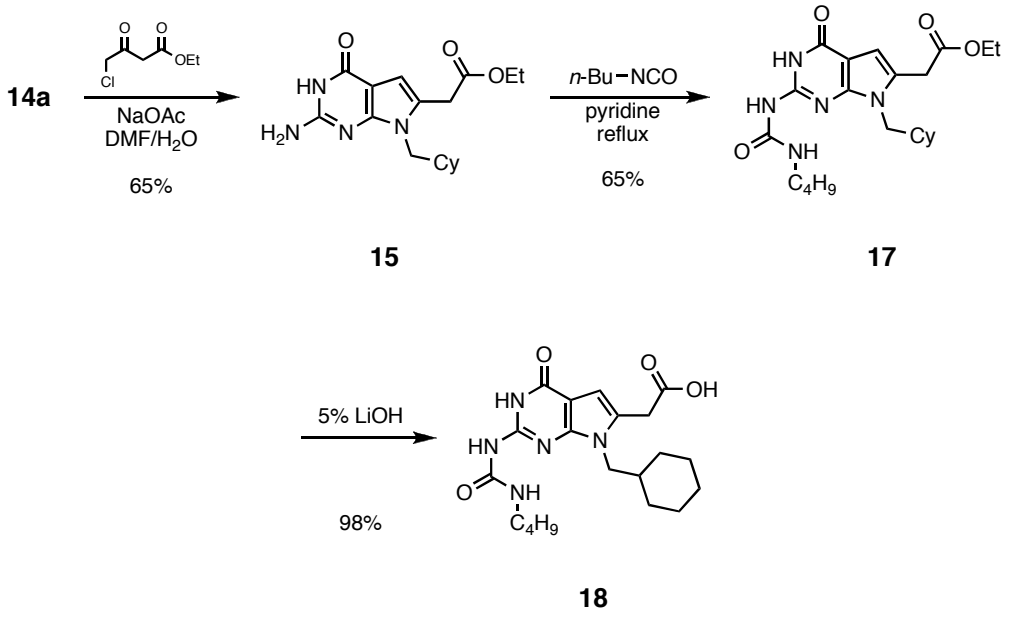

Previous work in our group had shown that the amino groups of similar compounds (guanines, pterins) are quite unreactive toward isocyanates.[8h,17] For example, in the synthetic route to UG, activation of the precursor amine via deprotonation using a sub-stoichiometric amount of sodium hydride was required.[17] However, this route proved less than reliable and gave unacceptably poor yields in the case of deazaguanine **15**. It was found that treatment of **15** with an excess of *n*-butyl isocyanate in refluxing pyridine gave DeUG acetic acid ethyl ester **17** in good yield. Lithium hydroxide mediated hydrolysis of the ethyl ester in 1:1 ethanol/H_2O afforded analytically pure carboxylic acid functionalized DeUG **18** in excellent yield after purification via recrystallization from ethanol.

Thus, relatively minor changes to the previously reported synthesis resulted in an approximately threefold to fourfold improvement in overall yield, while at the same time reducing the cost. Analytically pure DeUG acetic acid **18** can be routinely prepared on

multigram scale (> 10 g) in an overall yield of approximately 35% over six steps without the need to employ column chromatography for purification at any stage.[27]

One of the overarching goals of this project was to develop a modular approach to the covalent incorporation of hydrogen bonding modules into other compounds and materials. The copper-catalyzed azide-alkyne cycloaddition (CuAAC) has emerged as the preeminent reaction among those that meet Sharpless' criteria for "click" chemistry for many reasons, including high yield, functional group tolerance and scope, simple reaction conditions and non-chromatographic purification.[28] Therefore, as a demonstration of the ease with which DeUG acetic acid **18** can be functionalized with "clickable" groups, both alkyl azide and terminal alkyne variants were prepared.

Scheme 4

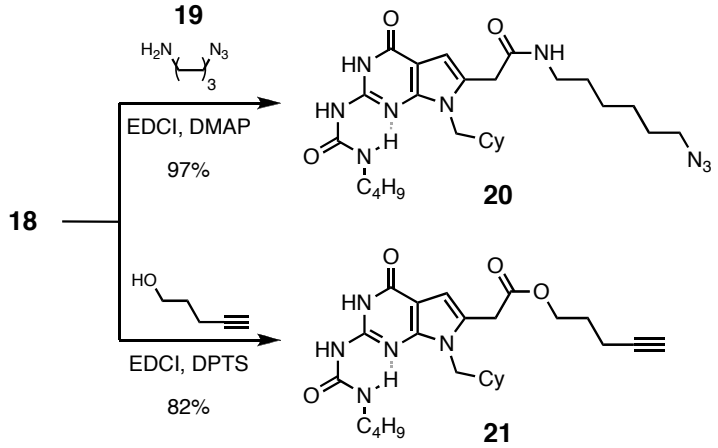

As illustrated in Scheme 4, DeUG hexyl azide **20** can be prepared in excellent yield from DeUG carboxylic acid **18** and 6-azidohexan-1-amine **19** with 1-ethyl-3-(3-dimethylaminopropyl) carbodiimide (EDCI) and catalytic *N,N*-dimethylaminopyridine (DMAP). Additionally, DeUG pentynyl ester can be prepared in good yield from **18** and

4-pentyn-1-ol with EDCI and catalytic 4-(dimethylamino)pyridinium 4-toluenesulfonate (DPTS).[29] DeUG propargyl amide **22** was also prepared (Scheme 5) for applications where the higher stability of the amide linkage is advantageous and because of its lower cost. Cyrus Anderson has also developed a convenient transesterification of DeUG alkyl esters, such as **17**, to glycol esters.[27]

Scheme 5

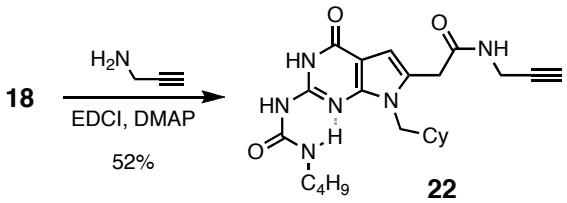

2.2.3 Characterization of DeUG

^{1}H NMR dilution experiments of DeUG **17** in deuterated chloroform were performed to investigate its self-association behavior. Both the *N*1-H and the aromatic *C*7-H resonances gave adequate signal-to-noise ratios over an appropriate concentration

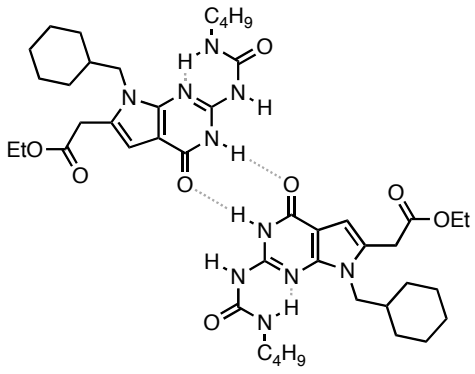

17·17

Figure 11. One of several possible modes of dimerization for DeUG **17**.

range. However, the *N*2-H and the *N*3-H resonances showed substantial broadening at low concentrations and could not be used in determining a dimerization constant. The data were fit to a standard 1:1 binding isotherm using nonlinear, least squares regression (Figure 12).[30,31] Self-association constants (K_{dimer}) of 520 M^{-1} and 700 M^{-1} (average 610 M^{-1}) were determined by following *N*1-H and *C*7-H, respectively. Not unexpectedly, the self-association of DeUG **17** is approximately twofold higher than that reported for UG **5**, which can be attributed to **17** being preorganized in the ADDA motif.

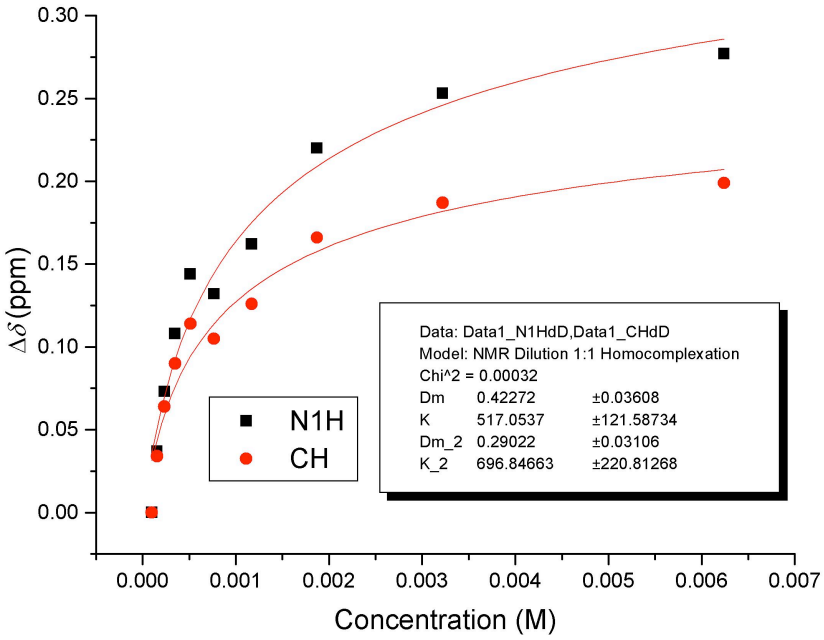

Figure 12. ^{1}H NMR dilution study of DeUG **17** in deuterated chloroform at 25 °C.

Interestingly, the maximum chemical shift change observed in this case, $\Delta\delta_{max}$ = 0.414 ppm, was significantly lower than that typically observed for protons engaged in strong, intermolecular hydrogen bonds. Similar, low values for $\Delta\delta_{max}$ have been reported for analogous ureas of 7-deazaguanine and other compounds.[32] Although the exact

nature of the small $\Delta\delta_{max}$ remains unknown, it is possible that it is due to multiple modes of dimerization and or oligomerization.

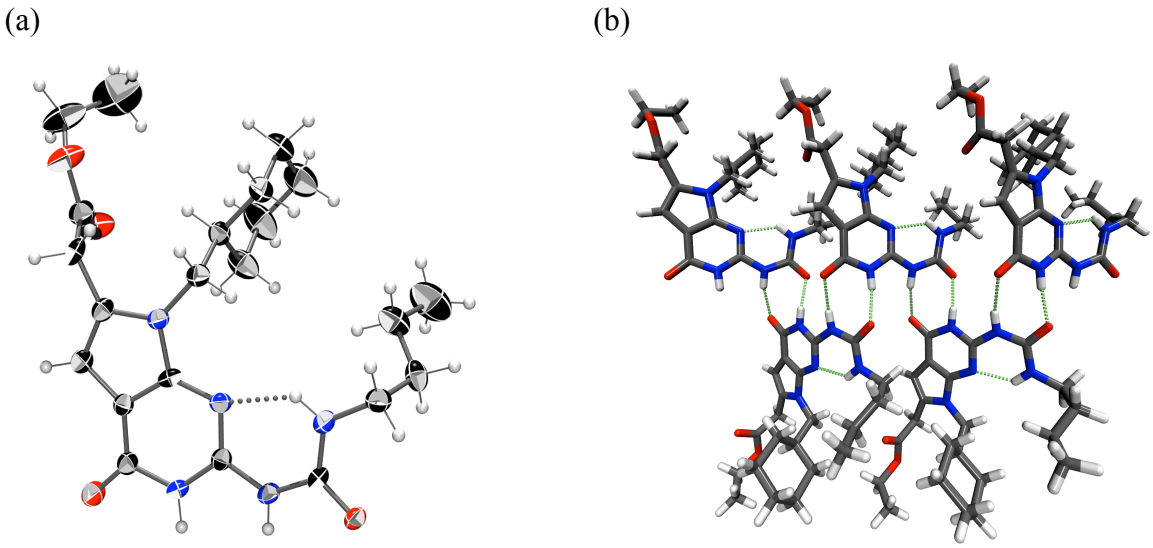

Figure 13. X-ray analysis of DeUG, **17**: (a) ORTEP representation of **17**. Thermal ellipsoids represent 50% probability. (b) Licorice representation of **17** highlighting the zipper-like hydrogen bonding assembly in the solid state.

Orthorhombic crystals of DeUG ethyl ester **17** suitable for X-ray analysis were obtained via recrystallization from acetone. Although some disorder was observed in both the cyclohexanemethyl and ethyl groups, the structure revealed an interesting "zipper-like" (vernier-type) hydrogen bonding assembly via repeating lactam-urea contacts and confirmed the preorganized acceptor-donor-donor-acceptor (ADDA) motif exists in the solid state (Figure 13a).[33] To accommodate the steric bulk of the molecule, the average plane defined by the heterocycles for each of any two hydrogen bonded DeUG units lie at a 58.6° angle to one another (Figure 13b), with the lactam-urea N-H···O hydrogen bond length being 1.90(2) Å (angle, 165°) and the urea-lactam N-H···O

hydrogen bond length being 2.00(2) Å (angle, 173°). The intramolecular N-H···N hydrogen bond, which preorganizes DeUG into the desired motif, was found to be 2.02(3) Å (angle, 133°).

Table 1. Summary of solid-state hydrogen bond geometries for **17**.*

D-H···A	d(D-H, Å)	d(H···A, Å)	d(D-H, Å)	∠(D-H···A, °)
lactam-urea N-H···O	0.90(2)	1.90(2)	2.780(4)	165(3)
urea-lactam N-H···O	0.89(2)	2.00(2)	2.888(4)	173(3)
intramolecular N-H···N	0.88(2)	2.02(3)	2.692(4)	133(3)

*Complete crystallographic structure data can be found in Appendix A.

2.3 Diamidonaphthyridine (DAN) Analogues

2.3.1 Synthetic Approaches to DAN Analogues

Synthetic approaches to 2,7-diamino-1,8-naphthyridine (**23**) have traditionally begun with the formation of 2-amino-1,8-naphthyridone (**26**), by a methodology first reported by Newkome and coworkers[34] where 2,6-diaminopyridine is reacted with racemic malic acid and concentrated sulfuric acid. The conversion of **26** to **23** then typically proceeds via acylation of the aminonaphthyridone followed by activation, typically using phosphorus oxychloride, and finally displacement of the chloride using ammonia[35] or an amine, such as *p*-methoxybenzylamine, that serves as an ammonia surrogate (Scheme 6).[36]

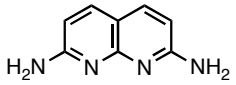

23

Figure 14. 2,7-Diamino-1,8-naphthyridine.

Scheme 6

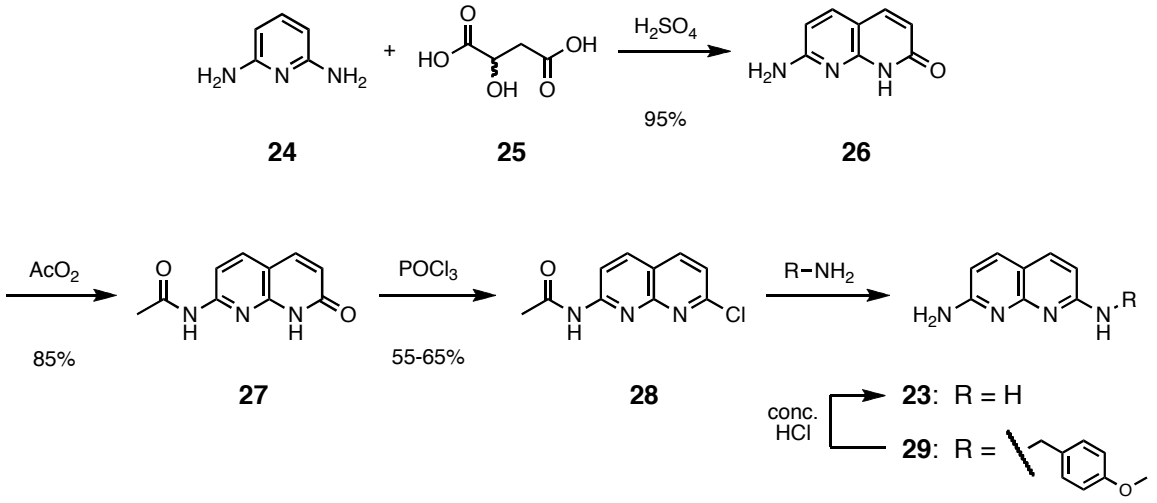

Although the approaches to **23** described above are reliable, they do have their disadvantages. In the case of the **28** to **23** transformation, the scale can be limited by virtue of the reaction being performed under high pressure in sealed glass tubes. In the case of the **28** to **29** transformation, use of the amine surrogate can become prohibitively expensive for routine use, as well as introducing the extra step of unmasking the amine. The use of amine surrogates has the added disadvantage of low atom economy.

Scheme 7

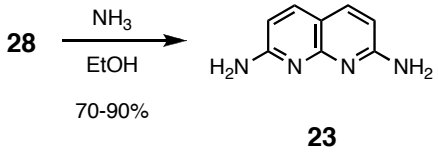

For routine preparation of diaminonaphthyridine **23**, ammonolysis of **28** under high pressure in a steel bomb, in a manner similar to that previously reported,[35] was found to be the most reliable, giving the most pure product in the highest overall yield on

average (Scheme 7). Using the small rocker in the high pressure facility in Roger Adams Laboratory, up to 10 g of **23** can be readily prepared in a single batch. Due care must be exercised to exclude water from the reaction mixture, as chloronaphthyridines are easily reverted to naphthyridone **26** via hydrolysis under these conditions.

For incorporation of diamidonaphthyridines into materials and other compounds, ready access to monofunctional naphthyridines that can be further elaborated is required. The synthesis of amidonaphthyridine **30** was initially attempted using a method previously developed in the Zimmerman laboratory wherein diaminonaphthyridine **23** is treated with heptanoyl chloride in the presence of catalytic DMAP in DMF.[17] However, this approach suffered from a lack of reproducibility and often gave unacceptably poor yields.

Scheme 8

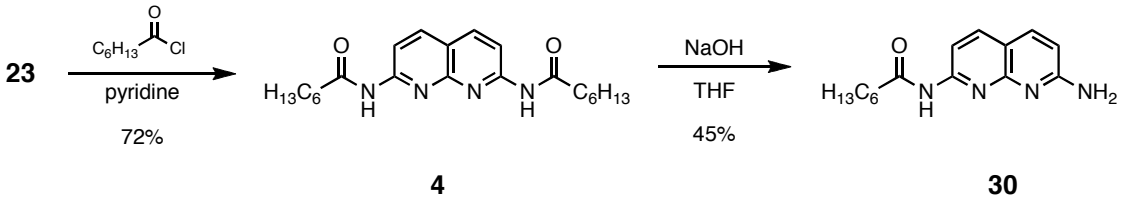

An alternative approach, as reported by Li and coworkers,[37] was used to prepare serviceable quantities of **30** via base promoted hydrolysis of diamidonaphthyridine **4** (Scheme 8). Although this method does have its disadvantages, including low atom efficiency and only moderate to good yields, it is reproducible and, under the right conditions, has a conversion just slightly higher than the yield, which allows for convenient recycling of unreacted **4** after column chromatography.

An obvious approach to **23** via **28** involves displacement of the chloride group with a different, more atom economical amine surrogate, such as an azide. Azides can typically be transformed in high yield to amines by a Staudinger reduction or other means. After surveying chloronaphthyridine **28** and several acylated chloronaphthyridines without success, it was discovered that **32** could be reliably transformed into the azide, which quickly and, to the best of our knowledge, irreversibly isomerizes into tetrazole **34**, as evidenced by the lack of a diagnostic peak by IR corresponding to the azide (Scheme 9). It was recognized that, if the tetrazole could be reduced, this would provide a convenient means to monofunctional amidonaphthyridines.

Scheme 9

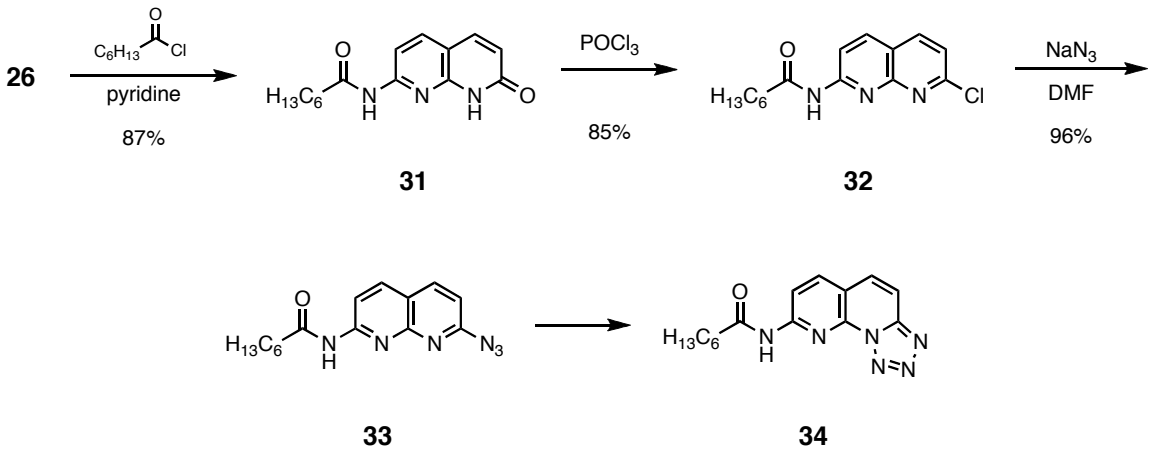

Unfortunately, **34** was never successfully reduced by Staudinger's method or any other that we tried. Monitoring the **32** to **34** transformation by ReactIR suggested that an *in situ* reduction may be possible. However, this also proved fruitless. Goswami and coworkers reported that they were able to reduce tetrazoles analogous to **34** to their corresponding amines in excellent yield using zinc and acetic acid.[38] However, in our

hands this route was completely unsuccessful. We were also unable to reproduce the synthesis of the reported precursor tetrazole.

Meijer has reported a palladium-catalyzed amidation route to monofunctional amidonaphthyridines[39] and, for routine access to some monofunctional amido-naphthyridines, Cyrus Anderson has recently developed a high yielding, copper-catalyzed amination of bromonaphthyridines.[40]

Scheme 10

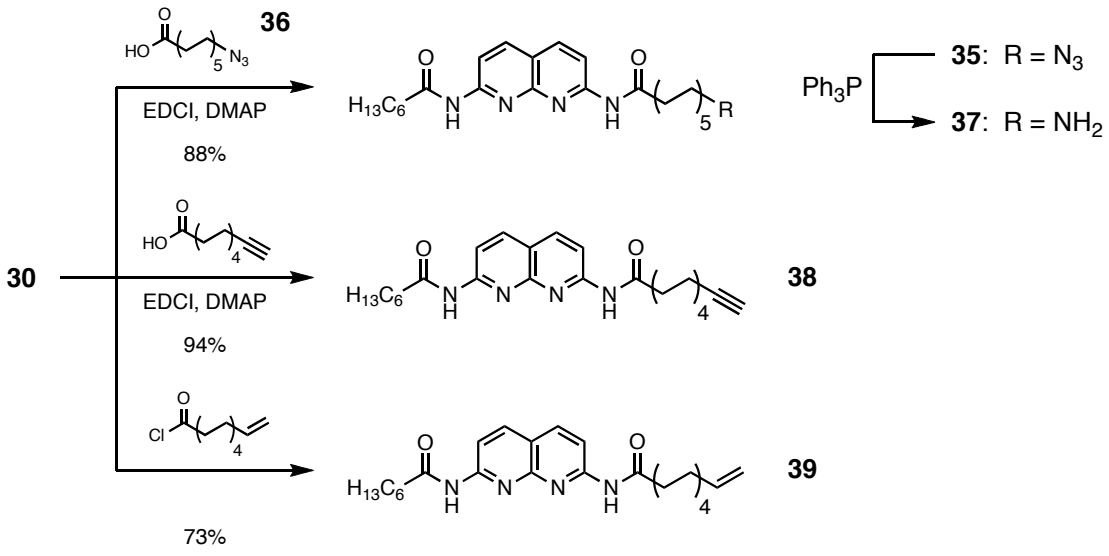

As with DeUG, we sought to synthesize a series of diamidonaphthyridines with reactive functionality that can be used to readily incorporate DAN into other structures. As illustrated in Scheme 10, 11-azidoundecanoic acid (7-heptanoylamino-[1,8]naphthyridin-2-yl)-amide **35** can be prepared in excellent yield from heptanoic acid (7-amino-[1,8]naphthyridin-2-yl)-amide **30** and 11-azidoundecanoic acid **36** with 1-ethyl-3-(3-dimethylaminopropyl) carbodiimide (EDCI) and catalytic *N,N*-

dimethylaminopyridine (DMAP). Staudinger reduction of **35** affords alkyl amine **37**. Additionally, 10-undecynoic acid (7-heptanoylamino-[1,8]naphthyridin-2-yl)-amide **38** can be prepared in good yield from **30** and 10-undecynoic acid with EDCI and catalytic DMAP. Lastly, 10-undecenoic acid (7-heptanoylamino-[1,8]naphthyridin-2-yl)-amide **39** can be readily prepared in moderate to good yield by reaction of 10-undecenoyl chloride with **30**.

2.4 Characterization of the DeUG·DAN Heterocomplex

The association constant (K_{assoc}) for the DeUG·DAN (**17·4**) heterocomplex was expected to be beyond the limit of detection by ^{1}H NMR titration studies based on previously reported competition studies, which indicated that the DeUG·DAN heterocomplex was more stable than the UG·DAN heterocomplex.[18] Indeed, this was found to be the case. Large downfield shifts in the N-H resonances for both compounds were observed over a concentration range of 10 μM to 10 mM. Assuming 5% dissociation went undetected, K_{assoc} was estimated to be greater than 10^7 M^{-1}.

In order to more accurately determine the K_{assoc} for complexes with such high binding affinity, a more sensitive technique needed to be employed. Isothermal titration calorimetry (ITC) is a powerful method for quantifying the thermodynamics of binding events because a single experiment gives K_{assoc}, ΔH, ΔS and the stoichiometry of complexation (n). Moreover, ITC can quantify association constants of the order of 10^2-10^9 M^{-1}.[41]

Titration of a 0.323 mM solution of DeUG in chloroform with a 3.27 mM solution of DAN in chloroform gave a K_{assoc} of 1.3×10^7 M^{-1}, a ΔH of -6.9 kcal mol^{-1} and a $T\Delta S$ of 2.8 kcal mol^{-1} from the best fit curve (Figure 15). However, the integrated data display an increasing amount of heat evolved per injection up to approximately 0.9 equivalents of DAN, which compromises the goodness of fit. Clearly, the enthalpy, which is the difference between the top and the bottom of the isotherm, is underestimated by the best fit curve.

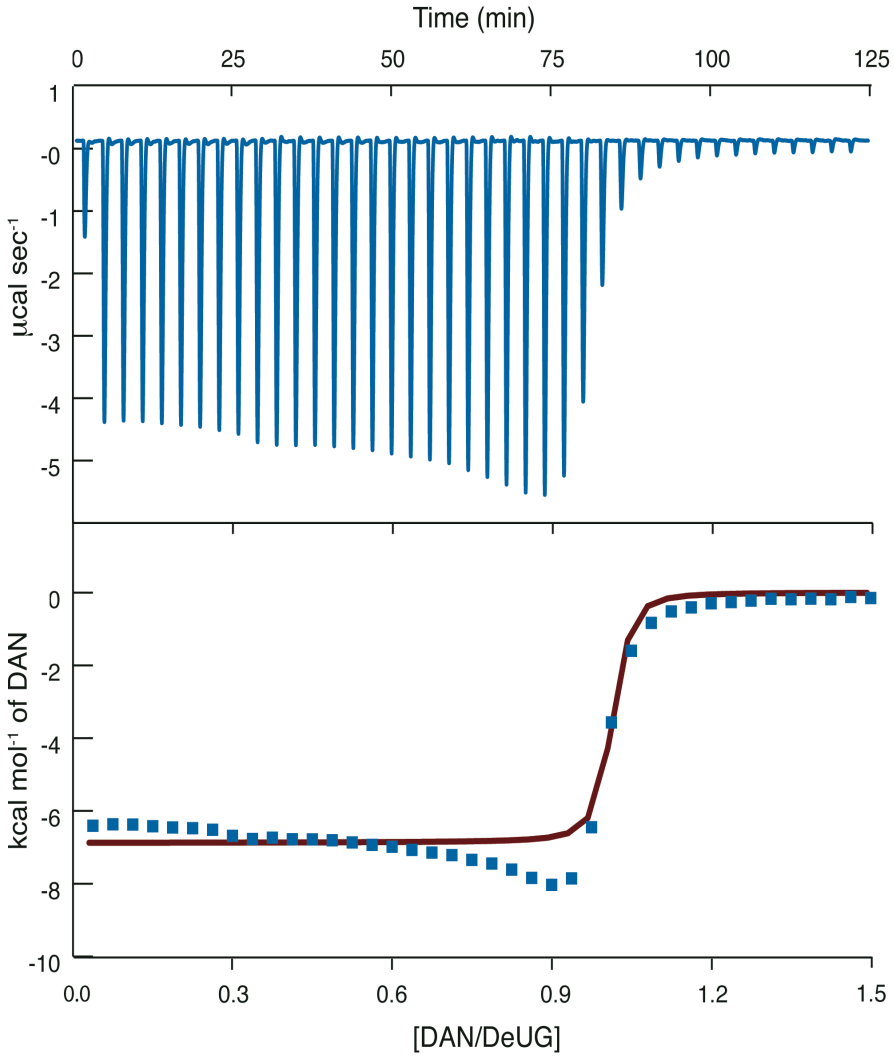

Figure 15. ITC of DeUG·DAN **17·4** in $CHCl_3$ at 25 °C showing the enthalpic attenuation resulting from dissociation of the DeUG dimer.

It was hypothesized that this apparent anomaly arose from an *enthalpic attenuation* caused by the endothermic cost of dissociating the DeUG homocomplex. Specifically, heterocomplexation of DeUG with DAN during the titration shifts the DeUG self-association equilibrium toward free DeUG. In this case, the total enthalpy measured for any single injection (up to 1:1 stoichiometry) is the sum of the endothermic homocomplex dissociation and the exothermic heterocomplex association—that is, the enthalpy of heterocomplexation is being *attenuated* by the enthalpy of homo-decomplexation. As the titration approaches 1:1 stoichiometry, the DeUG self-association equilibrium is being perturbed in favor of a larger and larger fraction of monomeric DeUG. Thus, the enthalpic attenuation diminishes with each successive injection, leading to the observed slope in the initial portion of the isotherm.

According to this hypothesis, the difference between the enthalpy for the first aliquot (injection) of the titration and the most exothermic aliquot (at ca. 0.9 equivalents) should closely correspond to the enthalpy of self-association for DeUG **17**. Moreover, an analysis of the concentration of each species through the titration should reveal that the DeUG dimerization equilibrium is being perturbed as proposed. Indeed, a plot of these concentrations shows that this is the case (Figure 16).

An analysis of the concentrations of monomeric and dimeric species throughout the titration proves revealing. The most important metric is illustrated as the red curve (which is plotted on the right, logarithmic axis) in Figure 16, which is the ratio of free DeUG to DeUG dimer. As predicted by the hypothesis, this ratio increases steadily up to near the equivalence point, where a dramatic increase occurs.

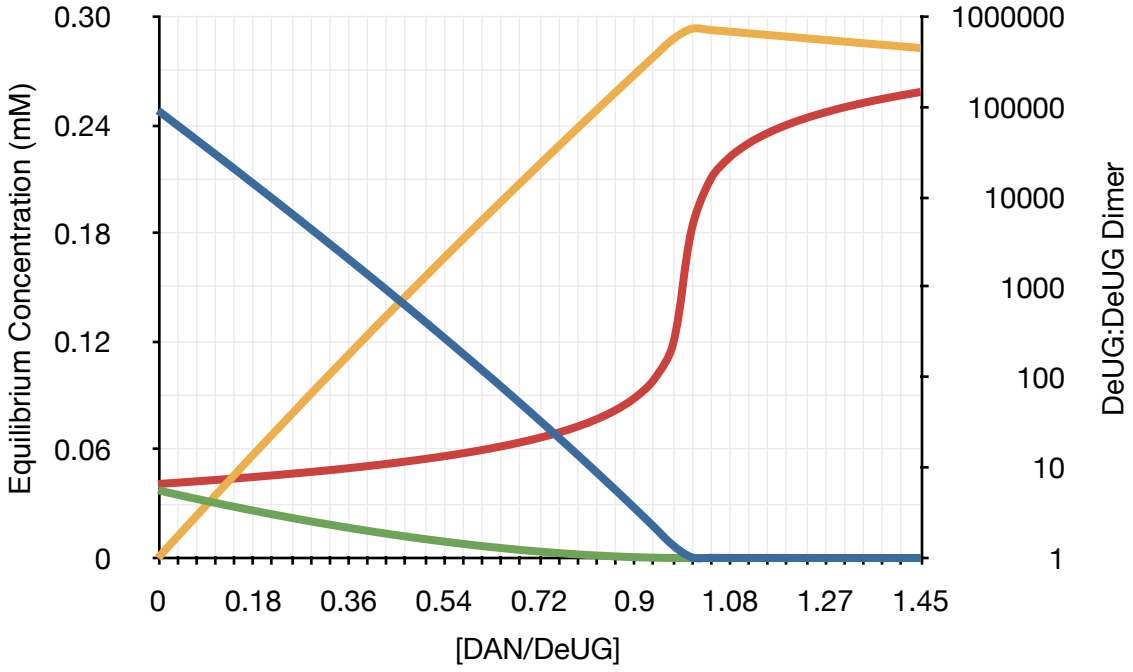

Figure 16. Equilibrium concentrations of major species (left ordinate) and ratio of DeUG to DeUG dimer (right ordinate) vs. DAN/DeUG molar ratio throughout the ITC experiment shown in Figure 12 for **17·4**.

The ΔH for DeUG dimerization as determined by ITC in the aforementioned manner was -1.6 kcal mol^{-1}. An independent determination of this quantity was found to be -1.7 kcal mol^{-1} via a ^{1}H NMR van't Hoff experiment over a temperature range of 5 °C to 41 °C (Figure 17), which is in good agreement with that determined by calorimetric methods. Thus, the DeUG·DAN (**17·4**) K_{assoc} value was estimated to be 1.9×10^{8} M^{-1} by correcting the enthalpy of heterocomplexation by an amount equal to the enthalpy of DeUG dimerization. This places the DeUG·DAN heterocomplex among the most stable of its kind reported to date.

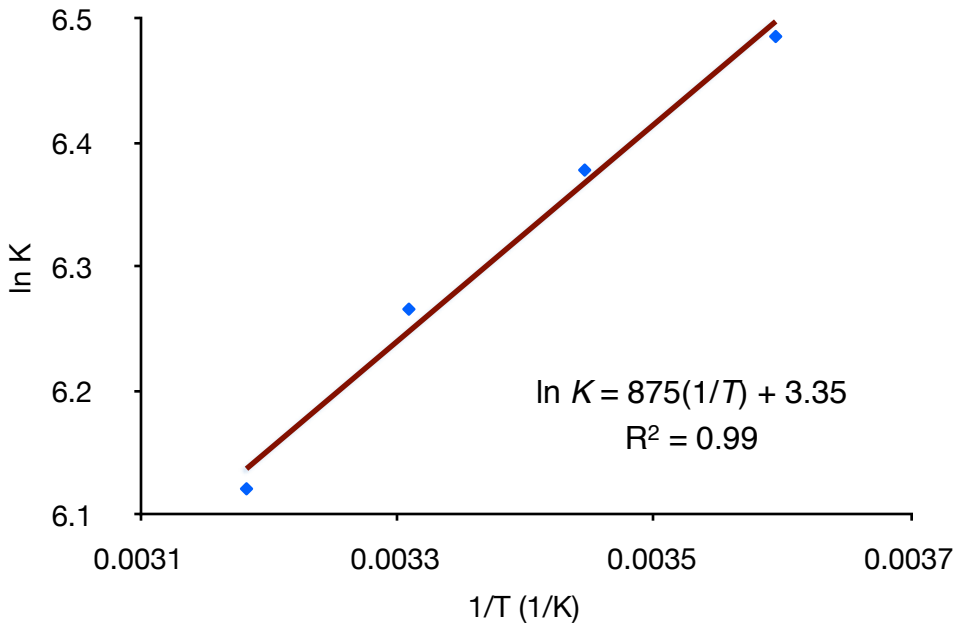

Figure 17. ^{1}H NMR van't Hoff plot for the self-association of DeUG **17** over a temperature range of 5 to 41 °C.

As shown in Figure 18, an ITC experiment was also performed in 5% DMSO/ $CHCl_3$, a more competitive solvent that was expected to reduce the contribution of DeUG self-association and, thus, diminish the enthalpic attenuation observed in $CHCl_3$. From titrations of DAN **4** into DeUG **17** at 25 °C in this solvent mixture, the best fit curve gave a K_{assoc} value of 2.1 × 10^4 M^{-1}, a ΔH of -6.9 kcal mol^{-1} and a $T\Delta S$ of 2.8 kcal mol^{-1}. Moreover, the isotherm did not display any enthalpic anomalies. This association constant falls within the previously reported range as estimated by ^{1}H NMR.[18]

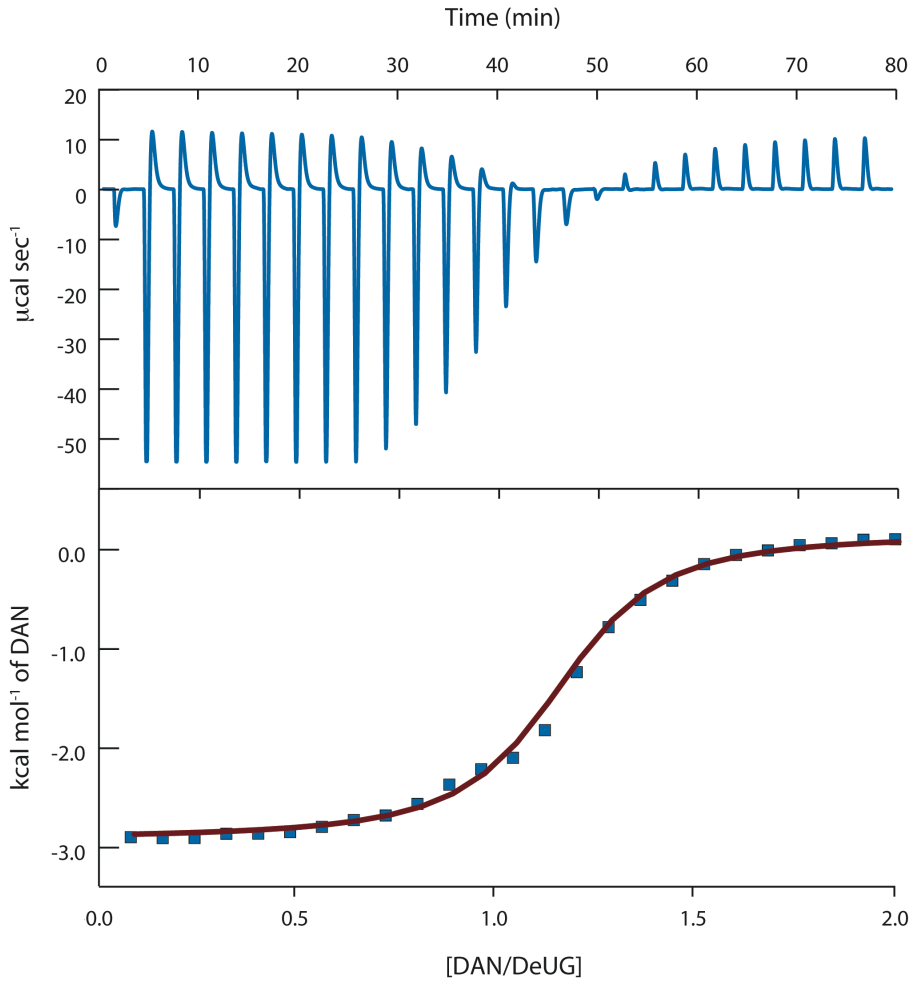

Figure 18. ITC of DeUG·DAN **17·4** in 5% DMSO/$CHCl_3$ at 25 °C.

Repeated attempts to obtain crystals of the **17·4** heterocomplex suitable for X-ray analysis proved unsuccessful. However, using the previously reported[18] 1,1,3,3-tetramethylbutyl urea DeUG analogue, **18**, Mr. Yi Gui Gao of the George C. Clark X-Ray Facility and 3M Materials Laboratory at the University of Illinois at Urbana-Champaign was able to obtain triclinic crystals of the **18·4** heterocomplex suitable for X-ray analysis via slow evaporation from chloroform (Figure 19).[33,42]

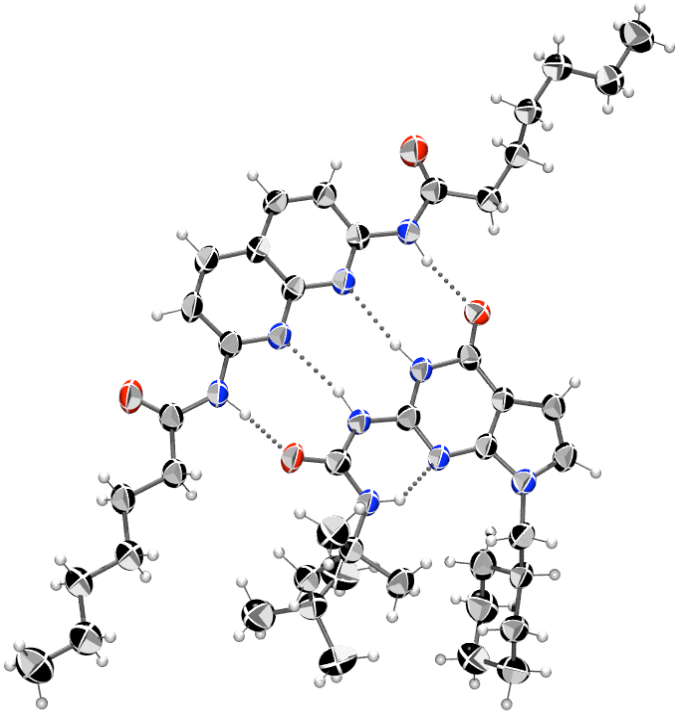

Figure 19. ORTEP representation of a DeUG·DAN (**18·4**) heterocomplex. Thermal ellipsoids represent 50% probability.

2.5 Miscellaneous Quadruply Hydrogen Bonding Modules

2.5.1 *tert*-Butyl Ureideodeazapterin (DeAP)

Recently, Todd and Zimmerman reported on the utility of a ditopic hydrogen bonding module based on the ureidodeazapterin (DeAP, **40**) motif, which was used in the construction of supramolecular star polymers. These polymers possess many interesting properties, including remarkable stability, forming large amounts of assembled material that persist even in DMF at elevated temperature.[43,44] Although this high degree of stability may be desirable in a number of applications, it may prove to be disadvantageous if the assembly is so thermodynamically robust that it is essentially

Scheme 11

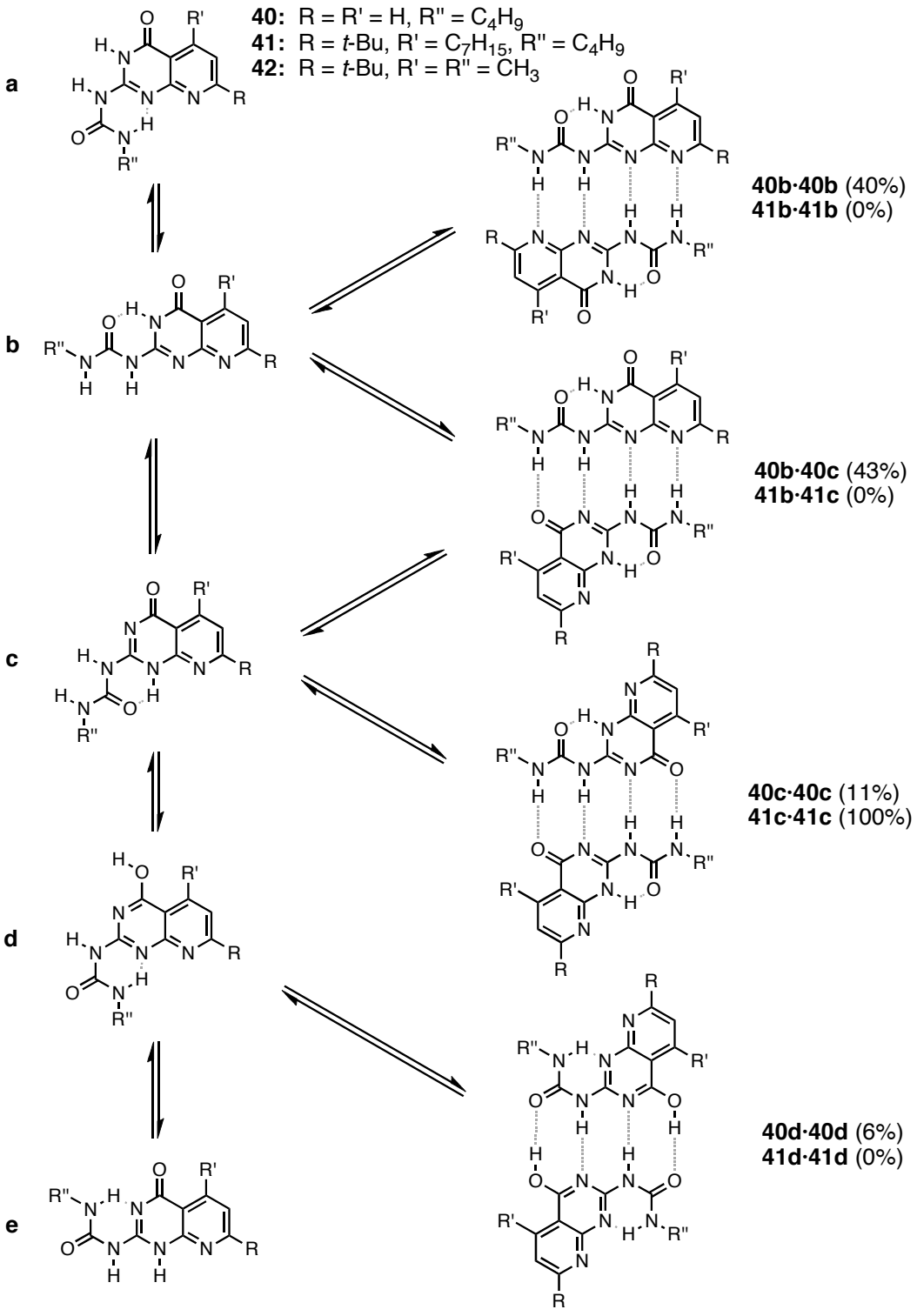

irreversible. From the beginning, DeAP was designed as a self-complementary unit that can assemble regardless of protomeric form (Scheme 11, numbers in parentheses are mol

% by ^{1}H NMR).[45] However, the presence of multiple protomeric forms can unnecessarily complicate analysis. Thus, efforts toward controlling the mode and attenuating the strength of association of DeAP based supramolecular assemblies were undertaken.

Todd proposed that perhaps the most straightforward approach to achieve both attenuation of the strength of the assembly and control over the mode of association is by judicious placement of a sterically encumbering group on the DeAP heterocycle.[46] By careful consideration of the species present in the parent DeAP system (*vide supra,* Scheme 11), it was rationalized that incorporation of a bulky group at *C*7, such as a *tert*-butyl group, would either preclude the formation or significantly diminish the contribution of complexes **40b·40b** and **40b·40c** via destabilizing steric interactions between the *tert*-butyl group and the *n*-butyl urea. Because lactim dimer **40d·40d** does not contain any of the proposed steric constraints, its formation was not anticipated to be perturbed.

In order to assess the viability of this approach, semi-empirical molecular modeling (RM1) of a simplified *tert*-butyl ureidodeazapterin (*tert*-butyl DeAP, **42**) was undertaken. Shown in Table 2 are the calculated energies and dipole moments for each protomeric and dimeric species. The relative energies indicate that dimer **42c·42c** can be expected to be more stable than mixed dimer **42b·42c** and homodimer **42b·42b** by approximately 1.5 and 1.8 kcal mol^{-1}, respectively, and nearly 16 kcal mol^{-1} more stable than lactim dimer **42d·42d**. Dimer **42c·42c** was also predicted to have the lowest dipole moment in the series as well as an over 4 kcal mol^{-1} lower enthalpy of association.

Table 2. RM1 energies and dipole moments for *tert*-butyl DeAP **42**.

Species	Dipole (D)	Relative energy (kcal mol^{-1})	Enthalpy of association (kcal mol^{-1})
42a	2.98	0.00	---
42b	4.42	3.91	---
42c	4.80	6.46	---
42d	5.88	10.1	---
42e	5.37	2.78	---
42b·42b	3.37	1.78	-24.2
42b·42c	5.17	1.52	-27.0
42c·42c	0.00	0.00	-31.1
42d·42d	0.08	15.7	-22.7

*Monomers are referenced to **42a** and dimers are referenced to **42c·42c**.

Because **41** is forced to dimerize through higher energy protomeric form **41c**, it was expected to possess a weaker self-association constant compared to parent DeAP **40**. However, the ^{1}H NMR spectrum of **41** in $CDCl_3$ did not change upon dilution down to 300 μM. Unfortunately, any difference in the association constants between DeAP **40** and *tert*-butyl DeAP **41** does not fall in the range observable by ^{1}H NMR. Furthermore, the equilibrium constant for diamidonaphthyridine **4** breaking up the *tert*-butyl DeAP dimer, as determined via ^{1}H NMR titration studies, was found to be the same (within error) as that reported for the parent DeAP system, suggesting that the two possess similar self-association constants.[45]

The synthesis and characterization of *tert*-butyl DeAP **41** have been reported elsewhere.[46] Monoclinic crystals of *tert*-butyl DeAP **41** suitable for X-ray analysis were

obtained via recrystallization from 20% chloroform in methanol (Figure 20).[33] The proposed mode of dimerization for **41** was confirmed to exist in the solid state structure.

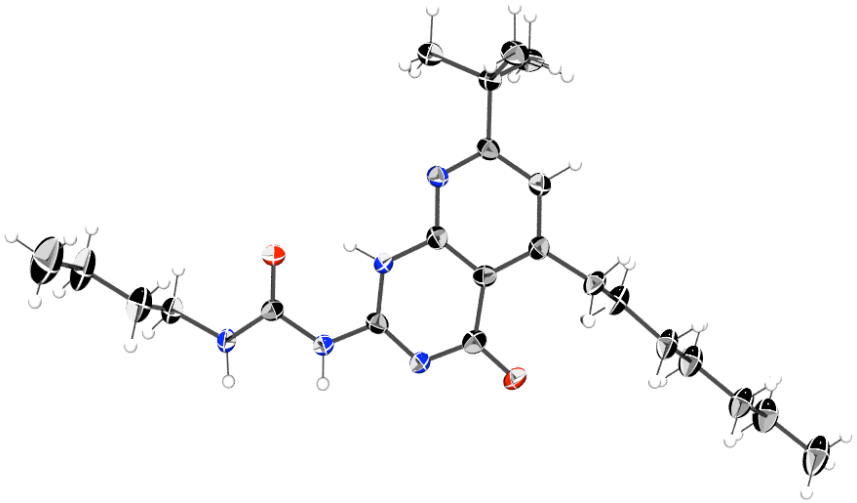

Figure 20. ORTEP representation of *tert*-butyl DeAP (**41**). Thermal ellipsoids represent 50% probability.

Table 3. Summary of solid-state hydrogen bond geometries for **41**.*

D-H···A	d(D-H, Å)	d(H···A, Å)	d(D-H, Å)	∠(D-H···A, °)
N-H···O	0.91(3)	1.84(3)	2.762(5)	166(5)
N-H···N	0.89(3)	2.12(3)	3.002(6)	176(4)
intramolecular N-H···O	0.88(2)	1.80(3)	2.580(5)	145(5)

*Complete crystallographic structure data can be found in Appendix A.

Todd reported on the self-assembly of discrete cyclic structures based on a bis-*tert*-butyl DeAP module (analogous to the bis-DeAP system) and telechelic polymers.[46] A publication covering all of these aspects of the *tert*-butyl DeAP module has been prepared and should be forthcoming.

2.5.2 2-(Heptanoylamido)-1,8-naphthyridine-7-one

A potentially useful and interesting self-complementary, quadruple hydrogen bonding module —naphthyridone **31**—can be easily synthesized in the course of synthesizing 2,7-diamino-1,8-naphthyridines (Figure 21). As shown in Scheme 9 (*vide supra*), this module can be synthesized in high yield in only two steps. Additionally, the inherent asymmetry allows for the facile introduction of functional groups on the alkyl amide—making it synthetically ideal for use in supramolecular architectures. However, there are no reports of its use in such a capacity. Although Alkorta has previously reported the crystal structure of the acetamide homologue,[47] there have been only limited reports of its self-association or heterocomplexation behavior. McKay reported the dimerization for **31·31** to be greater than 1.0×10^5 M^{-1} in chloroform. Importantly, it was also reported that the association constant of **31** with DAN **4** was less than 5 M^{-1} in chloroform.[48] Although apparently only possessing a moderate dimerization constant, the lack of promiscuity in binding displayed by **31** makes it an ideal candidate for use in multicomponent supramolecular architectures that also employ diamidonaphthyridines.

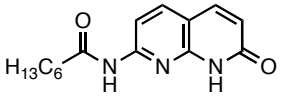

31

Figure 21. 2-(Heptanoylamido)-1,8-naphthyridine-7-one.

To further the study of this interesting class of quadruply hydrogen bonding modules and to determine its hydrogen bonding motif in the solid state, triclinic crystals of naphthyridone **31** suitable for X-ray analysis were obtained via slow evaporation from chloroform (Figure 22).[33]

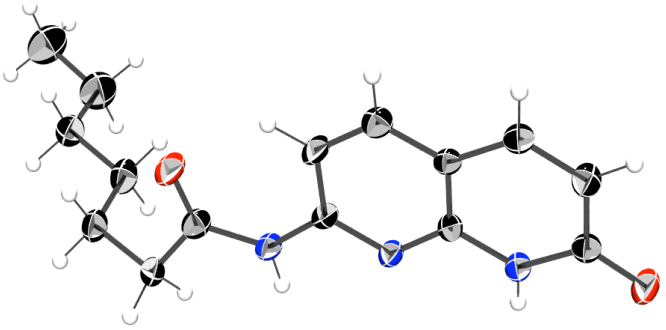

Figure 22. ORTEP representation of naphthyridone (**31**). Thermal ellipsoids represent 50% probability.

The mode of dimerization in the solid state was confirmed to be via the ADAD motif, as previously proposed. The hydrogen bonding geometries for the **31**·**31** dimer are summarized in Table 4, below.

Table 4. Summary of solid-state hydrogen bond geometries for **31**.*

D-H···A	d(D-H, Å)	d(H···A, Å)	d(D-H, Å)	∠(D-H···A, °)
N-H···N	0.93(2)	2.16(2)	3.072(4)	167(3)
N-H···O	0.89(2)	1.95(2)	2.833(4)	171(3)

*Complete crystallographic structure data can be found in Appendix A.

2.5.3 Thermogravimetric Analyses (TGA)

An understanding of the thermal stability of hydrogen bonding modules is of primary importance for determining their compatibility with conventional materials processing techniques such as melt processing, extrusion and injection molding.[49] Moreover, thermogravimetric profiling should aid in the identification of labile structural

features and, thus, could provide insight when designing more thermally robust analogues.

Armstrong and Buggy have studied the thermal stability of UPy **1** as well as benzoic acid-dipyridyl complexes by TGA and differential scanning calorimetry (DSC). The authors report that 89% of the initial mass of **1** was lost over a temperature range of 227 - 350 °C. The gaseous fragments of the thermal degradation were analyzed by GC-MS, with the mass of the primary fragment formed between 225 - 244 °C corresponding to butyl isocyanate. [50,51]

We were interested in comparing the thermal profiles of several other hydrogen bonding modules. To this end, TGA was performed on selected hydrogen bonding modules to assess their thermal stabilities (Figure 23). The modules were chosen to assess the effects of different functional groups.

DAN **4** and the *t*-butyl amide of deazaguanine (**43**) were found to have the greatest thermal stability in the series with onset temperatures of 313 °C and 304 °C, respectively. The profiles for **4** and **43** were strikingly similar, with approximately 75% of the mass loss occurring in a single step between 300 °C and 400 °C. DeUG **17** displayed a similar profile as that reported for UPy, with a slightly higher onset temperature of 240 °C with approximately 80% of the mass loss occurring in a single step over a temperature range of 240-525 °C. DeAP **40** had an onset temperature of 205 °C with approximately 35% of the mass loss occurring over a temperature range of 205-245 °C. A second decomposition event had an onset temperature of 400 °C with an additional 25% mass loss. Deazaguanine ethyl ester **15** had the lowest thermal stability of the series

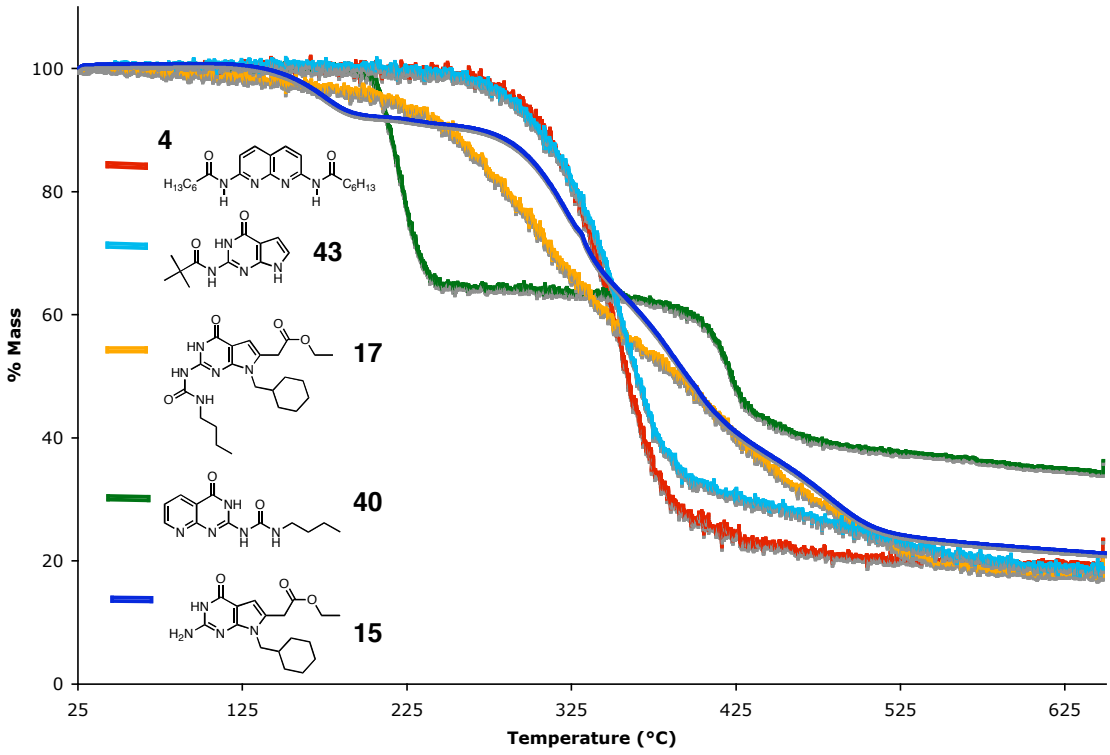

Figure 23. Thermogravimetric analysis (TGA) profiles for selected hydrogen bonding modules. Samples were heated from 25 °C to 650 °C at a rate of 10 °C min^{-1}.

with an initial onset temperature of approximately 150 °C corresponding to an 8% mass up to 290 °C. Another 70% of the mass was lost in a second step. Interestingly, all compounds showed approximately 40% mass loss at around 350-360 °C.

2.6 Conclusion

A convenient, scalable synthesis for the supramolecular building block 7-deazaguanine urea (DeUG), which displays high-affinity, high-fidelity complexation with 2,7-diamido-1,8-naphthyridines (DAN), was successfully accomplished. Analytically pure DeUG can be synthesized in an overall yield of approximately 35% over six steps without the need for column chromatography at any stage. Additionally, DeUG was

readily functionalized with several common reactive groups in preparation for materials applications. A key finding was that DeUG has an exceptionally high affinity for DAN as determined by combined isothermal titration calorimetry (ITC) experiments, van't Hoff experiments and modeling of the heterocomplexation equilibrium.

Additional advancements were made in the characterization of *t*-butyl deazapterin (*t*-butyl DeAP) and with 2-(heptanoylamido)-1,8-naphthyridine-7-one. In the case of the naphthyridone, it represents an ideal candidate for the construction of complex supramolecular architectures in conjunction the DeUG·DAN pair. It is anticipated that developing and testing supramolecular materials will be made more accessible by the ready availability of these new quadruply hydrogen bonding modules.

Part II: Materials Applications of the DeUG·DAN Heterocomplex

Chapter 3

Reversible Supramolecular Network Polymer Formation

3.1 Background

Supramolecular polymers are macromolecular structures that have some noncovalent component that contributes to their formation, organization and/or stability.[52] Supramolecular polymers can be broadly classified by the location of the noncovalent interaction (Figure 24). In main-chain supramolecular polymers, the noncovalent interaction occurs in the backbone of the polymer and, thus, is responsible for the formation of the polymer itself. Main-chain supramolecular polymers can be further sub-divided by the number and type of non-covalent interactions. A single, self-complementary monomer forms a homopolymer, whose degree of polymerization is related to the strength of the noncovalent interaction (Figure 24a).[53] When two or more

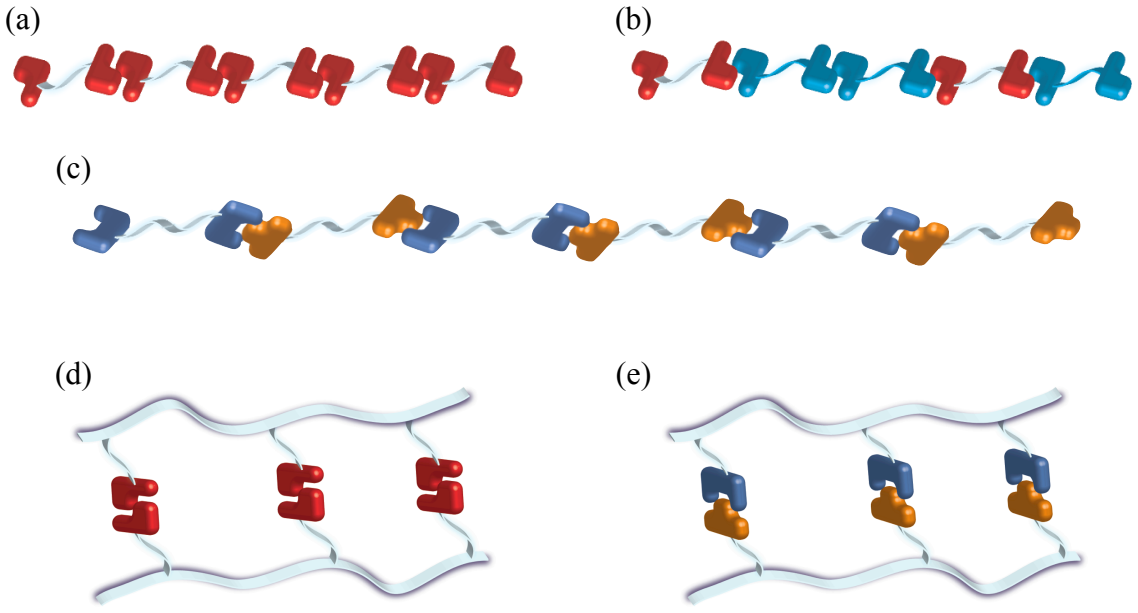

Figure 24. Classes of supramolecular polymers organized by location of the noncovalent interaction.

mutually complementary monomers are used, a random block copolymer results, whose architecture is dictated by the relative strengths of the self-complementary and hetero-complementary association constants (Figure 24b). On the other hand, when highly orthogonal noncovalent interactions are used, a strictly alternating block copolymer is the result (Figure 24c).[54]

Supramolecular network polymers represent another interesting class. In these materials, the noncovalent interaction is typically displayed on a side chain and acts as a crosslinking agent to create the polymer network. Again, these can be created from self-complementary noncovalent units (Figure 24d) or orthogonal units (Figure 24e). Previous work in our laboratories has shown the utility of the network architecture illustrated in Figure 24e in creating polymer blends between otherwise thermodynamically incompatible polymers.[16] Supramolecular network polymers often lead to robust, and, sometimes, intractable gels. Other types of supramolecular polymers, such as supramolecular star polymers, are beyond the scope of the present discussion and, thus, are not included here.

Organogels and hydrogels have been the subject of much scientific inquiry in recent years due to their unique properties and, therefore, a wide range of practical and theoretical applications. Many types of gels have been reported—some with extraordinary properties.[55] Gels were defined by Flory as macroscopic, multi-component, colloidal dispersions that display solid-like rheological behavior.[56] Often, gel deformation and formation can be achieved by simple heating and cooling cycles. However, for applications ranging from drug delivery to chemical sensors and polymer

processing, engineering a means of externally modulating gel deformation and formation would be advantageous.[57]

Much effort in our research laboratories has been devoted to the design and synthesis of molecular recognition units that have application in the formation of supramolecular polymers and polymer blends. A major, ongoing goal is to create a robust, stimuli-responsive molecular recognition unit capable of reversible binding. Indeed, there are few reports of stimuli-responsive, multiply hydrogen bonded modules in the literature.[58]

3.2 A Photoresponsive DAN (pDAN)

3.2.1 Design Principles and Modeling

Initially, to develop a means of modulating the binding event between DeUG and DAN, we set out to create a molecule bearing a pendant moiety capable of reversibly and noncovalently competing for the naphthyridine binding face. The most straightforward approach involved the use of an azobenzene group that would act as a "hinge" and be able to swing the pendant moiety from being proximal to the naphthyridine binding face to being distal to it.

Scheme 12

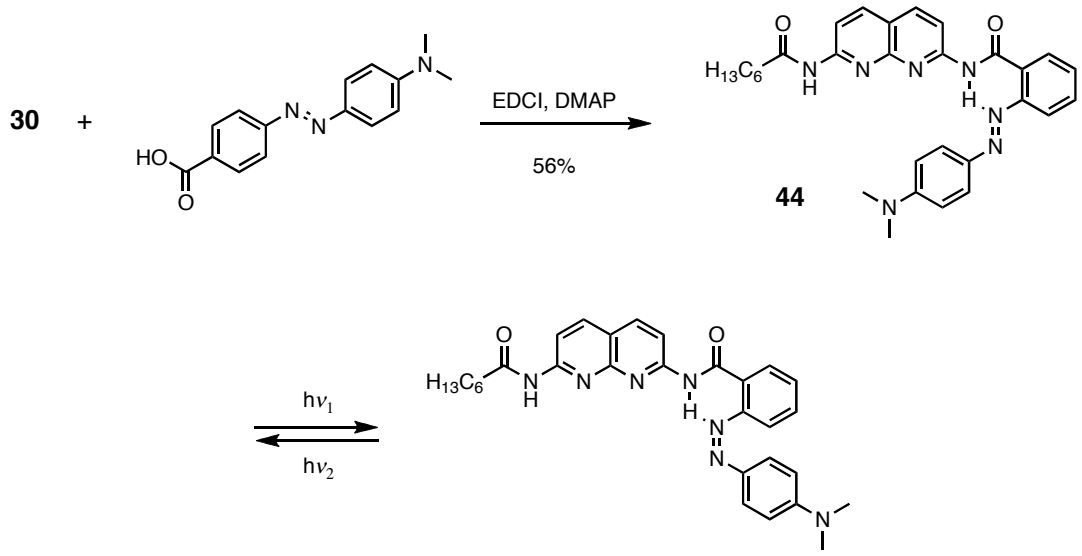

A relatively simple molecule was synthesized to gauge the feasibility of this approach. Methyl red, a common indicator, met the design criteria quite well and was appended onto amidonaphthyridine **30** under standard coupling conditions to give DAN-methyl red conjugate **44** (Scheme 12). It was anticipated that in the *trans* form, **44** would

present sufficient steric bulk to the binding face of the naphthyridine (by virtue of an intramolecular hydrogen bond) that affinity for DeUG would be significantly diminished, while binding to DeUG would be largely unperturbed when in the *cis* form. However, preliminary studies suggested binding to DeUG by *trans*-**44** was actually enhanced, possibly due to π-π interactions between DeUG and azobenzene. Indeed, semi-empirical molecular modeling suggested this was the case. It was decided that a more sterically-encumbering pendant group would be needed to realize effective competition for the naphthyridine binding face. This goal became the independent project for another member of the research group.

We instead turned our attention to appending moieties capable of photodimerization to DAN. Bassani and coworkers[58] had recently demonstrated photochemical modulation of binding to barbital using a bisanthracene-modified Hamilton receptor.[59] The study of the photodimerization of anthracene has a long history. Anthracene is known to readily undergo photooxidation under aerobic conditions giving anthraquinone. It has been proposed that anthracene itself acts as a sensitizer, generating singlet oxygen, which then reacts with anthracene.[60]

Despite this drawback, we decided to use the general approach reported by Bassani to create an analogous photoresponsive DAN (pDAN). Semi-empirical molecular modeling (RM1) was used to gauge the optimum linker length between the naphthyridine and the anthracene moieties (Figure 25). Modeling suggested that four methylene groups would offer the best balance between allowing for intramolecular

dimerization of the pendant anthracenes and providing maximum steric hindrance to the naphthyridine binding face.

(a) (b)

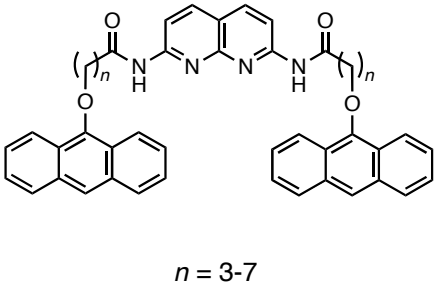

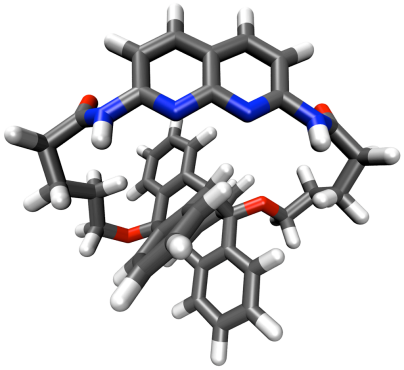

Figure 25. (a) pDAN structures that were modeled. (b) Licorice representation of the semi-empirical (RM1) equilibrium geometry of pDAN where n = 4, showing steric encumbrance of the naphthyridine binding face.

3.2.2 Synthetic Approaches to pDAN

The synthesis of pDAN **45** was accomplished in three convergent steps, following the general approach reported by Bassani.[58a] As shown in Scheme 13, alkylation of anthrone with ethyl 5-bromovalerate using potassium carbonate afforded ethyl 5-(9-anthryloxy)valerate, which was subsequently hydrolyzed to carboxylic acid **46** (75% yield over two steps). Diaminonaphthyridine **23** then underwent an EDCI-promoted double coupling with carboxylic acid **46** to afford pDAN **45** in good yield.

Scheme 13

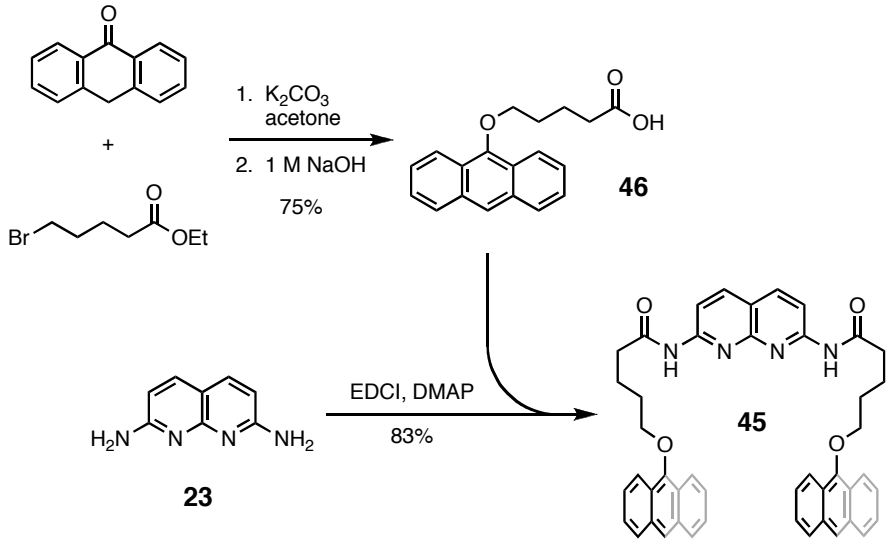

Because anthracene is prone to photooxidation, pDAN **45** was typically stored as macrocycle **47** (Scheme 14). Photodimerization of pDAN was carried out in rigorously degassed acetonitrile due to the discovery that the naphthyridine moiety rapidly decomposes in halogenated solvents (CH_2Cl_2 and $CHCl_3$) when irradiated at 365 nm. This decomposition of the naphthyridine also occurred in control experiments using diamidonaphthyridine **4**. Continued irradiation of **45** for 3 hours using a high-power 365 nm light-emitting diode array gave macrocyclic photodimer **47**.[61]

Scheme 14

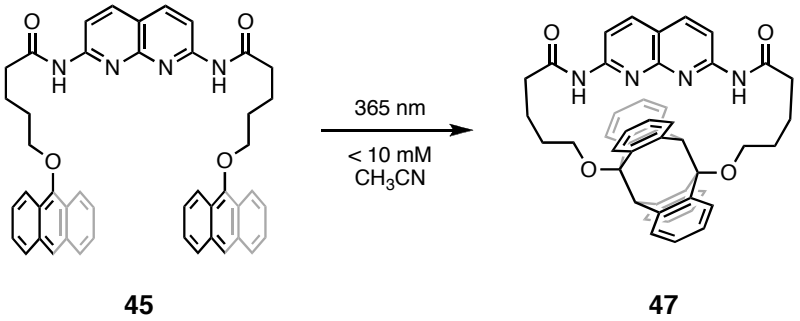

The head-to-tail isomer for the anthracene dimer is shown as it is known to be more stable than the head-to-head isomer.[60] However, we have not unequivocally established which isomer is dominant in **47**.

3.2.3 Characterization of pDAN

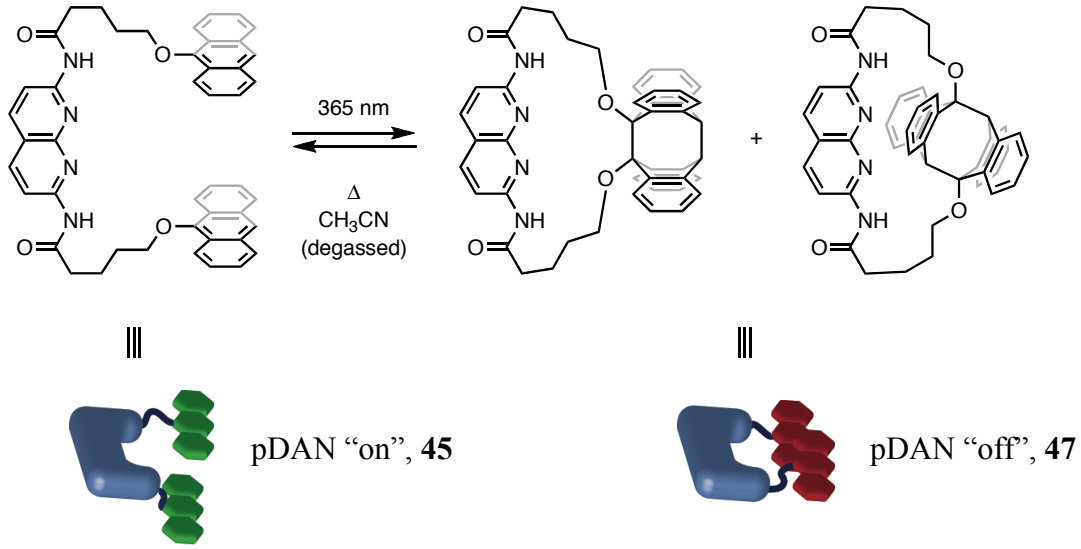

Figure 26. Schematic of the pDAN photochemical cycloaddition and thermal cycloreversion.

Investigations of the photochemical cycloaddition and thermal cycloreversion[62] of pDAN were initially made by UV-vis spectroscopy. As shown in Figure 27a, the characteristic absorption bands due to anthracene between 350 nm and 400 nm completely disappear after irradiation (365 nm, 3 h, 100 μM **45** in rigorously degassed CH_3CN).

To further assess the ability of pDAN to cycle through its "on" and "off" states, a fatigue study was performed by monitoring the absorbance at 368 nm. A 100 100 μM

solution of **45** in rigorously degassed CH_3CN was irradiated at 365 nm for 3 hours and the UV-vis spectrum recorded. The solution was then heated at 70 °C for 24 hours and the UV-vis spectrum was again recorded. This cycle was repeated three more times. As shown in Figure 27b, the absorbance at 368 nm decreases by less than 10% after four complete cycles between the two states.

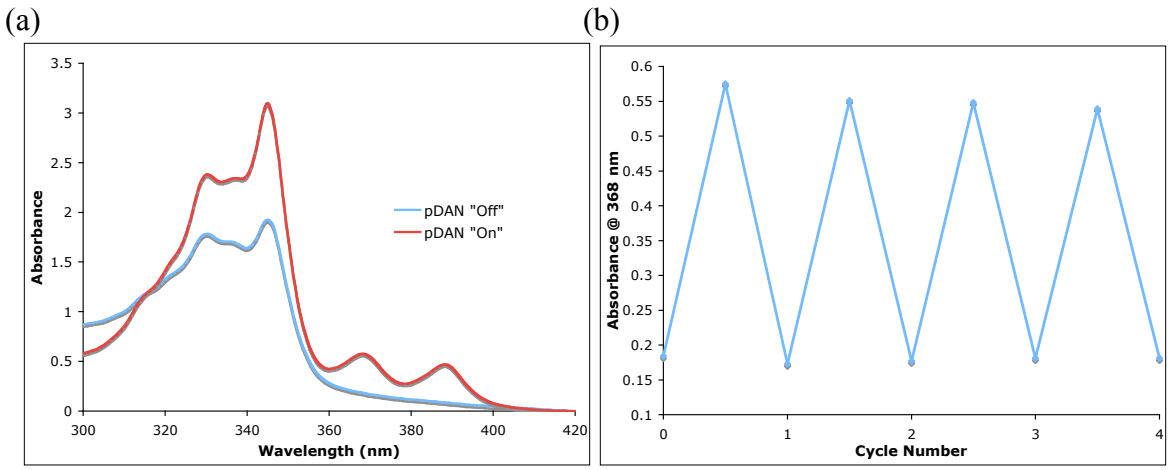

Figure 27. (a) UV-vis spectra of pDAN "on" (**45**) and pDAN "off" (**47**). (b) UV-vis fatigue study of **45**/**47**.

^{1}H NMR studies showed evidence for pDAN **45** reversibly binding DeUG **17** (Figure 28). The ^{1}H NMR spectra for 500 μM solutions of **17** and **45** CD_3CN are shown in Figures 28a and 28b, respectively. The resonance for *C*7-H in free DeUG appears at 6.30 ppm, while the resonance for the N-Hs in free pDAN appear at 9.03 ppm. However, as shown in Figure 28c, a 1 mM solution of a 1:1 mixture of **17**·**45** in CD_3CN shows a large downfield shift (2.5 ppm, from 9.03 to 11.5 ppm) in the *N*-H resonances for pDAN and an upfield shift (0.17 ppm, from 6.30 to 6.13 ppm) in the *C*7-H resonance for DeUG, both of which are consistent with the formation of a strongly bound complex.

Unfortunately, we were unable to discern the chemical shifts of the *N*-H resonances of DeUG in deuterated acetonitrile.

The 1 mM solution **17·45** was then irradiated at 365 nm for 3 hours and the ^{1}H NMR spectra was recorded. As shown in Figure 28d, the *C*7-H resonance for DeUG moves downfield by 0.12 ppm, consistent with a large fraction of DeUG being unbound. Unfortunately, the signals for the *N*-H's in pDAN were not observed. We propose that

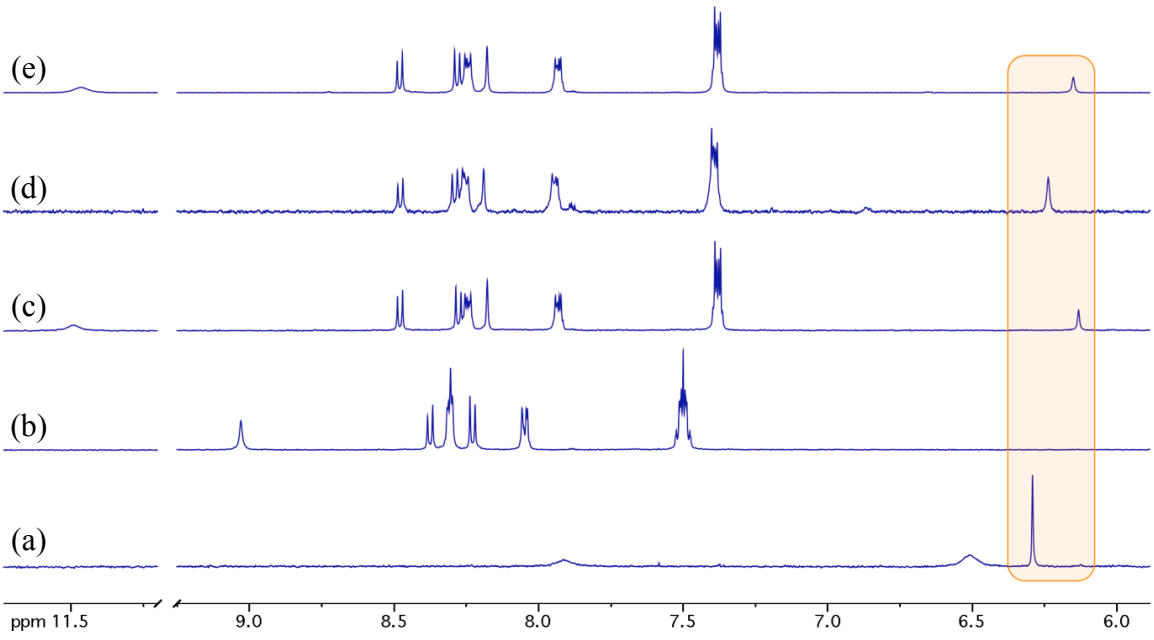

Figure 28. ^{1}H NMR study of DeUG·pDAN complexes **17·45** and **17·47**.

this is due to pDAN being partitioned across many different states and conformations, which caused the signals to be broadened out, which is consistent with ^{1}H NMR studies of **47** alone. The spectrum is most consistent with the equilibrium between **17·45** and **17·47** being shifted toward **17·47**, based on the time-averaged chemical shift change observed for DeUG *C*7-H.

The solution was then heated at 70 °C for 24 hours and the ^{1}H NMR spectra was again recorded (Figure 28e). The *N*-H resonances for pDAN reappear near 11.5 ppm and the *C*7-H resonance for DeUG appears at 6.15 ppm, both of which are consistent with the reformation of the **17·45** heterocomplex when compared to Figure 28c. Upon close inspection, the characteristic resonances for anthraquinone are just barely discernible indicating that a small amount of photooxidation of **45** had occurred.

Although a quantitative determination of the association constants for DeUG·pDAN complexes **17·45** and **17·47** was never made, the combined results of the UV-vis and ^{1}H NMR experiments strongly suggested that the behavior would be sufficient to demonstrate the modulation of sol-gel transitions in supramolecular polymers.

3.3 Supramolecular Polymer Syntheses

There are two traditional methods used in the preparation of side-chain functionalized supramolecular polymers with architectures akin to those illustrated in Figure 24 (*vide supra*). The first involves copolymerization of two monomers—one with and the one without the molecular recognition unit.[63,64] The other is post-polymerization functionalization. For the preparation of the polymers used in the following studies, we chose the former method due to its simplicity and because the heterocyclic recognition units are incompatible with many post-polymerization techniques.[65]

Scheme 15

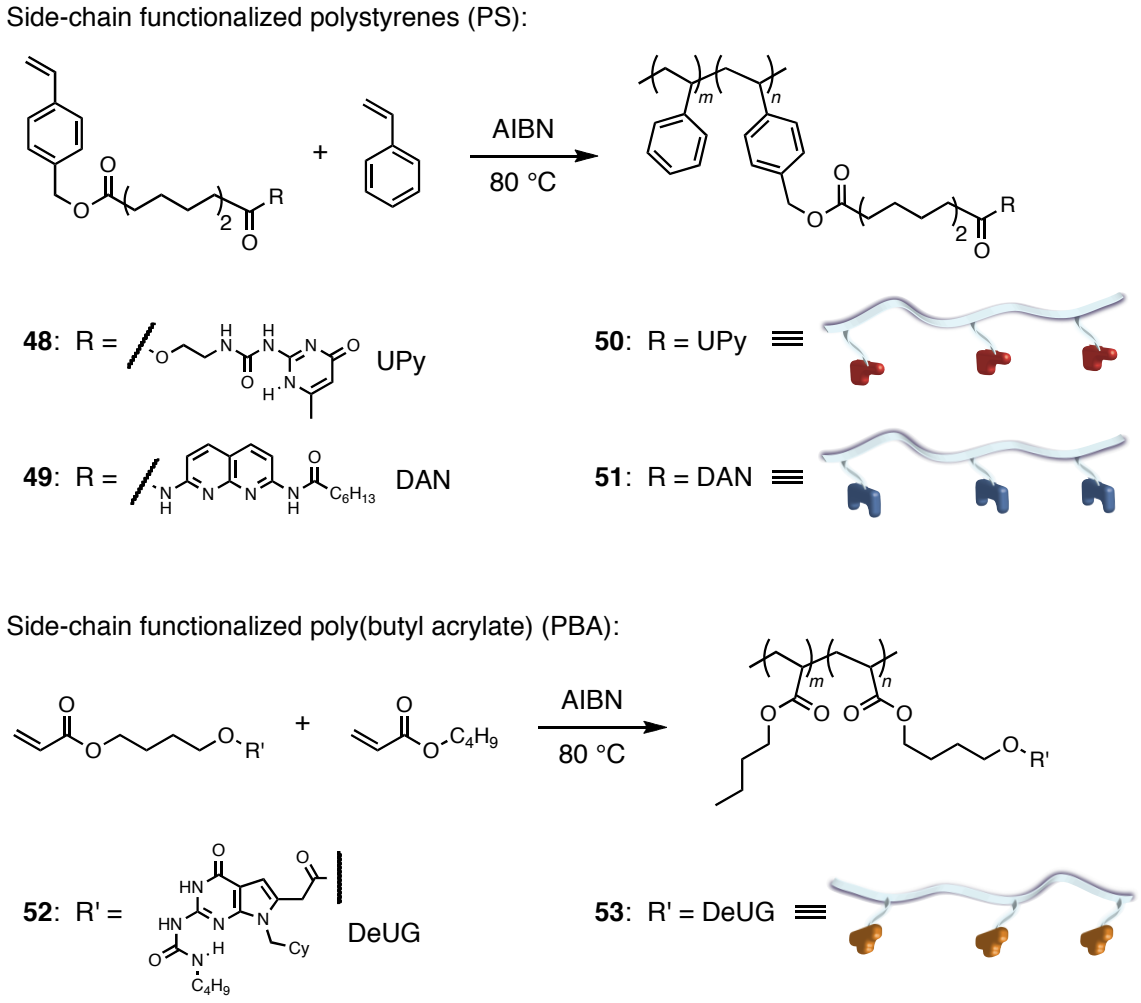

As shown in Scheme 15, side-chain functionalized UPy-polystyrene (UPy-PS, **50**) and DAN-polystyrene (DAN-PS, **51**) were prepared by free radical copolymerization of functional monomers **48** and **49**, respectively, with styrene. Likewise, side-chain functionalized DeUG-poly(butyl acrylate) (DeUG-PBA, **53**) was prepared by free radical copolymerization of functional monomer **52** with butyl acrylate. In all cases, the loading of functional comonomers **48**, **49** and **52** in the resultant polymers was controlled by varying the comonomer feed ratio. Each polymer was characterized by ^{1}H NMR and

analytical size-exclusion chromatography (SEC). The results are summarized in Table 5, below.

Table 5. Summary of supramolecular polymers.

Polymer	M_n (kDa)	Module	mol % Loading*
50, UPy-PS	57	UPy	11
51, DAN-PS	22	DAN	5
53, DeUG-PBA	10	DeUG	6

*Loading determined by ^{1}H NMR integration.

3.4 Modulation of Sol-Gel Transition in Supramolecular Polymers

UPy-PS **50** was found to form a robust organogel in a variety of organic solvents that persisted even after heating at 80 °C in toluene for 14 hours. However, as illustrated in Figure 29, this gel can be irreversibly disrupted by the addition of just 2 equivalents of DAN **4** and mild heating at 40 °C for 10 min.

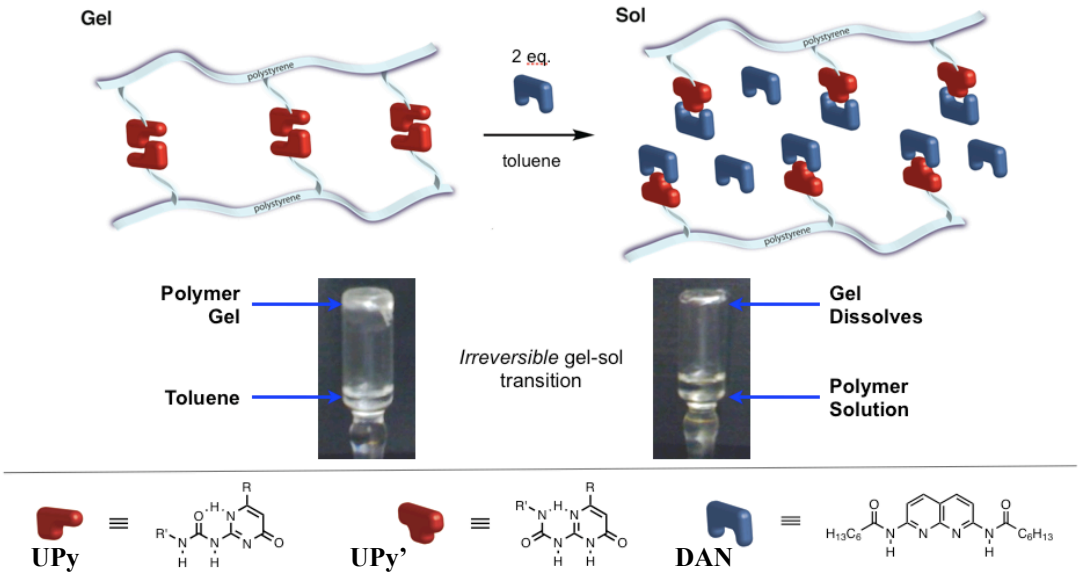

Figure 29. Irreversible disruption of UPy-PS **50** organogel using DAN **4**.

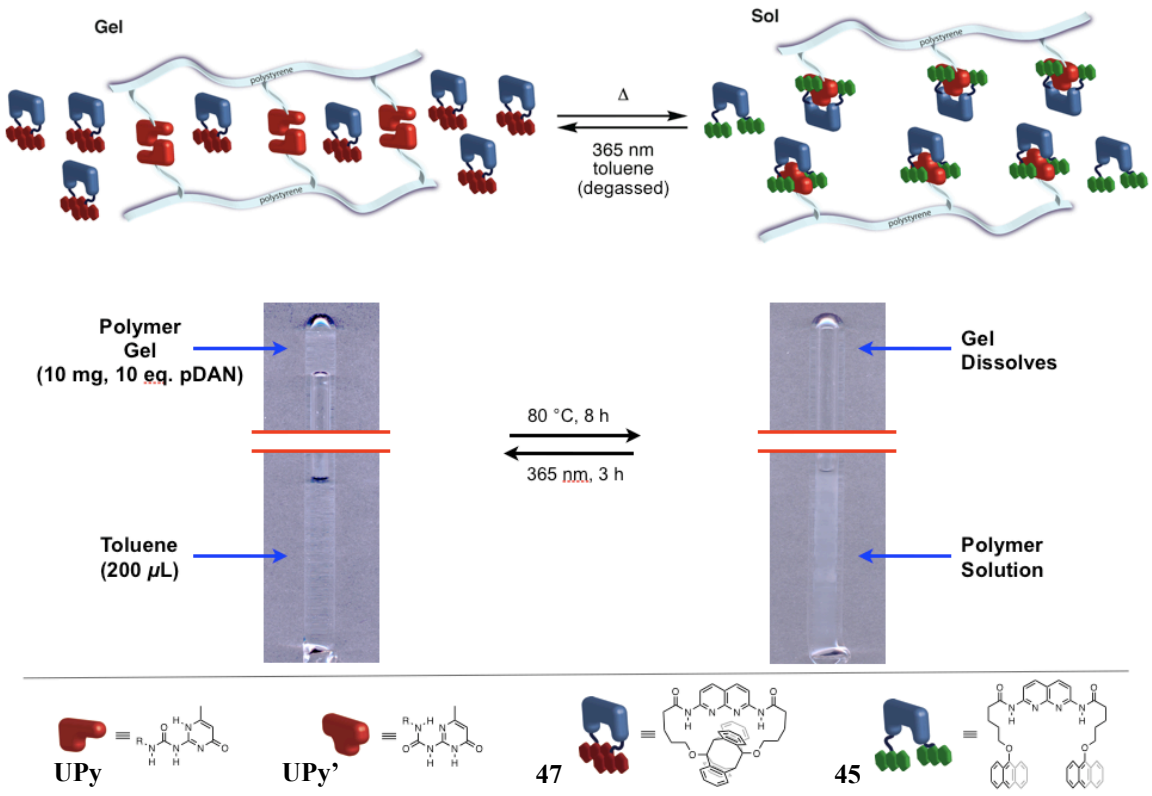

Figure 30. Reversible formation of UPy-PS **50** organogel using pDAN **45/47**.

Without a means to remove or otherwise render **4** inactive, this represents a one-way transformation from the gel to the sol state. The experiment was therefore repeated using pDAN. In a typical experiment, 10 mg of UPy-PS **50** was placed in a thick-walled NMR tube and was swelled via addition of 200 μL of toluene containing 10 equivalents of pDAN-"off" **47** via microsyringe. The contents were subjected to seven freeze-pump-thaw cycles and flame-sealed under argon. As shown in Figure 30, the UPy-PS gel persisted for a minimum of 24 hours in the presence of **47**. The sample was then heated at 80 °C for 8 hours in the dark. After this time, the gel was found to be completely dissolved. The sample was then irradiated at 365 nm. After 3 hours, visual inspection indicated that no additional gel was forming. This cycle was repeated 3 additional times.

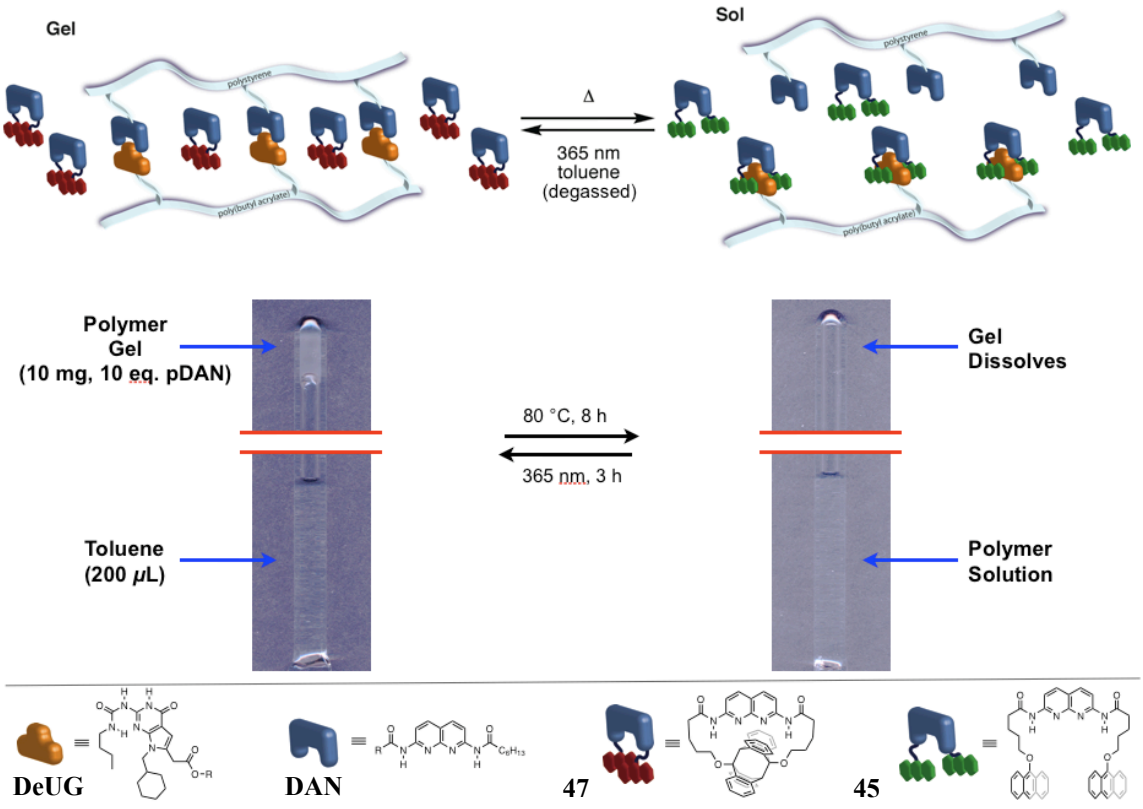

Figure 31. Reversible formation of DAN-PS/DeUG-PBA organogel using pDAN **45**/**47**.

We next endeavored to demonstrate the same application of pDAN toward supramolecular network polymer blends of DAN-PS **51** and DeUG-PBA **53** (Figure 31). Zimmerman and Park had previously reported on the utility of the UG·DAN heterocomplex toward the formation of supramolecular network polymer blends between traditionally incompatible polymers such as PS and PBA.[17] The experiment was repeated under the same conditions detailed for UPy-PS·pDAN (*vide supra*) with an essentially identical outcome.

In both cases (UPy-PS·pDAN and DAN-PS/DeUG-PBA·pDAN), visually discernible decreases in the amount of gel reformed upon irradiation were observed after

an average of three cycles. Analysis of the supernatant from each experiment revealed a complex mixture of compounds to be present—among them, small amounts of anthraquinone. It is important to note that, when pDAN undergoes photooxidation, a completely active form of diamidonaphthyridine is generated, which would prevent reformation of the gel. However, due to the complexity of the compounds found in the supernatant, it is likely that photooxidation of pDAN is contributing to the lack of gel reformation to only a small extent, and that the major contributing factor is the photobleaching of the recognition units themselves.

3.5 Conclusion

A photoresponsive diamidonaphthyridine (pDAN, **45**) was successfully synthesized and characterized. It was demonstrated to act as a means of reversibly modulating binding to DeUG **17**. Due to the propensity of anthracene to undergo photooxidation, this approach is feasible only under strictly anaerobic conditions. A key finding was that DAN rapidly undergoes a presently unknown mechanism of photobleaching when irradiated at 365 nm in halogenated solvents.

It was further demonstrated that pDAN is useful as a method to reversibly control the formation and deformation of supramolecular network polymers and polymer blends. After an average of three gel-sol cycles, the amount of gel reformed significantly decreased. This is likely a result of photobleaching of the pendant molecular recognition units from the polymer backbone, although more studies are indicated in order to unequivocally establish the reason for the limited lifetime of these systems.

Chapter 4

Supramolecular Chemistry on Surfaces

4.1 Background

Self-assembly of nanoscale objects and multilayer organic thin films on surfaces represents one of the most versatile, simple and elegant methods to approach the "bottom-up" construction of functional devices. Many types of nanoscale objects have been deposited onto several substrate classes via covalent attachment, electrostatic interactions and hydrogen-bonding interactions[66] with the goal of fabricating devices with possible applications ranging from optics to molecular sensing.[67-69]

With regard to multilayer construction methods, the popular Langmuir-Blodgett (LB) technique is limited to specific classes of molecules[70,71] while the more general layer-by-layer (LbL) deposition of alternating layers of polyanionic and polycationic species on charged substrates, pioneered by Decher,[72] has its own limitations due to the polyionic nature of the materials. More recently, non-specific hydrogen-bonding has been employed as means of fabricating multilayer thin films of several types of nonionic polymers.[73,74] However, to enable a higher level of control over the intra- and interlayer architecture in such systems, it may be advantageous to employ specific, orthogonal molecular recognition units.

The following chapter begins with our initial attempts to apply the DeUG·DAN heterocomplex towards self-assembly on surfaces and finishes with an exploration of using the heterocomplex towards interfacial adhesion promotion.

4.2 Preparation of DeUG-Modified Surfaces

4.2.1 Silica Nanoparticles and Polystyrene Resins

Propylamine functionalized silica particles were prepared via a one-pot method involving a slight modification to the well-known Stöber method,[75] as reported by Lee and coworkers (Scheme 16).[76] Tetraethyl orthosilicate (TEOS) was added to a 1.5 M solution of ammonium hydroxide in ethanol. After 12 h, 3-aminopropyltrimethoxysilane (APTMS) was added directly to the aforementioned solution giving **55** after workup (Scheme 16). The presence of the amino group was confirmed via a Kaiser test.[77] Aqueous dynamic light scattering (DLS) experiments revealed the hydrodynamic radius (R_H) of these nanoparticles to be 63-65 nm.

Scheme 16

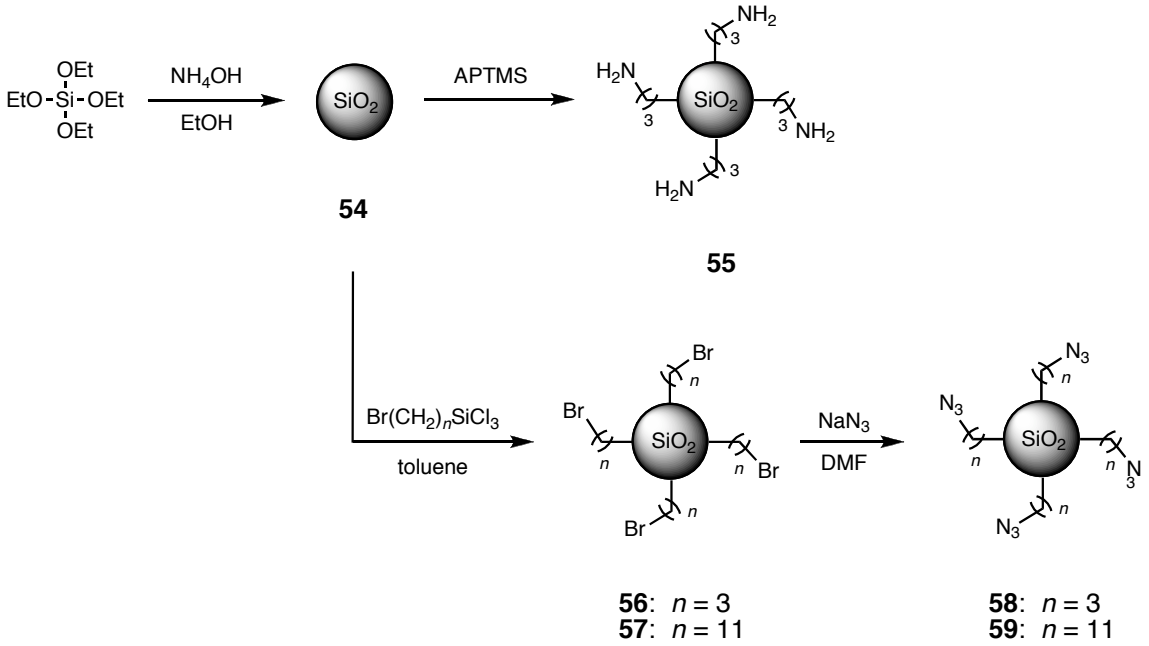

Reports of hydrogen bonding module functionalized surfaces suggest that, as expected, the length of the surface-bound tether has a pronounced effect on intra-surface self-association. Shorter tethers were shown to contribute to reducing the extent of intra-surface self-association.[78] With this in mind, alkylbromide-tailored silica nanoparticles were prepared by reacting either 3-bromopropyltrichlorosilane or 11-bromoundecyltrichlorosilane with **54** to give **56** and **57**, respectively. Treatment of each **56** and **57** with sodium azide in DMF afforded azide-tailored silica nanoparticles **58** and **59** (Scheme 16). In each case, confirmation of the presence of the azide group was accomplished using IR spectroscopy (ν = 2104 cm^{-1}). Identical surface modifications to those shown in Scheme 1 were also performed on 230-400 mesh (40-63 μm) silica gel.

Scheme 17

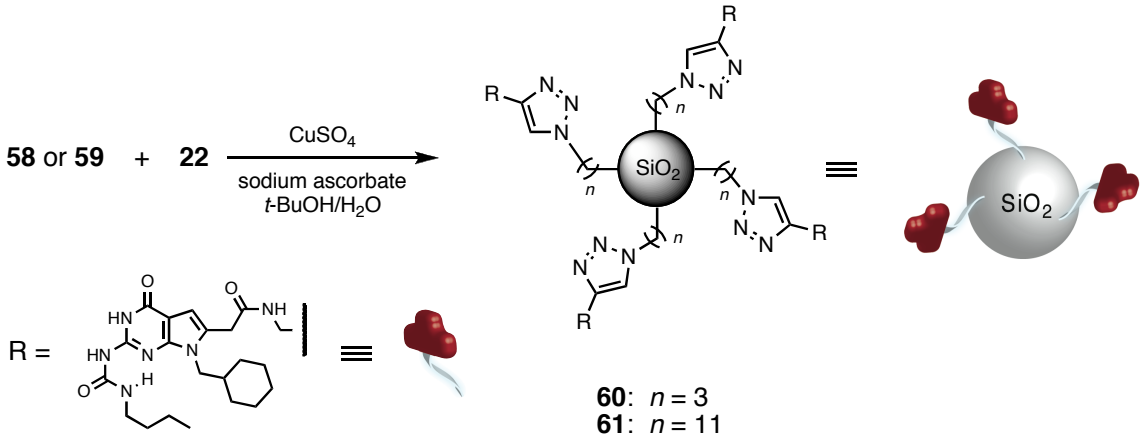

As shown above in Scheme 17, DeUG propargyl amide **22** was attached to azide functionalized silica nanoparticles **58** and **59** via copper-catalyzed azide-alkyne cycloaddition (CuAAC) using catalytic cupric sulfate and sodium ascorbate (NaAsc), following the general procedure reported by Sharpless.[28] The presence of the DeUG

modules was confirmed by IR spectroscopy, which revealed three diagnostic peaks corresponding to the three carbonyl-containing functional groups (Figure 32). The IR spectrum of also revealed the presence of residual azide groups.

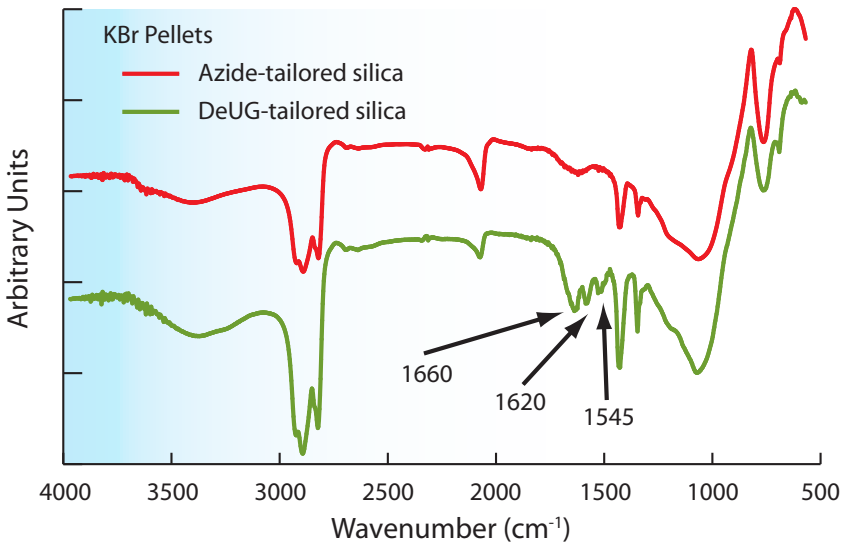

Figure 32. IR spectra of azide-tailored silica nanoparticles **58** and DeUG-tailored silica nanoparticles **60**.

Investigations of the self-assembly of DAN **4** on DeUG-tailored silica nanoparticles **60** were performed via UV-vis spectroscopy (Figure 33). In a typical experiment, a 56 μM solution of **4** was prepared in chloroform. The concentration was verified by comparison to a standard curve, also generated by UV-vis. To this solution was added 40 mg of nanoparticles. The solution was vigorously shaken for 15 min and centrifuged. The concentration of **4** in the supernatant was then determined by UV-vis. As controls, the above experiment was repeated using propylbromide-tailored silica nanoparticles **56** and unfunctionalized silica nanoparticles. The results are summarized in Figure 33b.

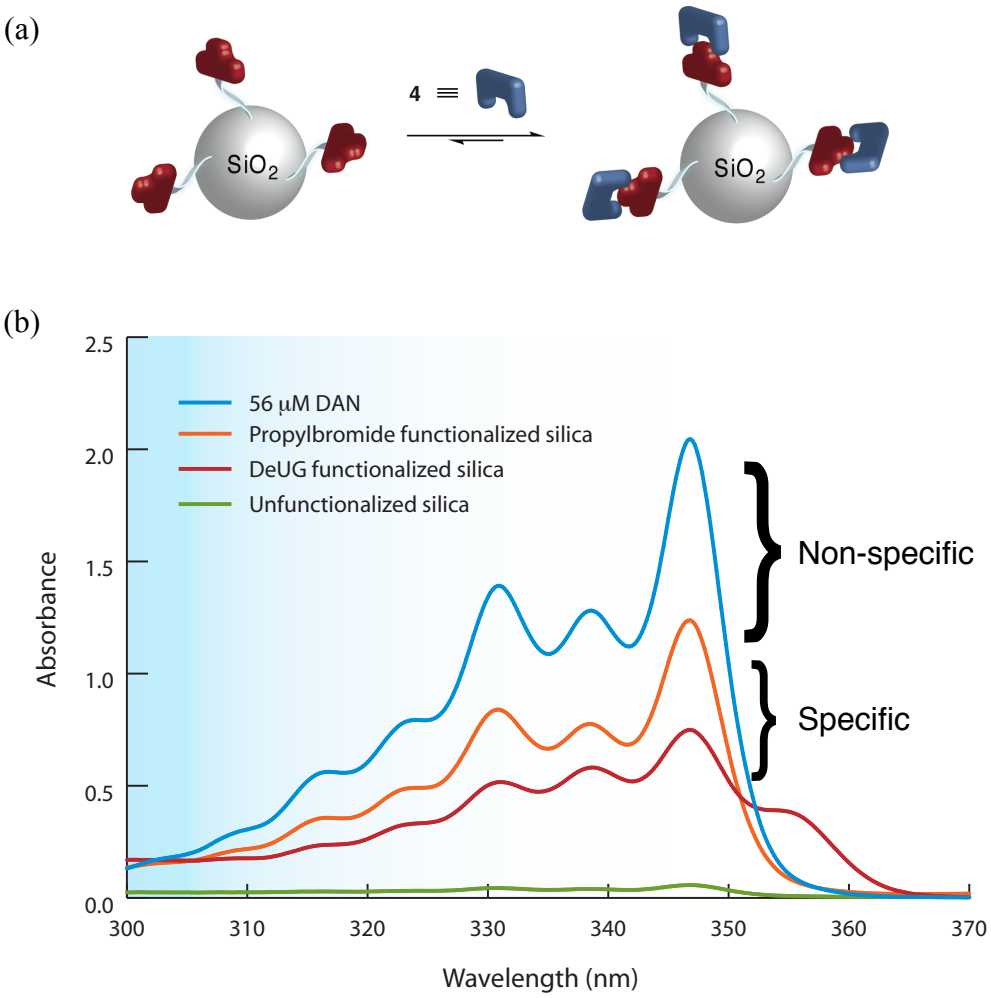

Figure 33. (a) Schematic of the self-assembly of DAN **4** on DeUG-tailored silica nanoparticles **60** and (b) UV-vis experiment in $CHCl_3$ showing extent of adsorption and self-assembly of DAN **4** on differently functionalized silica nanoparticles.

As expected, unfunctionalized silica nanoparticles showed virtually complete adsorption of DAN from solution, while the propylbromide-tailored silica nanoparticles showed a 40% decrease in absorbance, suggesting that the siliceous surface had only been partially passivated. DeUG-tailored silica nanoparticles showed a 55% decrease in absorbance, down to 0.58 from 1.28. Assuming that the extent of passivation, and, thus, the extent of nonspecific adsorption, between samples **56** and **60** are approximately equal, which is a reasonable assumption as **60** was prepared from the same batch of **56** used in

the experiments, and further assuming 90% DeUG·DAN complexation, a lower limit for DeUG loading of 360 nmol g^{-1} could be estimated. As shown in Figure 33, the results suggest that both nonspecific adsorption and specific, molecular recognition driven adsorption are operative.

To test this hypothesis, polystyrene (PS) beads in the form of Merrifield resin were functionalized in a manner similar to the silica nanoparticles (Scheme 18). Using this approach, nonspecific interactions between recognition units and the substrate should be minimized.

Scheme 18

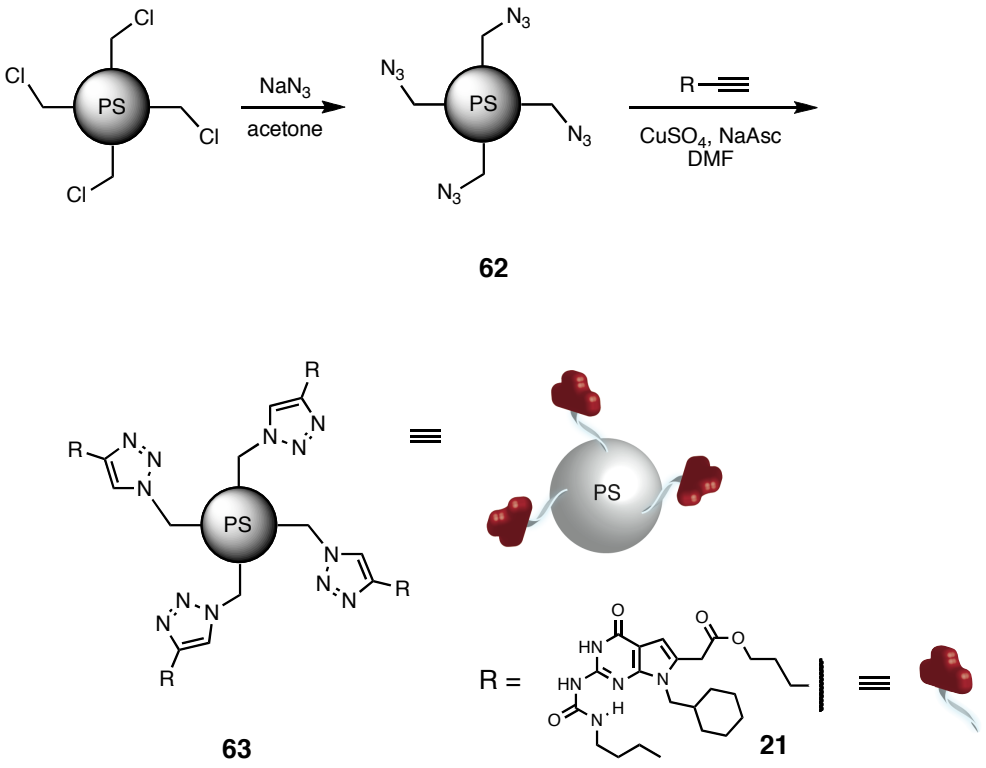

Azide-tailored Merrifield resin **62** was prepared by treating commercially available Merrifield resin (2% crosslinked, 200-400 mesh, 2.25 mmol g^{-1} Cl) with sodium

azide in acetone. As before, the presence of the azide was confirmed by IR spectroscopy. DeUG pentynyl ester **21** was attached to **62** via CuAAC chemistry using catalytic cupric sulfate and sodium ascorbate in DMF to give DeUG-tailored PS beads **63**. The presence of the DeUG modules was again confirmed by IR spectroscopy, as shown in Figure 34. The IR spectra for the DeUG-tailored PS beads is scaled to match the spectra for **21** for ease of comparison. In the present case, no residual azide groups were observed indicating that near quantitative incorporation of DeUG had occurred.

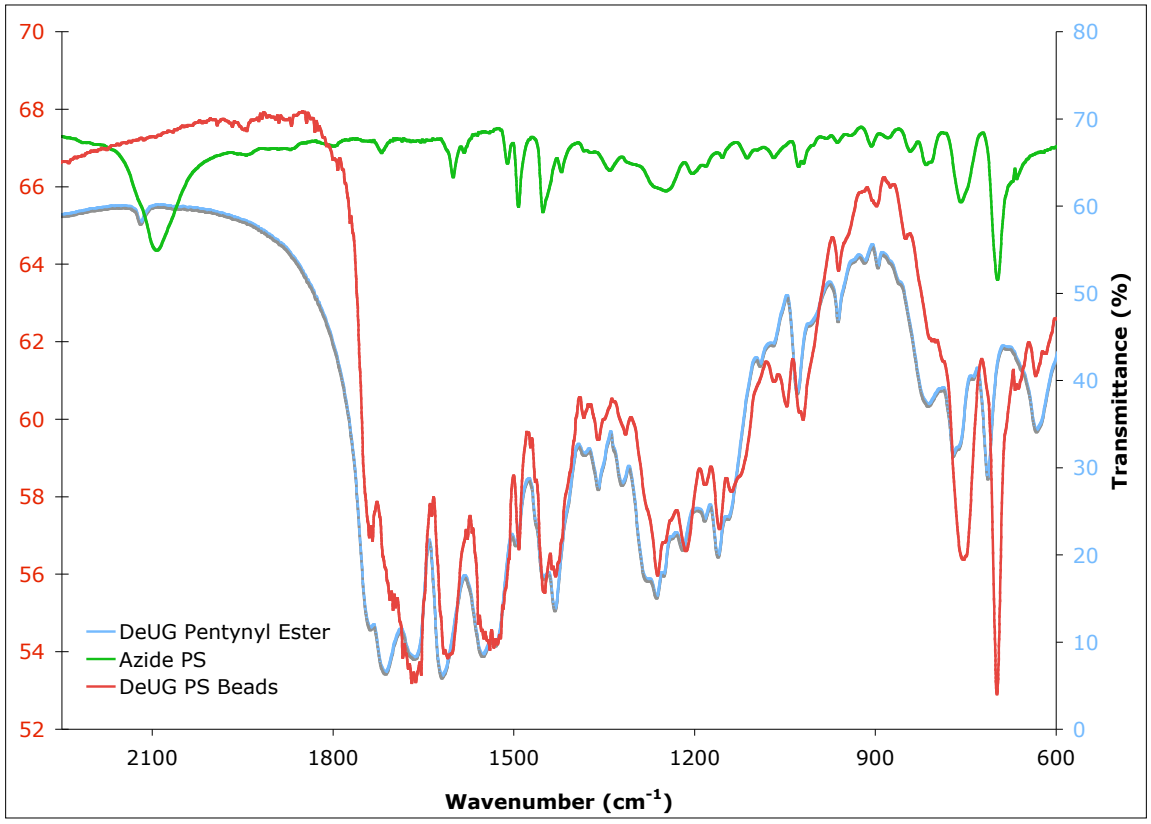

Figure 34. IR spectra of azide-tailored Merrifield resin **62**, DeUG-tailored Merrifield resin **63** and DeUG pentynyl ester **21**.

As before, investigations of the self-assembly of DAN **4** on DeUG-modified Merrifield resin **63** were performed via UV-vis spectroscopy (Figure 35). In a typical experiment, a 52 μM solution of **4** was prepared in chloroform. The concentration was verified by comparison to a standard curve, also generated by UV-vis. To this solution was added 40 mg of the appropriate Merrifield resin. The solution was vigorously shaken for 15 min and centrifuged. The concentration of **4** in the supernatant was then determined by UV-vis. As controls, the above experiment was repeated using azide-modified Merrifield resin **62** and "off-the-shelf" Merrifield resin.

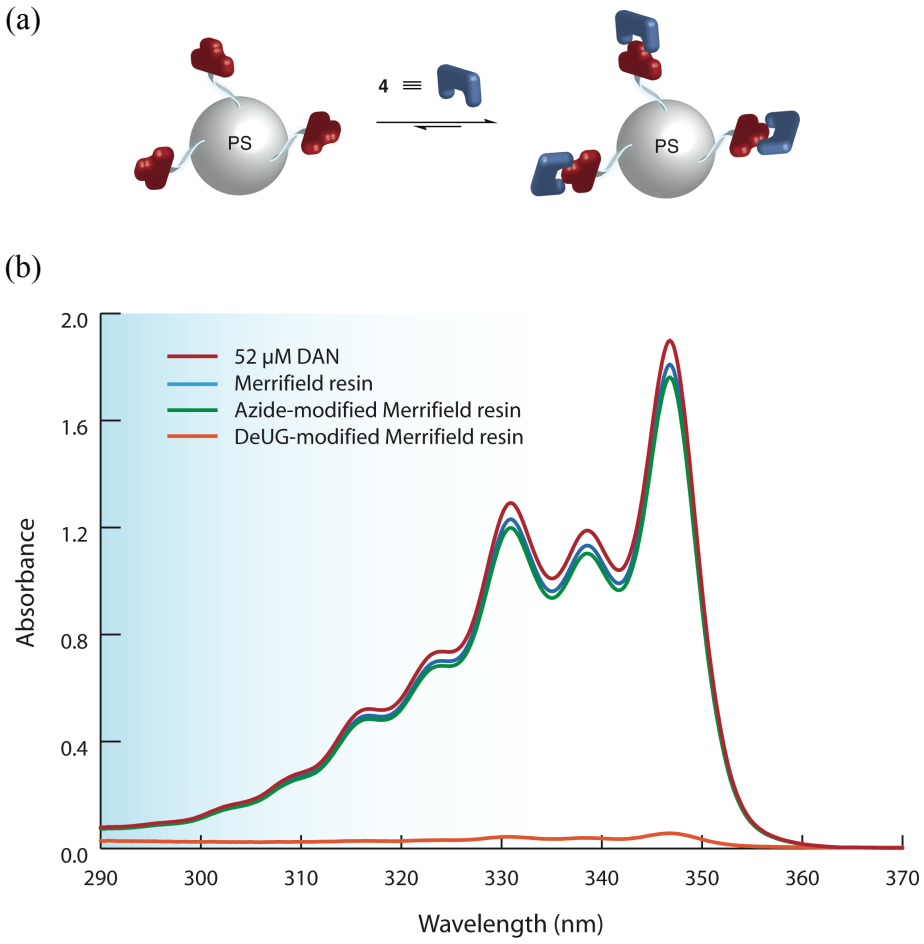

Figure 35. (a) Schematic of the self-assembly of DAN **4** on DeUG-modified Merrifield **63** and (b) UV-vis experiment in $CHCl_3$ showing extent of adsorption and self-assembly of DAN **4** on differently functionalized Merrifield resins.

As shown in Figure 35, both off-the-shelf Merrifield resin and azide-modified Merrifield resin showed minimal adsorption (< 10%) of **4** from solution. This small amount of loss of **4** can be attributed to physical entrapment in the cross-linked resin and/or experimental error. However, DeUG-modified Merrifield resin **63** showed nearly complete adsorption of DAN **4** from solution. If quantitative functionalization through the **61** → **63** synthetic modifications was achieved (which is supported by IR), **63** should contain ca. 2.25 mmol of DeUG g^{-1}. Total adsorption of **4** then corresponds to only ca. 0.6% of the recognition sites on the resin being occupied. It is reasonable to assume that complexation occurred primarily on the surface-exposed recognition units due to less than maximum swelling of the resin in chloroform.

4.2.2 Glass Slides and Silicon(111) Wafers

Our attention was next focused on the functionalization of planar silicon-based substrates such as glass, quartz and silicon. Prior to functionalization, silicon-based substrates are typically cleaned and/or activated using various chemical and physical techniques. Because of its simplicity and effectiveness, we chose to clean and activate all of our silicon-based substrates using a 30 min room temperature piranha treatment (7:3 conc. H_2SO_4/30% H_2O_2).[79] Because the surface morphology and, thus, the surface energy, of the substrate is expected to have a pronounced effect on the physical properties of the surface, readily available glass slides (Fisherbrand) were studied by atomic force microscopy (AFM).

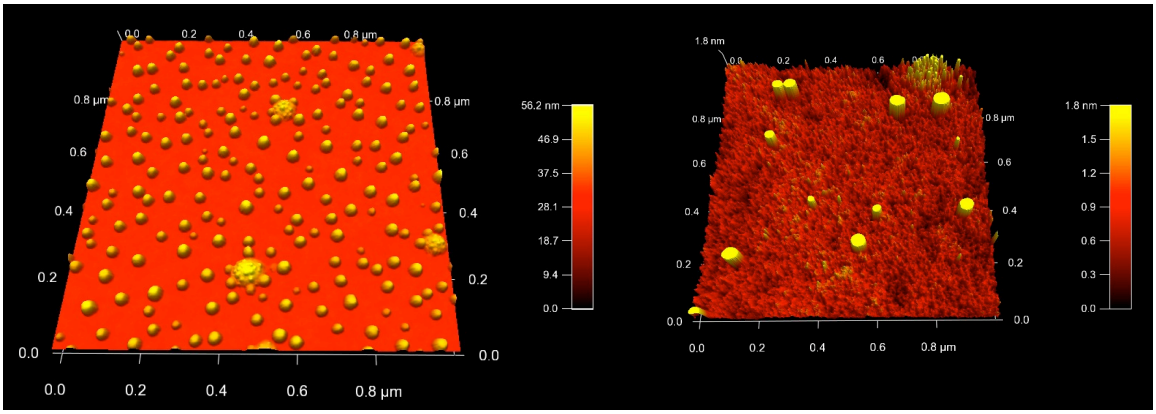

Figure 36. AFM images of piranha treated Fisherbrand glass slides showing large, anomalous surface features.

Galipeau has reported on the surface changes, namely surface roughness, induced by the most widely used surface cleaning techniques.[80] As shown in Figure 36, tapping mode AFM images of piranha treated Fisherbrand glass slides revealed large, anomalous surface features (20-50 nm). These features appeared to be rigid as evidenced by the AFM trace and retrace profiles, which were identical. Similar features were also found to be present on the untreated glass slides from all batches sampled. However, by applying a mask to these features, root mean square (RMS) roughness values of the could be determined (*vide infra*, Table 6) and were largely consistent with those reported by Galipeau. In later studies, a different brand of glass slides (Gold Seal) was used as they were found to have a much more normal surface that lacked these large, anomalous features as evidenced by AFM.

Scheme 19

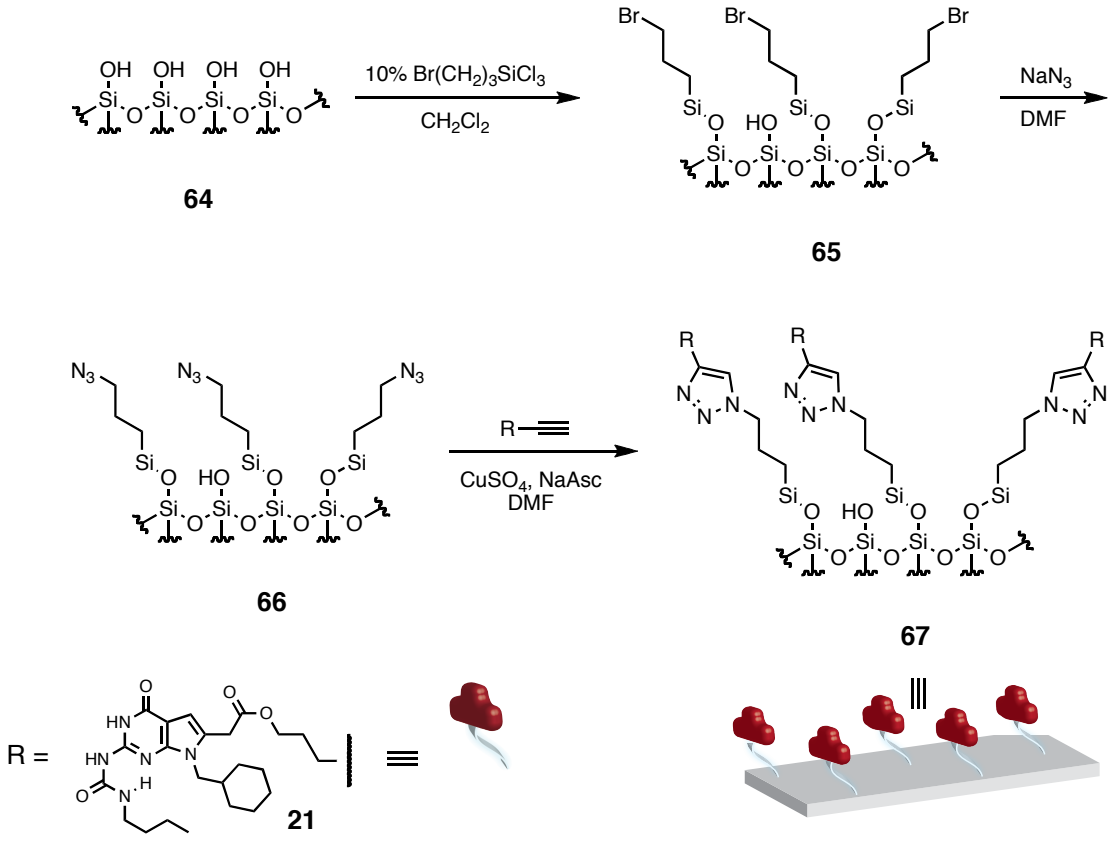

As shown in Scheme 19, glass and silicon substrates were, after piranha treatment, functionalized using a protocol similar to that reported above for silica nanoparticles and polymer resins. Covalent modifications to planar silicon-based substrates using alkylsiloxanes has been widely studied and are known to typically lead to densely packed and ordered silane monolayers.[81] Hoffman was the first to demonstrate the utility of combining this approach with the Huisgen 1,3-dipolar cycloaddition ("click" reaction) to avoid many of the synthetic pitfalls of creating siloxane functionalized reagents for direct derivatization of siliceous surfaces.[82]

Glass slides were treated with a piranha solution for 30 min. After thorough rinsing, the glass slides were then treated with 3-bromopropyltrichlorosilane to give **65**. The bromo functionalized slides were then transformed to the corresponding azide via treatment with sodium azide in DMF. The resulting azide-tailored slides **66** were were next subjected to CuAAC conditions using DeUG pentynyl ester to give DeUG-tailored slides **67**. Samples of slides at each stage of the derivatization protocol were studied by contact angle goniometry and AFM, the results of which are summarized in Table 6.

Table 6. Summary of aqueous contact angle measurements and AFM roughness values for differently functionalized glass surfaces.

Surface	Contact Angle (deg)	RMS Roughness (nm)
Untreated glass	9.0	0.25-0.42
Piranha treated glass, **64**	5.9	0.33-0.55
Propylbromide, **65**	98.9	0.98-1.2
Propylazide, **66**	41.8	1.0-1.1
Propyl DeUG, **67**	74.5	1.1-1.5

Contact angle measurements provided an initial assessment of the changes in the hydrophilicity of the differently derivatized glass slides. An small increase in hydrophilicity is seen after the piranha treatment, followed by a dramatic decrease in hydrophilicity after silanization. Introduction of the polar azido group increased the hydrophilicity, as was expected. After CuAAC modification with DeUG, the contact angle again showed a decrease in the hydrophilicity of the surface. RMS roughness values as determined by AFM showed only moderate changes to the surface roughness

after piranha treatment. However, after silanization, the RMS roughness values markedly increased (2- to 3-fold).

Secondary ion mass spectrometry (SIMS) is a powerful surface analysis technique in which a sample is exposed to a beam of primary ions, such as Ga^+, Ar^+ or various alkali metal ions. These primary ions impact the surface of a sample and liberate secondary ions (and neutral species) which are subsequently analyzed via standard MS detection techniques.[83] Time-of-flight (TOF) SIMS was employed as a means to observe the masses of molecular fragments liberated from the surfaces of differently functionalized glass and silicon substrates.

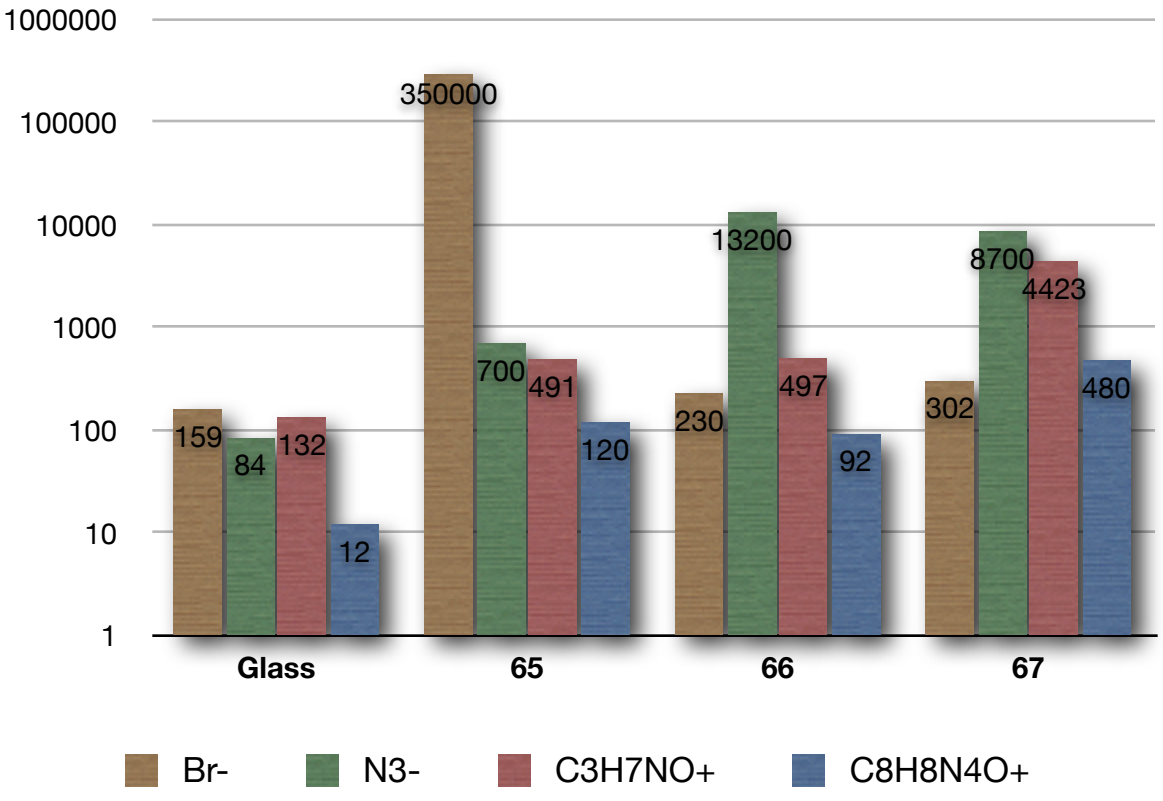

Figure 37. Ion counts for differently functionalized glass surfaces as determined by TOF-SIMS.

Diagnostic ions were monitored by TOF-SIMS at each stage of surface derivatization. Importantly, each sample came from a batch of the preceding sample. For example, the samples of DeUG-tailored glass **67** were prepared from the same batch of azide-tailored glass **66** used in the TOF-SIMS experiments. The results of the TOF-SIMS experiments are summarized in Figure 37. Propylbromide-tailored glass slides **65** showed a dramatic increase of over 3-orders of magnitude in the number of counts for a mass which corresponds to bromide ion versus that observed for unfunctionalized glass, as well as a significant increase in the amount of a small organic fragment ($C_3H_7NO^+$), consistent with successful functionalization of the surface with the alkylbromide. After treatment of **65** with sodium azide, the counts for bromide ion on **66** decrease to close to that observed for unfunctionalized glass (background levels), indicating nearly quantitative displacement of bromide ion by the azide. Moreover, a concomitant increase in the mass corresponding to the azide ion was observed from **65** to **66**, while the counts for the small organic fragment remained unchanged. After treatment of **66** with DeUG pentynyl ester under CuAAC conditions, the counts corresponding to the azide only modestly, but significantly, decreased. An increase in the small organic fragment as well as a large organic fragment ($C_8H_8N_4O^+$) were also observed. Importantly, image maps of diagnostic fragments show the surfaces to be relatively uniformly derivatized (Figure 38).

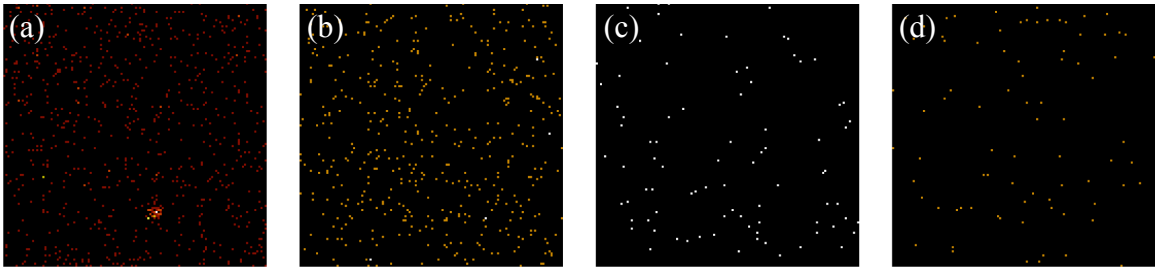

Figure 38. TOF-SIMS image maps (50 μm × 50 μm) for diagnostic fragments (a) $C_3H_7NO^+$, (b) $C_8H_8N_4O^+$, (c) $C_{15}H_{18}N_4O_2^+$ and (d) $C_{19}H_{28}N_5O_2^+$.

Probable molecular fragments of DeUG responsible for two of the larger organic fragments (> 200 amu), albeit in low total counts, observed by TOF-SIMS are shown in Figure 39. Taken together, the results strongly suggest that DeUG was successfully incorporated onto the glass surface.

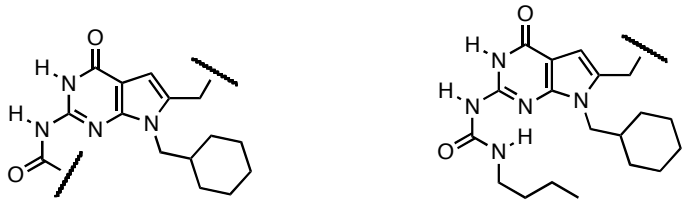

Figure 39. Some possible molecular fragments from DeUG consistent with large masses observed by TOF-SIMS.

As complementary evidence for the presence of the desired functionality at each stage of the treatment protocol, X-ray photoelectron spectroscopy (XPS) was employed, which can provide detailed chemical and electronic surface structural information.[84,85] Because glass is prone to charging under XPS conditions, Si(111) substrates were prepared under the same conditions as for the glass substrates, whose structures are

shown in Figure 40a.[86,87] Survey scans for each of the differently functionalized silicon substrates are shown in Figures 40b-d.

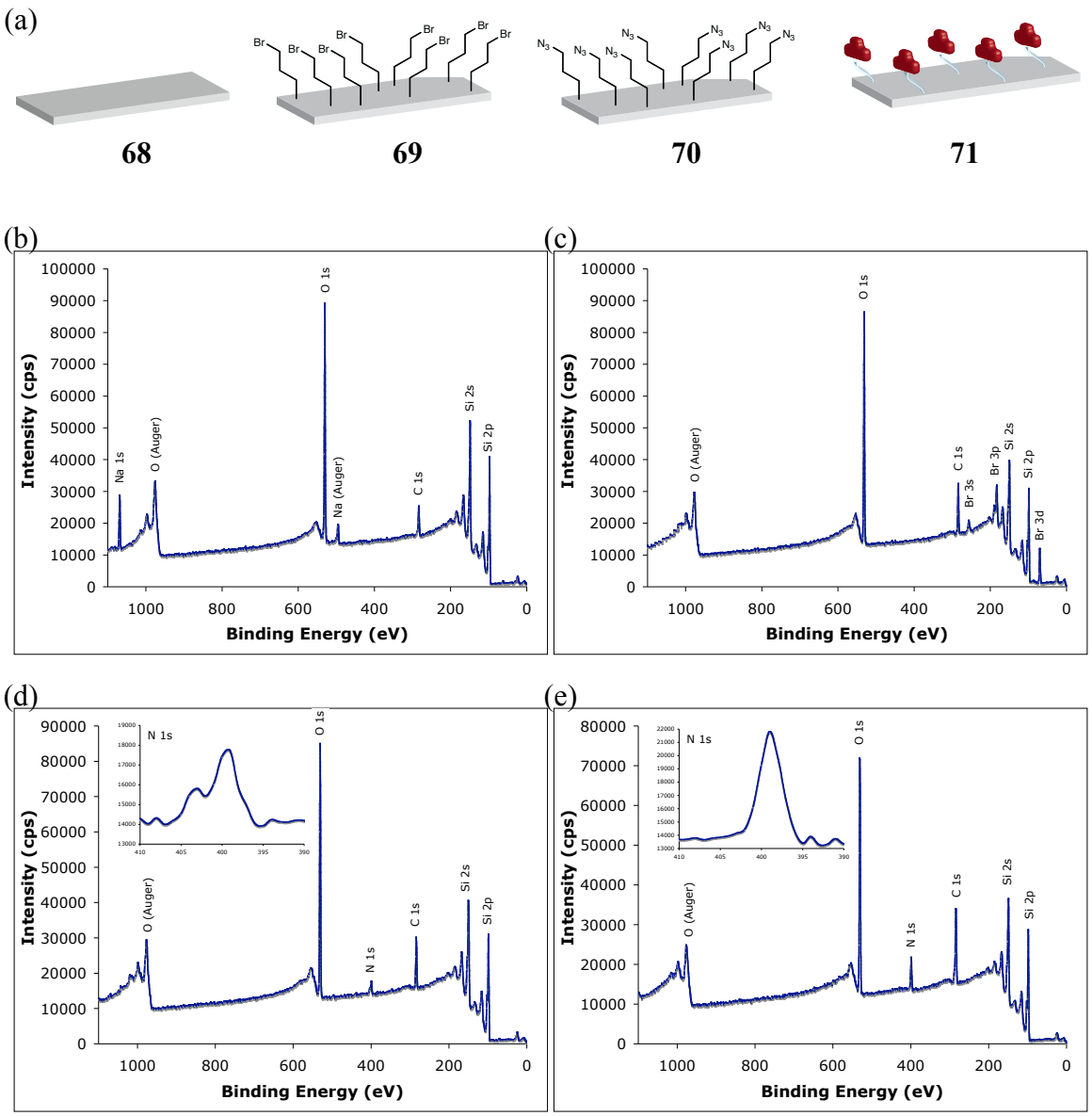

Figure 40. (a) Piranha treated Si(111) **68**, silane treated Si(111) **69**, azide treated Si(111) **70** and DeUG treated Si(111) **71**. XPS spectra for differently functionalized Si(111). (b) Piranha treated Si(111). (c) Silanization showing characteristic Br peaks. (d) Azide treatment showing characteristic 2:1 doublet peak (inset). (e) "Click" modification showing lack of doublet (inset).

Table 7. Summary of diagnostic XPS data for differently functionalized Si(111).

Diagnostic States	Binding Energy (eV)	Sample							
		68		69		70		71	
		cps	Atom %	cps	Atom %	cps	Atom %	cps	Atom %
Cu [2p]	958	0	0.00	0	0.00	0	0.00	228	0.05
O [1s]	531	25k	32.46	23k	32.22	21k	30.78	16k	29.02
N [1s]	399	96	0.22	90	0.22	1.1k	2.86	1.8k	5.72
C [1s]	284	2.5k	10.37	4.0k	17.48	4.0k	18.04	4.0k	25.39
Si [2p]	98	15k	56.92	12k	46.81	12k	48.17	7.6k	39.77
Br [3d]	70	19	0.02	2.6k	3.28	109	0.14	34	0.06

Piranha treated Si(111) (Figure 40b) clearly shows the lack of any characteristic peaks for either bromine or nitrogen. It can be seen in Figure 40c that the three characteristic peaks for bromine are present—Br [3d] at ~70 eV, Br [3p] at ~180 eV and Br [3s] at ~250 eV—indicating that the silanization was successful. Figure 40d is further evidence for near quantitative displacement of the bromide as none of the characteristic peaks were observed and a new peak at ~400 eV, consistent with N [1s], can be seen. This peak has been enlarged in the inset of Figure 40d where the characteristic 1:2 "doublet" structure is evident. This doublet, with the smaller peak at ~404 eV and the larger peak at ~400 eV, is strong evidence for the presence of a surface bound azide.[88-90] After the CuAAC modification, the N [1s] peak at ~400 eV (inset, Figure 40e) no longer shows the doublet structure characteristic of azides but appears as a broad singlet. This peak shape has been attributed to the presence of the 1,2,3-triazole after CuAAC

modification.[91] However, in our case, the presence of several structurally unique nitrogen atoms in the recognition unit is likely contributing as well. Importantly, increases in the intensities of the C [1s] and N [1s] peaks in after CuAAC modification are indicative of higher levels of carbon and nitrogen on the surface. Extremely small amounts of residual copper (Cu [2p] at ~260 eV) from the CuAAC modification can be seen in the quantitative scan (Table 7), although this peak is not apparent in the survey scan (Figure 40e).

Having successfully derivatized glass and Si(111) substrates with DeUG, we sought to demonstrate self-assembly on these surfaces using polymers bearing DeUG's complement, DAN **4**, as end groups. Although hydrogen-bonding mediated self-assembly on surfaces has been demonstrated in the past, it has not yet been achieved , or applied to materials, using such high-affinity and high-fidelity recognition units as the DeUG·DAN pair.[92,93]

Covalent modification of 4,4'-azobis(4-cyanovaleric acid) (ACVA) provides facile access to polymers with chain-end functionality. Chain-end DAN-functionalized polystyrene **73** was prepared via radical polymerization in dimethylsulfoxide (DMSO) using bisDAN modified ACVA **72** as the initiator. The bisDAN-functionalized initiator was synthesized in one step by standard EDCI coupling methods of ACVA to aminonaphthyridine **30** and proceeded in excellent yield (Scheme 20).

Scheme 20

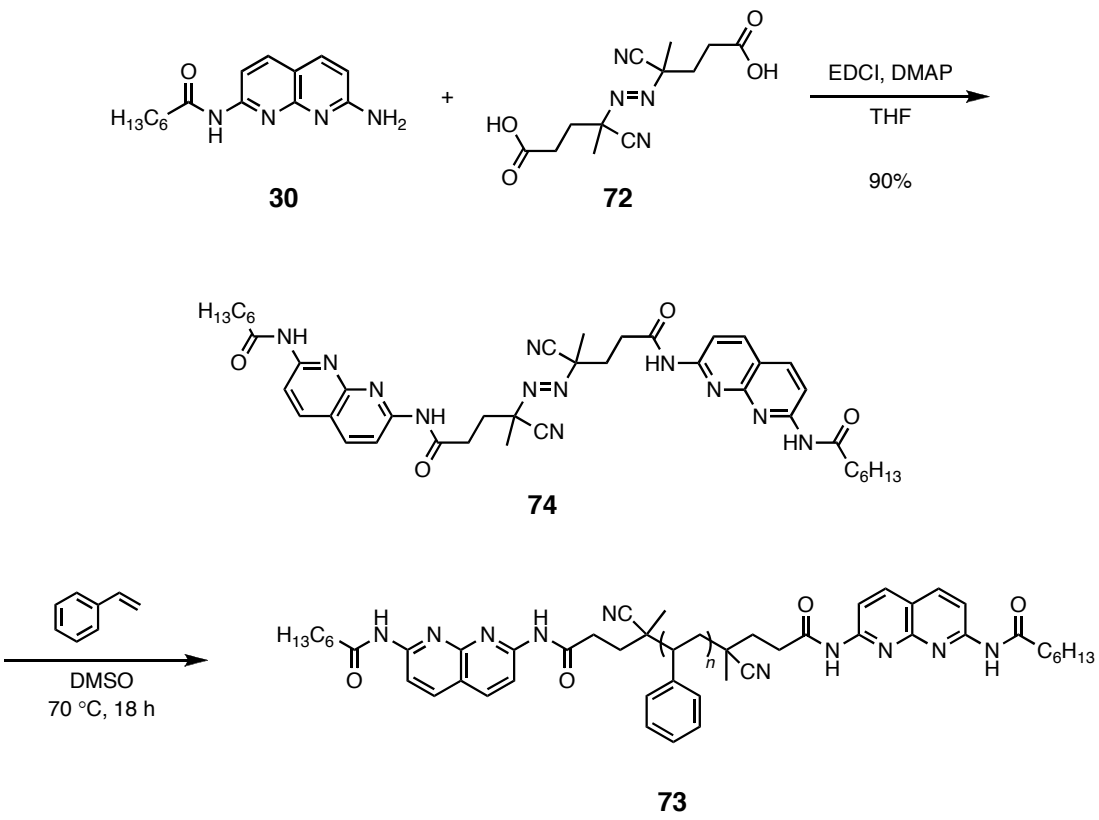

Polymer **73** was characterized by size exclusion chromatography (SEC), and UV-vis spectroscopy. The SEC determined M_w was 19.8 kDa while the M_n was 14.6 kDa, giving a polydispersity index (PDI) of 1.36. UV-vis spectroscopy was employed as an additional verification of the presence of the DAN unit. Although an absolute determination of the end group functionality was not unequivocally made, the species present were well suited to demonstrate self-assembly.

Preliminary investigations of the self-assembly of chain-end DAN functionalized polystyrene **73** on DeUG functionalized quartz and glass slides were performed. DeUG functionalized quartz slides were submersed in a 1 mg mL^{-1} solution of chain-end DAN functionalized polystyrene **73** in $CHCl_3$ for 15 min and then checked by UV-vis. The

UV-vis spectrum clearly shows the presence of the DAN unit, although in very small quantities (Figure 41). Moreover, the spectrum did not change appreciably after immersing in chloroform. However, after immersing in DMSO, the DAN-polystyrene was completely removed. Propylbromide-tailored quartz slides showed no adsorption of DAN-polystyrene, suggesting that DeUG·DAN complexation is responsible for the adsorption on the DeUG-functionalized quartz substrates.

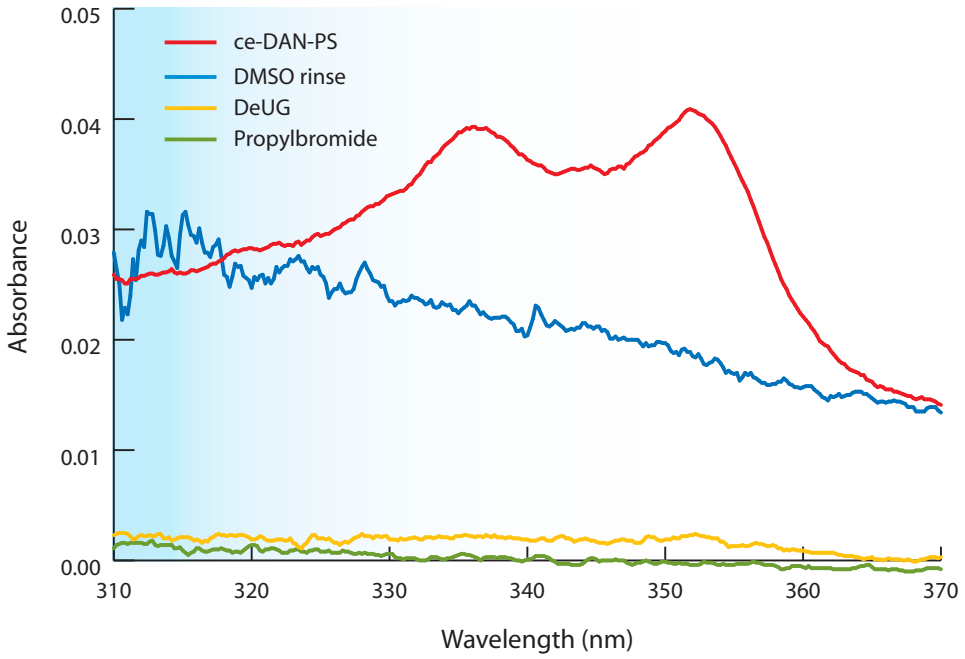

Figure 41. UV-vis experiment showing extent of adsorption and self-assembly of polymer **73** on DeUG functionalized quartz slides.

Having preliminarily demonstrated self-assembly on surfaces using the DeUG·DAN pair, we next turned our attention to developing this generalized phenomenon into a mechanism for promoting adhesion between materials of differing physical properties. This concept is vitally important in polymer composites and nanocomposites.

4.3 Supramolecular Interfacial Adhesion Promotion

For nearly two decades now, polymer nanocomposites (PNCs) have received widespread interest due to their improved thermal, mechanical and physical properties when compared to traditional fiber reinforced composite materials.[94] The term "polymer nanocomposite" has come to refer to materials that consist of a polymer, or polymer blend, and a nanoscale dispersant. From this perspective, the majority of nanocomposites reported thus far would be more accurately described as "nanoparticle-filled polymers".[95] A plethora of nanoparticle-filled polymers have been reported to date which incorporate isotropic[96] (e.g., gold) and anisotropic[97] (e.g., clay) nanoparticles. In these materials, uniform control over nanoparticle dispersion is important and remains a significant challenge to realizing maximum load transfer and reinforcement. It is largely for this reason that the mechanical properties of nanoparticle-filled polymers fall well below the theoretical maximum, except at low volume additions of the dispersant. Clearly, this points to a need to be able to precisely engineer the morphology of these materials and move from nanoparticle-filled polymers to true, tailored polymer nanocomposites. Several examples have recently appeared in the literature that attempt meet this challenge.[81] Using the layer-by-layer assembly technique pioneered by Decher,[72] Kotov and coworkers have recently shown that a polyvinyl alcohol/montmorillonite clay PNC displays mechanical properties which approach the theoretical maximum.[98]

Despite the popularity of PNCs, presently they represent only a fraction of global polymer composite production. Traditional fiber reinforced composites remain, as they have for decades, the material of choice for applications were both low weight and high

strength are required. However, polymer composites can suffer from poor adhesion between the polymer matrix, which is often non-polar, and the reinforcing material, which is often polar. As with polymer nanocomposites, polymer composites rely on a strong interaction between the matrix and the reinforcing material for load transfer and, thus, strength and durability.[99] These challenges must be overcome in order to realize novel materials based on unprecedented combinations of matrix and reinforcing agent.

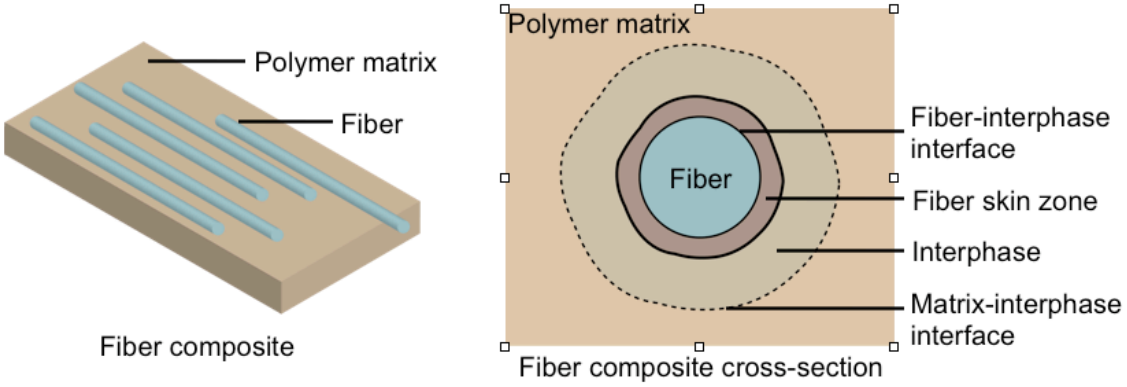

Figure 42. Schematic representations of a bulk polymer composite matrix (left), and a generalized fiber-matrix interaction (right).

As mentioned previously, in traditional fiber reinforced composites, the mechanical properties of the material depend critically upon the strength of interfacial adhesion. The zone where the matrix and, in this case, the fiber are mechanically indistinct is referred to as the interphase (Figure 42). It is the microstructure of this interphase region that is largely responsible for the material's mechanical properties.

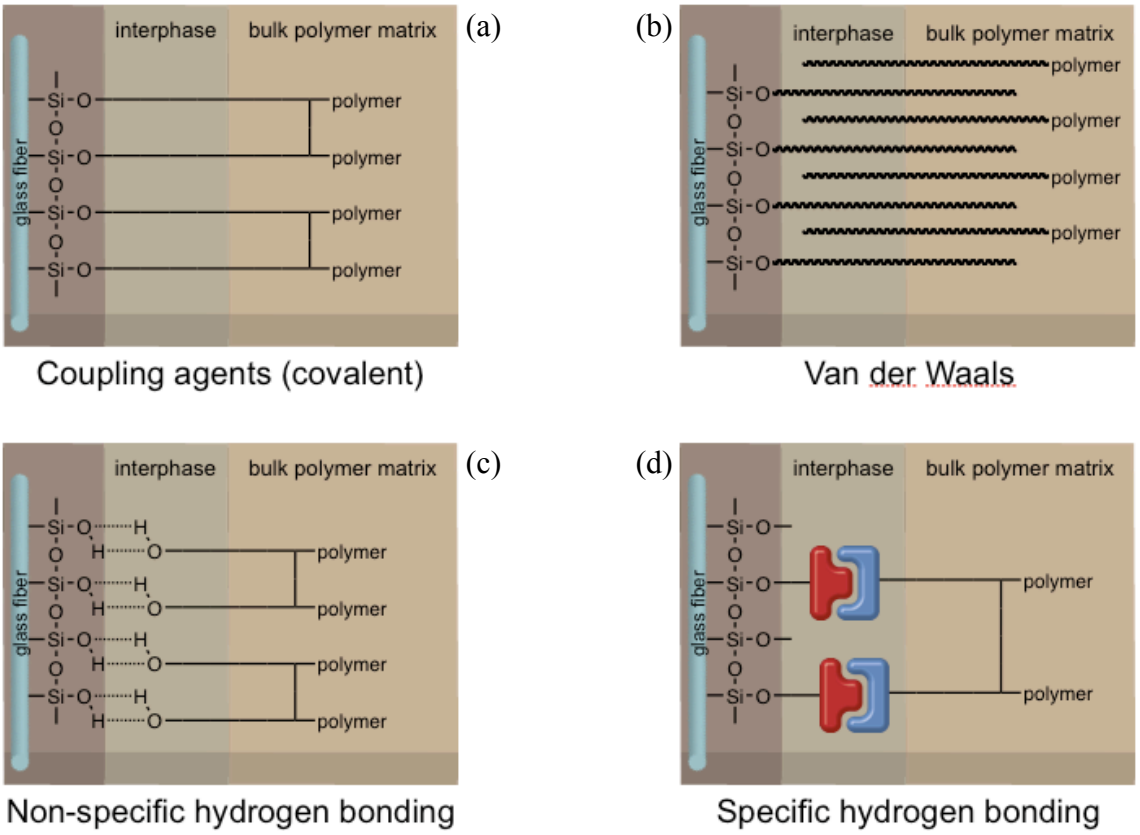

Figure 43. Schematic representations of a traditional approaches to fiber-matrix coupling: (a) covalent linkage, (b) van der Waals forces and (c) non-specific hydrogen bonding. Our proposal is to use specific hydrogen bonding units, as illustrated in (d).

Several approaches to enhancing the interfacial adhesion in fiber reinforced composites have appeared over the years.[100,101] As illustrated in Figure 43, these approaches can typically be categorized as covalent coupling of fiber to matrix (Figure 43a) and non-specific, non-covalent coupling of fiber to matrix (Figures 43b and 43c). We propose that the use of specific, non-covalent interactions may provide a novel and useful means to improve interfacial adhesion.

As an approximation to testing interfacial adhesion promotion in fiber-reinforced composites, lap-shear experiments were performed using functionalized glass substrates

as the adherend and complementarily side-chain functionalized polymer as the adhesive (Figure 44). This represents a worthwhile composite model and also allows us to test the possibility of using functional polymers as a bulk adhesive. Adhesion results from a complex set of interactions between adherend and adhesive. Many of these interactions are non-covalent and some have been engineered. The biomimetic approaches of Messersmith are particularly noteworthy.[102] Additionally, Craig and coworkers have used AFM to probe the forces of single molecule adhesion.[103] Using specific, high-affinity non-covalent interactions to improve interfacial adhesion may offer several potential advantages including self-healing.

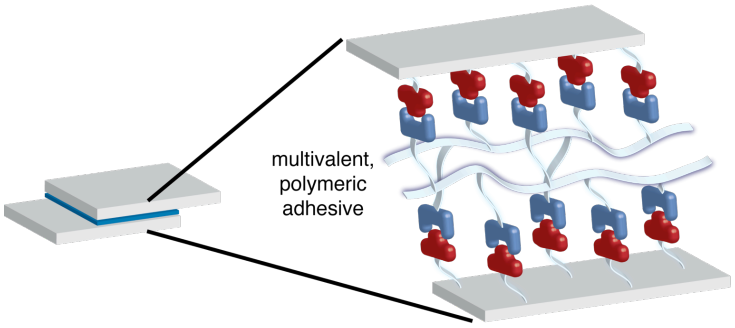

Figure 44. Schematic of supramolecular polymer adhesive concept.

4.3.1 Lap Shear Measurements

Initial lap-shear experiments were performed using DeUG-derivatized glass slides with DAN-functionalized polystyrene (DAN-PS) as the adhesive on a 220 N load cell. In a typical experiment, 10 μL of a 10 mg mL^{-1} solution of the indicated polymer in dichloromethane was placed on the appropriately functionalized glass slide, followed by

immediately placing another slide on top of this to create a 15 mm × 25 mm (375 mm^2) lap joint. The joints were then clamped in place and cured under dry nitrogen at ambient temperature for ca. 24 hours.

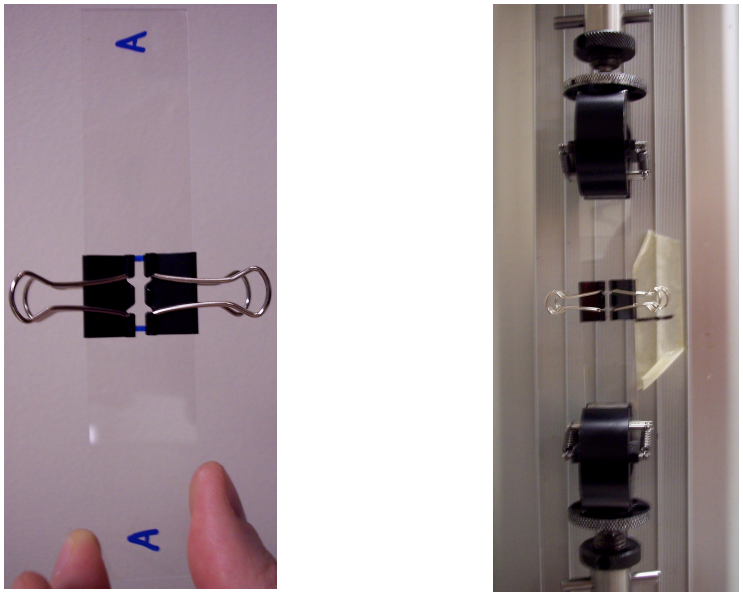

Figure 45. Freshly prepared lap-shear sample (left) and sample mounted on 220 N load cell (right).

DAN-functionalized polystyrenes were prepared via post-polymerization functionalization by Cyrus Anderson via the method of Bae.[104,105] The polymers used in lap-shear experiments are summarized in Figure 46, below.

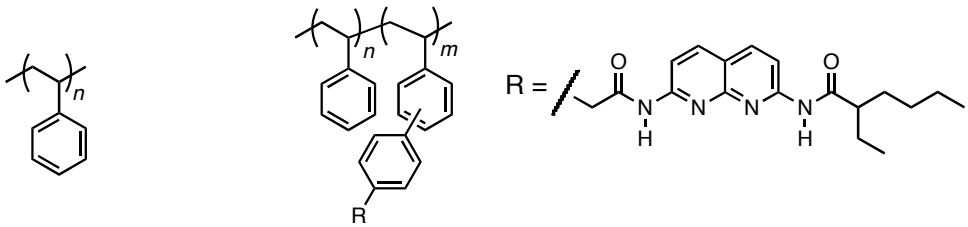

75
75k M_n Polystyrene (PS)

76: 11k M_n, 11 mol % DAN-PS
77: 235k M_n, 10 mol % DAN-PS

Figure 46. Polymers used as adhesives in lap-shear tests.

Lap-shear experiments were performed under ambient conditions under displacement control (1 mm min^{-1}) and the load versus displacement was recorded. In all experiments, the maximum load sustained (N) was used in calculating the shear strength (MPa). Using 11k M_n, 11 mol % DAN-PS **76**, the majority of lap-shear samples sustained the maximum load (220 N) and failed once they were removed from the load cell, indicating that the average shear strength is likely just over 0.60 MPa (Figure 47). Those samples that failed prematurely were inadvertently stressed upon mounting on the load cell.

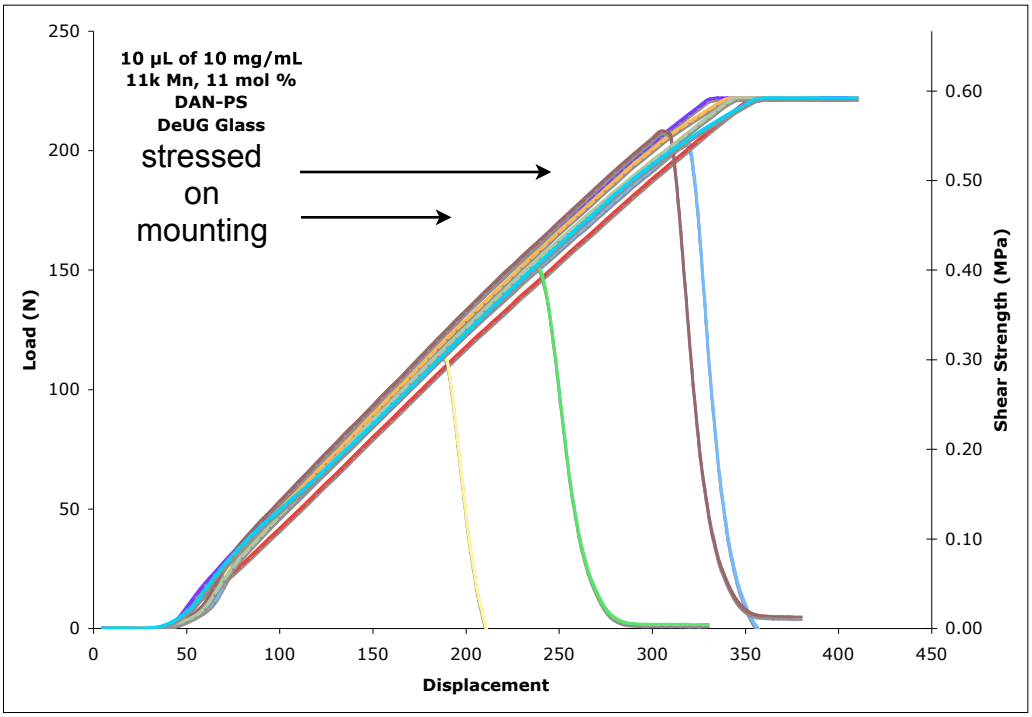

Figure 47. Load vs. displacement curves for 11k M_n, 11 mol % DAN-PS **76** on DeUG derivatized glass slides **67**.

Visual inspection of the failed samples suggested that the mode of failure was both adhesive and cohesive (Figure 48). In order to more accurately determine the shear strength, we switched to using a 500 N load cell.

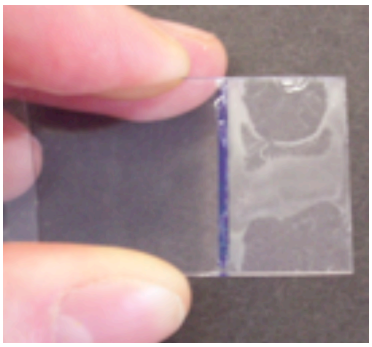

Figure 48. Failed lap-shear sample.

Pairwise samples using unfunctionalized polystyrene **75** and DAN-PS **77** as the adhesives, and unfunctionalized glass slides and DeUG-functionalized glass slides **67** as the adherends were prepared as previously described. The maximum load sustained was then measured, also as previously described. The results are summarized below in Figure 49.

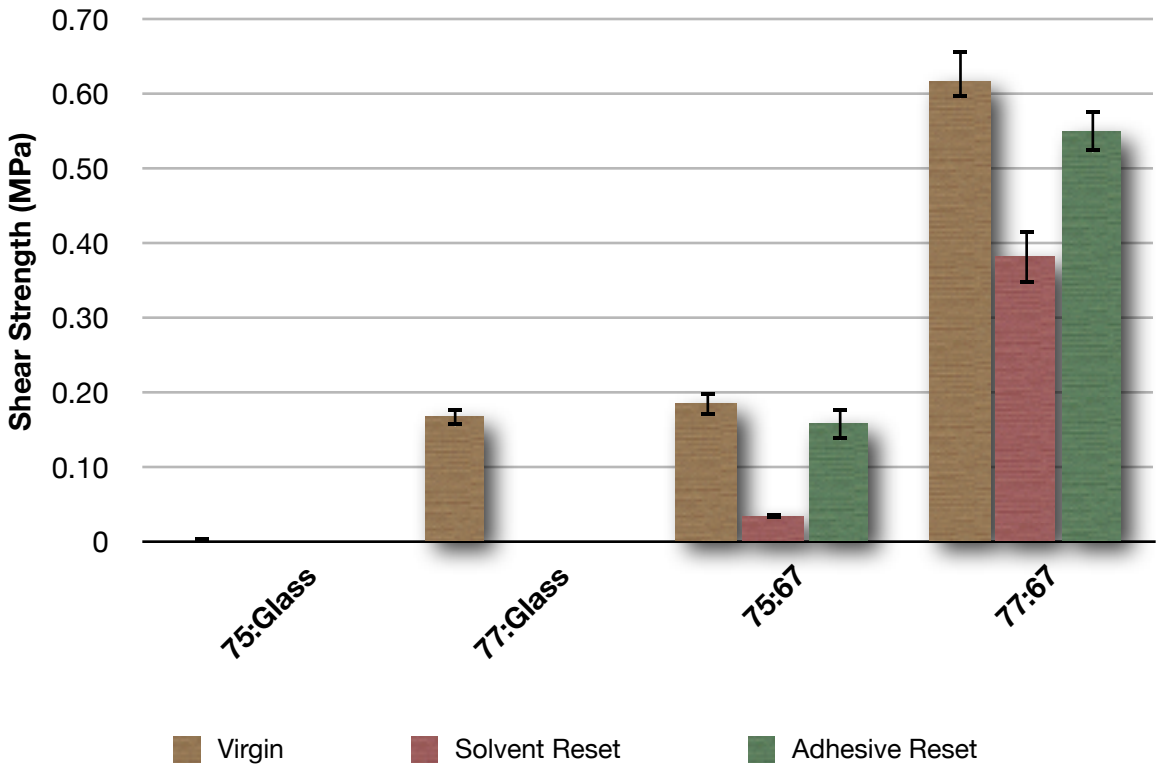

Figure 49. Shear strengths of pairwise combinations of glass, **67**, **75** and **77**. (adhesive:adherend). Error bars represent the standard error of the mean.

Virgin samples of homopolymer **75** on unfunctionalized glass actually failed under their own weight. From this observation, an upper limit for the shear strength was estimated to be 3.3×10^{-4} MPa. Virgin samples of both **77** on unfunctionalized glass and homopolymer **75** on DeUG functionalized glass **67** showed modest and comparable enhancements to the shear strength versus that of homopolymer **75** on unfunctionalized glass (0.17 and 0.18 MPa, respectively). This suggests that the presence of a recognition unit in either the adhesive or on the adherend increases non-specific interactions and, thus, adhesion. Virgin samples of DAN-PS **77** on DeUG functionalized glass **67** showed a significant increase in mean shear strength (0.63 MPa), a greater than 3-fold enhancement over **77:Glass** and **75:67**.

As previously noted, we are very interested in the possibility of self-healing in adhesives such as these. Failed samples of **75:67** and **77:67** were "reset" by applying 10 μL of methylene chloride to the lap joint area. The samples were cured as before and subjected to a second round of lap-shear testing. For the **75:67** sample (homopolymer on DeUG functionalized glass) reset with solvent, the mean shear strength was determined to be 0.034 MPa, or approximately 19% of the virgin material. In the case of the **77:67** sample (DAN-PS on DeUG functionalized glass) reset with solvent, the mean shear strength was determined to be 0.38 MPa, or approximately 61% of the virgin material.

As a further demonstration of the self-healing ability of the system, failed samples **75:67** and **77:67** were also "reset" by removing the residual adhesive from the substrate and applying 10 μL of a fresh 10 mg mL^{-1} polymer solution to the lap joint area. Again, the samples were cured as before and subjected to a second round of lap-shear testing.

For the sample of homopolymer **75** on DeUG functionalized glass **67**, the mean shear strength was determined to be 0.16 MPa, or approximately 85% of the strength of the virgin material. In the case of DAN-PS **77** on **67**, the mean shear strength was determined to be 0.55 MPa, or approximately 88% of the strength of the virgin material.

Although the enhancement to shear strength observed for the **77:67** combination versus the controls is only modest (ca. 3-fold), it is significant and was reproducible. It is worthwhile to compare the observed shear strengths with more common materials and their strengths. For example, approximately 1.38×10^{-22} kcal of energy is required to break a carbon-carbon single bond. The energy required to break the lap joints in the **77:67** combination is approximately 5.03×10^{-8} kcal—roughly the equivalent of 1 nmol of carbon-carbon single bonds or 10 nmol of DeUG·DAN interactions existing between the adherends. The significance of this magnitude of strength is more apparent when it is quantified against the amount of adhesive per unit area, which only 2.6 μg cm^{-2}. For comparison, the shear strengths of some common commercial adhesives are shown in Table 8, below.[106]

Table 8. Comparison of the shear strengths of some common adhesives.

Adhesive	Adherend	Shear Strength (MPa)
77	**67**	0.63
poly(vinyl alcohol)	bare glass	1.4
cyanoacrylate	bare glass	6.9
epoxy resin	bare glass	10.3

4.4 Conclusion

To summarize, we have successfully derivatized several types of surfaces with DeUG and demonstrated self-assembly of DAN and DAN-functionalized polymers on these surfaces. Key findings were that the DeUG·DAN pair are well suited for self-assembly on surfaces and that the extent of surface passivation and the type of surface have a pronounced effect on non-specific adsorption. These surfaces were demonstrated to have covalent incorporation of DeUG by several complementary surface analysis techniques such as SIMS and XPS.

Additionally, we were able to demonstrate the utility of the DeUG·DAN pair as adhesion promotors at interfaces between dissimilar materials via lap-shear experiments. It is anticipated that the model studies described herein will serve as the groundwork for investigations of adhesion promotion and self-healing in polymer composites and nanocomposites. A key finding was that the majority of the adhesion promotion (~60-90%) could be recovered by various resetting ("healing") methods. Although the exact magnitude of the contribution of the molecular recognition units to the shear strength enhancement in unclear, the data strongly suggests that it does play a significant role.

Chapter 5

Experimental for Parts I and II

5.1 Computational Methods

All molecular modeling (*ab initio* and semi-empirical) was performed using Spartan '04 or Spartan '06. In semi-empirical calculations, initial ground-state equilibrium geometries were determined via MMFF followed by optimization using the indicated method (AM1, PM3 or RM1). In *ab initio* calculations, initial ground-state equilibrium geometries were determined via MMFF followed by B3LYP/6-31G(d). Single-point energies were then determined using the B3LYP/6-311+G(d,p) basis set.

5.2 General Methods

2-Amino-4,6-dihydroxypyrimidine was purchased from AK Science and used as received. 1-(3-Dimethylaminopropyl)-3-ethylcarbodiimide hydrochloride (EDCI) was purchased from Advanced ChemTech and used as received. 4-(Dimethylamino)pyridinium 4-toluenesulfonate (DPTS),[29] styrene sebasic acid and DAN polystyrene **49**[107] were prepared as described in the literature. All other chemicals were purchased from Sigma-Aldrich and used without further purification unless otherwise indicated. Solvents were of reagent grade and used without further purification except as follows: *N,N*-dimethylformamide (DMF) was vacuum distilled from 4Å molecular sieves just prior to use. Tetrahydrofuran (THF) was distilled from sodium benzophenone ketyl just prior to use. Triethylamine (TEA) was distilled from calcium hydride (CaH_2) and stored over sodium hydroxide pellets. Methylene chloride (CH_2Cl_2) was washed with conc. sulfuric

acid (H_2SO_4), 5% sodium bicarbonate ($NaHCO_3$) and water before being distilled from CaH_2. Chloroform ($CHCl_3$) was passed over activated alumina before being distilled from CaH_2. Pyridine was distilled from CaH_2 just prior to use. All reactions were performed under a dry nitrogen atmosphere unless otherwise indicated. Reported reaction temperatures refer to the temperature of the heating medium.

Analytical thin-layer chromatography (TLC) was performed using 0.2 mm silica 60 coated, plastic plates with F254 indicator purchased from EM Science. Flash chromatography was performed in quartz columns using Ultra Pure SiliaFlash® P60 230-400 mesh (40-63 μm) silica gel (SiO_2) with fluorescence indicator green 254 nm (Fluka) following the general procedure reported by Still and coworkers.[108]

^{1}H NMR spectra were acquired using either a Varian Unity 400 MHz (^{13}C, 101 MHz) or Varian Unity 500 MHz (^{13}C, 126 MHz) spectrometer. ^{1}H NMR chemical shifts (δ) are reported in parts per million (ppm) and were referenced to the residual protio solvent peak at 7.26 ppm for $CDCl_3$ and 2.50 ppm for DMSO-d_6. ^{1}H NMR coupling constants (J) are reported in hertz (Hz). ^{13}C NMR chemical shifts are reported in ppm and were referenced to the solvent peak at 77.16 ppm for $CDCl_3$ and 39.52 ppm for DMSO-d_6. All NMR spectra were processed using iNMR. Mass spectra were obtained on Micromass Q-Tof Ultima (HR-ESI) and Micromass Quattro (LR-ESI) instruments. IR spectra were obtained on a Mattson-Galaxy FT spectrometer with major bands reported in cm^{-1}. Melting points were determined using a Thomas-Hoover melting point apparatus and are uncorrected. Elemental analyses were performed at the University of Illinois, School of Chemical Sciences Microanalytical Laboratory.

5.3 Synthetic Procedures

5.3.1 Synthetic Procedures for Part I

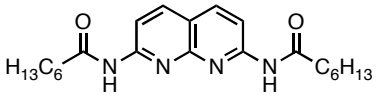

Heptanoic acid (7-heptanoylamino-[1,8]naphthyridin-2-yl)-amide (4). To a solution of 3.20 g (15.79 mmol) of 2,7-diamino-1,8-naphthyridine (**23**) in 100 mL of pyridine at 100 °C was added 9.80 mL (63.10 mmol) of heptanoyl chloride. The solution was allowed to stir for 2 d. The contents were allowed to cool to room temperature before concentrating *in vacuo*. The residue was dissolved in 100 mL of chloroform, washed with 3 × 100 mL portions of water, 1 × 50 mL of saturated sodium bicarbonate solution, dried over magnesium sulfate, gravity filtered and concentrated *in vacuo*. The residue was triturated with 30 mL of *n*-hexane and vacuum filtered. The product was purified via column chromatography using 9:1 (v/v) $CHCl_3$/MeOH as the eluent (R_f = 0.66) to afford 4.57 g (72%) of **4** as an off-white powder: mp 195-196 °C; ^{1}H NMR ($CDCl_3$) δ 8.61 (br s, 2H), 8.44 (d, J = 8.8, 2H), 8.11 (d, J = 8.8, 2H), 2.44 (t, J = 7.3, 4H), 1.71 (m, 4H), 1.31 (m, 12H), 0.86 (t, J = 6.8, 6H); ^{13}C NMR ($CDCl_3$) δ 172.62, 154.09, 153.76, 139.16, 118.42, 113.60, 38.09, 31.62, 28.95, 25.34, 22.60, 14.16; ESI-HRMS calcd for $(C_{22}H_{32}N_4O_2{\cdot}H)^+$ 385.2604, found 385.2618; UV ($CHCl_3$) λ_{max}, nm (ε): 330.5 (24900), 338.5 (22990), 346.5 (34660).

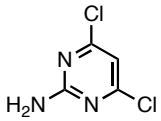

2-Amino-4,6-dichloropyrimidine (9). A vigorously stirred suspension of 103 g (810 mmol) of **12** in 240 mL (2.57 mol) of $POCl_3$ was heated to 60 °C and 220 mL (1.74 mol) of *N,N*-dimethylaniline was added at a rate of 4 drops per min. The suspension was stirred for one hour, allowed to cool to rt and placed in an ice bath. Excess $POCl_3$ was quenched by the careful addition of 750 mL of H_2O over ca. 3 h, being sure not to allow the internal temperature to exceed 60 °C. The resultant yellow powder was collected via vacuum filtration and washed with 1.5 L of H_2O to afford 121 g (91%) of **9**, which was judged to be sufficiently pure by ^{1}H NMR and carried on to the next step without further purification: mp 221-223 °C (lit. 219-222 °C); ^{1}H NMR (500 MHz, DMSO-d_6) δ 7.61 (br s, 2H), 6.87 (s, 1H); ^{13}C NMR (126 MHz, DMSO-d_6) δ 162.9, 161.0, 107.6; ESI-LRMS calcd for $(C_4H_3Cl_2N_3 \cdot H)^+$ 164.0, found 163.9. All characterization data were fully consistent with literature values.[24]

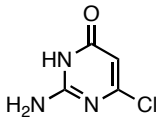

2-Amino-6-chloro-3*H*-pyrimidin-4-one (13). A suspension of 50.0 g (305 mmol) of **9** in 750 mL of 1 M NaOH was heated to reflux. After 2 h, the solution became homogeneous, was allowed to cool to rt and adjusted to pH 4 via addition of glacial acetic acid. The resultant thick, white precipitate was collected via vacuum filtration, washed with 1 L of H_2O on the filter paper and dried *in vacuo* to afford 42.2 g (95%) of **13**, which was judged to be sufficiently pure by ^{1}H NMR and was carried on to the next step without further purification: mp 254-255 °C dec (lit. 252 °C dec); ^{1}H NMR (500 MHz, DMSO-d_6) δ 11.14 (br s, 1H), 6.99 (br s, 2H), 5.59 (s, 1H); ^{13}C NMR (126 MHz, DMSO-d_6) δ 162.3, 159.5, 155.5, 99.4; ESI-LRMS calcd for $(C_4H_4ClN_3O{\cdot}H)^+$ 146.0, found 146.0. All characterization data were fully consistent with literature values.[24]

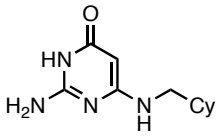

2-Amino-6-(cyclohexanemethylamino)-3*H*-pyrimidin-4-one (14a). To a suspension of 20.0 g (137 mmol) of **13** in 250 mL of *n*-butanol was added 38.0 mL (273 mmol) of TEA and 25.0 g (221 mmol) of cyclohexanemethylamine. The suspension was heated to 145 °C for 18 h (solution became homogeneous after ca. 2 h), cooled to room temperature and washed with 3 × 200 mL portions of water. The aqueous layers were combined and back-extracted with 2 × 50 mL portions of *n*-butanol. The organic layers were combined, dried over magnesium sulfate, gravity filtered and concentrated *in vacuo*. The resultant pale yellow solid was triturated with 150 mL of *n*-pentane and vacuum filtered to afford 29.6 g (97%) of **14a** as an off-white powder, which was judged to be sufficiently pure by ^{1}H NMR and carried on to the next step without further purification: mp 222-224 °C (lit. 227-228 °C); ^{1}H NMR (500 MHz, DMSO-d_6) δ 9.61 (br s, 1H), 6.36 (br s, 1H), 6.09 (br s, 2H), 4.39 (s, 1H), 2.85 (br s, 2H), 1.67 (m, 4H), 1.61 (m, 1H), 1.44 (m, 1H), 1.14 (m, 3H), 0.85 (m, 2H); ^{13}C NMR (126 MHz, DMSO-d_6) δ 164.5, 163.0, 154.9, 74.5, 47.3, 37.2, 30.6, 26.2, 25.5; ESI-HRMS calcd for $(C_{11}H_{18}N_4O{\cdot}H)^+$ 223.1559, found 223.1570.

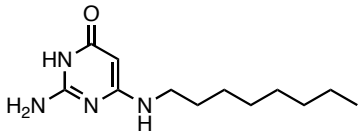

2-Amino-6-(octylamino)-3*H*-pyrimidin-4-one (14b). To a suspension of 202 mg (1.39 mmol) of 2-amino-6-chloro-3*H*-pyrimidin-4-one **13** in 15 mL of *n*-butanol was added 1.0 mL (7.17 mmol) of TEA and 1.15 mL (6.87 mmol) of octylamine. The suspension was heated to 145 °C for 18 h (solution became homogeneous after ~2 h), cooled to room temperature and washed with 2 × 15 mL portions of water. The aqueous layers were combined and back-extracted with 2 × 10 mL portions of *n*-butanol. The organic layers were combined, dried over magnesium sulfate, gravity filtered and concentrated *in vacuo*. The resultant pale yellow solid was triturated with 10 mL of *n*-pentane and vacuum filtered to afford 281 mg (86%) of **14b** as a white solid which was judged to be > 95% pure by ^{1}H NMR and carried on to the next step without further purification: ^{1}H NMR (DMSO-d_6) δ 9.70 (br s, 1H, NH), 6.38 (br s, 2H, NH_2), 6.33 (br s, 1H, NH), 4.37 (s, 1H, CH), 2.98 (br s, 2H, CH_2), 1.43 (m, 2H, CH_2), 1.24 (m, 10H, CH_2), 0.85 (t, J = 7.2, 3H, CH_3); MS (ESI) m/z 239.2 ($[M+H]^+$, 100).

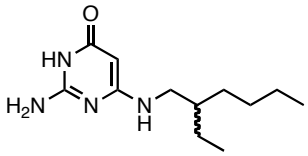

(±)-2-Amino-6-(2-ethylhexylamino)-3*H*-pyrimidin-4-one (14c). To a suspension of 0.506 g (3.48 mmol) of 2-amino-6-chloro-3*H*-pyrimidin-4-one (**13**) in 15 mL of *n*-butanol was added 0.70 mL (5.02 mmol) of TEA and 0.75 mL (4.47 mmol) of (±)-2-ethylhexylamine. The suspension was heated to 145 °C for 18 h (solution became homogeneous after ~2 h), cooled to room temperature and washed with 2 × 15 mL portions of water. The aqueous layers were combined and back-extracted with 2 × 15 mL portions of *n*-butanol. The organic layers were combined, dried over magnesium sulfate, gravity filtered and concentrated *in vacuo*. The resultant pale yellow solid was triturated with 10 mL of *n*-pentane and vacuum filtered to afford 0.697 g (85%) of **14c** as an off-white solid which was judged to be > 95% pure by ^{1}H NMR and carried on to the next step without further purification: mp 210-211 °C; ^{1}H NMR (DMSO-d_6) δ 9.67 (br s, 1H, NH), 6.32 (br s, 1H, NH), 6.09 (br s, 2H, NH_2), 4.41 (s, 1H, CH), 2.92 (br s, 2H, CH_2), 1.33 (m, 9H, CH, CH_2), 0.86 (t, J = 7.3, 3H, CH_3), 0.83 (t, J = 7.4, 3H, CH_3); MS (ESI) m/z 239.2 ($[M+H]^+$, 100).

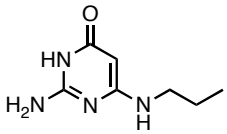

2-Amino-6-(propylamino)-3*H*-pyrimidin-4-one (14d). To 40.0 g (275 mmol) of chloropyrimidinone **13** in a 1 L flask was added 500 mL of *n*-butanol and 225 mL (2.74 mol) of *n*-propylamine. The contents were heated to reflux with stirring. After 18 h, the contents were allowed to cool to room temperature and was concentrated *in vacuo*. The residue was dispersed in 500 mL of chloroform and washed with 3 × 250 mL of water. The aqueous layers were combined and back extracted with 6 × 100 mL of chloroform. the organic layers were combined, dried over magnesium sulfate, gravity filtered and concentrated *in vacuo*. The resultant pale yellow solid was triturated with 300 mL of *n*-pentane and vacuum filtered to afford 39.3 g (85%) of **14d** as an off-white solid which was judged to be > 95% pure by ^{1}H NMR and carried on to the next step without further purification: mp 250-251 °C; ^{1}H NMR (DMSO-d_6) δ 9.67 (br s, 1H, NH), 6.32 (br s, 1H, NH), 6.09 (br s, 2H, NH_2), 4.41 (s, 1H, CH), 2.97 (s, 2H, CH_2), 1.43 (m, 2H, CH_2), 0.85 (t, J = 7.3, 3H, CH_3); ^{13}C NMR (DMSO-d_6) δ 164.5, 163.1, 155.0, 74.9, 42.9, 22.5, 11.8; ESI-HRMS calcd for $(C_7H_{12}N_4O{\cdot}H)^+$ 169.1089, found 169.1095.

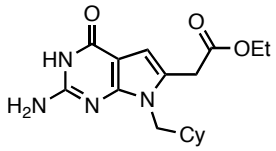

(2-Amino-7-cyclohexylmethyl-4-oxo-4,7-dihydro-3H-pyrrolo[2,3-d]pyrimidin-6-yl)-acetic acid ethyl ester (15). To a stirred suspension of 27.9 g (126 mmol) of **14a** in 500 mL of 4:1 DMF/H_2O was added 12.4 g (151 mmol) of sodium acetate. The pale yellow solution was stirred for 10 min and 35 mL of ethyl 4-chloroacetoacetate was added via syringe pump at a rate of ca. 0.34 mL/min. The solution took on a deep red color through the addition and settled to a pale orange color ca. 6 hr after addition was complete. The contents were allowed to stir for 5 d and were poured into 1 L of water. Vacuum filtration afforded an orange solid, which was dispersed in 1:1 acetone/water and heated to 60 C for 2 h. Vacuum filtration and drying under high vacuum afforded 27.1 g (65%) of **15** as a pale yellow powder: mp 241-243 °C; ^{1}H NMR (500 MHz, DMSO-d_6): δ 10.24 (br s, 1H), 6.16 (br s, 2H), 6.11 (s, 1H), 4.09 (q, J = 7.1, 2H), 3.71 (d, J = 7.7, 2H), 3.69 (s, 2H), 1.69 (m, 1H), 1.64 (m, 2H), 1.59 (m, 1H), 1.42 (m, 2H), 1.19 (t, J = 7.1, 3H), 1.09 (s, 3H), 0.92 (m, 2H); ^{13}C NMR (126 MHz; DMSO-d_6): δ 170.1, 158.3, 152.0, 151.1, 124.8, 101.3, 99.1, 60.5, 47.3, 37.8, 32.3, 30.1, 26.0, 25.3, 14.1; ESI-HRMS calcd for $(C_{17}H_{24}N_4O_3{\cdot}H)^+$ 333.1927, found 333.1923. Anal. calcd for $C_{17}H_{24}N_4O_3$: C, 61.43; H, 7.28; N, 16.86. Found: C, 61.36; H, 7.43; N, 16.55.

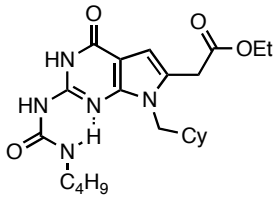

[2-(3-Butylureido)-7-cyclohexanemethyl-4-oxo-4,7-dihydro-3H-pyrrolo[2,3-d]pyrimidin-6-yl]-acetic acid ethyl ester (DeUG ethyl ester, 17). To a solution of 24.0 g (72.2 mmol) of **15** in 250 mL of pyridine was added 25 mL (224 mmol) of *n*-butyl isocyanate via syringe. The solution was heated to 140 °C for 16 h, cooled to rt and concentrated *in vacuo*. The residue was triturated under ultrasonication with 100 mL of a 1:1 (v/v) solution of petroleum ether/acetone. Vacuum filtration afforded 20.3 g (65%) of **17** as a buff-colored powder: mp 188-190 °C; ^{1}H NMR (500 MHz, $CDCl_3$) δ 11.25 (br s, 1H), 9.43 (br s, 1H), 9.02 (br s, 1H), 6.87 (s, 1H), 4.18 (q, J = 7.1, 2H), 3.84 (d, J = 7.6, 2H), 3.73 (s, 2H), 3.47 (dt, J = 5.8, J = 7.1, 2H), 1.68 (m, 6H), 1.58 (m, 2H), 1.47 (m, 2H), 1.27 (t, J = 7.1, 3H), 1.16 (m, 3H), 0.97 (t, J = 7.4, 3H), 0.95 (m, 2H); ^{13}C NMR (126 MHz, $CDCl_3$) δ 170.1, 159.4, 154.2, 148.7, 146.4, 127.6, 103.5, 102.5, 61.5, 49.3, 40.2, 39.0, 33.4, 32.2, 31.2, 26.4, 25.9, 20.5, 14.3, 14.0; ESI-HRMS calcd for $(C_{22}H_{33}N_5O_4 \cdot H)^+$ 432.2611, found 432.2613.

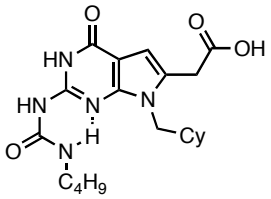

[2-(3-Butylureido)-7-cyclohexanemethyl-4-oxo-4,7-dihydro-3H-pyrrolo[2,3-d]pyrimidin-6-yl]-acetic acid (DeUG acetic acid, 18). A suspension of 12.0 g (27.8 mmol) of **17** in 300 mL of a 1:1 (v/v) mixture of 10% aqueous LiOH/ethanol was stirred at room temperature for 30 min. The homogeneous solution was washed with 3 × 100 mL portions of chloroform. The organic layer was discarded and the aqueous layer was neutralized and the product precipitated via the dropwise addition of 5% aqueous HCl. Vacuum filtration, water rinse on the filter paper and recrystallization from ethanol afforded 10.9 g (98%) of **18** as an off-white powder: mp 177-179 °C; ^{1}H NMR (500 MHz, DMSO-d_6) δ 12.12 (br s, 1H), 11.34 (br s, 1H), 9.49 (br s, 1H), 7.25 (br s, 1H), 6.26 (s, 1H), 3.80 (d, J = 7.8, 2H), 3.68 (s, 2H), 3.17 (dt, J = 5.9, J = 6.8, 2H), 1.73 (m, 1H), 1.63 (m, 3H), 1.45 (m, 4H), 1.32 (m, 2H), 1.11 (m, 3H), 0.94 (m, 2H), 0.90 (t, J = 7.3, 3H, CH3); ^{13}C NMR (126 MHz, DMSO-d_6) δ 171.5, 156.8, 154.6, 148.2, 146.7, 127.7, 101.7, 101.6, 47.9, 38.8, 37.9, 32.5, 31.5, 30.2, 25.9, 25.3, 19.5, 13.7; ESI-HRMS calcd for $(C_{25}H_{35}N_5O_4 \cdot H)^+$ 404.2298, found 404.2297. Anal. calcd for $C_{20}H_{29}N_5O_4$: C, 59.54; H, 7.24; N, 17.36. Found: C, 59.15; H, 7.40; N, 17.04.

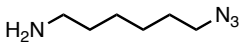

6-Azidohexan-1-amine (19). Following the procedure reported by Kim:[109] To 100 mL of a vigorously stirred 9:1 (v/v) mixture of DMF/H_2O was added 4.76 g (19.5 mmol) of 1,6-dibromohexane and 3.80 g (58.5 mmol) of sodium azide. The contents were heated to 80 °C for 22 h. The contents were allowed to cool to room temperature and were extracted with 3 × 50 mL portions of ether. The organic layers were combined, dried over magnesium sulfate, gravity filtered and concentrated *in vacuo* to afford 3.22 g (98%) of 1,6-diazidohexane as a light brown oil: ^{1}H NMR (400 MHz, $CDCl_3$) δ 3.27 (t, J = 6.9 Hz, 2H), 1.60 (m, 2H), 1.40 (m, 2H); ^{13}C NMR (101 MHz, $CDCl_3$) δ 51.4, 28.8, 26.4; IR (KBr, thin film) 2940, 2863, 2102, 1456, 1349, 1260.

To 20 mL of a 1:1 (v/v) mixture of ethyl acetate and ether was added 16 mL of 2 M HCL. The contents were vigorously stirred, cooled in an ice water bath and 1.15 g (6.84 mmol) of 1,6-diazidohexane was added. After 10 min, 1.76 g (6.71 mmol) of triphenylphosphine was added in small portions over 1 h. The flask was removed from the bath and stirred at room temperature for 20 h. The contents were poured into a separatory funnel containing 20 mL of water and the organic layer was discarded. The aqueous layer was extracted with 3 × 20 mL portions of CH_2Cl_2 and carefully basified with 1 M NaOH. The aqueous layer was extracted with 3 × 30 mL portions of CH_2Cl_2 and the combined organic layers were dried over magnesium sulfate, gravity filtered and concentrated *in vacuo* to afford 0.540 g (56%) of **19** as a colorless oil: ^{1}H NMR (500

MHz, $CDCl_3$) δ 3.22 (t, J = 6.9, 2H), 2.65 (t, J = 7.0, 2H), 1.59-1.54 (m, 2H), 1.40 (m, 2H), 1.35-1.31 (m, 4H), 1.20 (br s, 2H); ^{13}C NMR (126 MHz, $CDCl_3$) δ 51.4, 42.1, 33.6, 28.8, 26.6, 26.5; IR (KBr, thin film) 3422, 3020, 2935, 2860, 2100, 1215, 755, 670; ESI-HRMS calcd for $(C_6H_{14}N_4 \cdot H)^+$ 143.1297, found 143.1297.

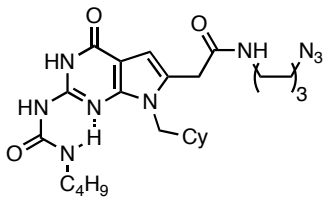

***N*-(6-Azidohexyl)-2-[2-(3-butylureido)-7-(cyclohexylmethyl)-4-oxo-4,7-dihydro-3*H*-pyrrolo[2,3-*d*]pyrimidin-6-yl]ethanamide (DeUG azide, 20).** To a suspension of 0.510 g (1.26 mmol) of **18** in 25 mL of CH_2Cl_2 was added 0.360 g (2.53 mmol) of **19**, 3 drops of DMF and 0.031 g (252 μmol) of DMAP. The suspension was stirred at rt and 0.363 g (1.89 mmol) of EDCI was added. After 12 h, the contents were homogeneous and were heated to reflux for 6 h. The contents were washed with 3 × 50 mL of water, dried over magnesium sulfate, gravity filtered and concentrated *in vacuo*. The residue was purified via column chromatography using 9:1 $CHCl_3$/MeOH as the eluent (R_f = 0.49) followed by precipitation from chloroform (3 mL) via addition of PE to afford 0.650 (97%) g of **20** as a pale yellow powder: mp 137-139 °C; ^{1}H NMR (500 MHz, $CDCl_3$) δ 11.26 (br s, 1H), 9.40 (br s, 1H), 8.88 (br s, 1H), 6.79 (s, 1H), 6.30 (br s, 1H), 3.82 (d, J = 6.7, 2H), 3.64 (s, 2H), 3.40 (m, 2H), 3.23 (m, 4H), 1.69 (m, 4H), 1.64 (m, 3H), 1.55 (m, 4H), 1.47

(m, 3H), 1.36 (m, 2H), 1.30 (m, 2H), 1.13 (s, 3H), 0.98 (t, J = 7.4, 3H), 0.94 (m, 2H); ^{13}C NMR (126 MHz, $CDCl_3$) δ 169.0, 159.2, 153.9, 149.1, 146.5, 128.8, 103.9, 102.4, 51.4, 49.3, 40.3, 40.0, 38.9, 35.7, 32.3, 31.1, 29.6, 28.9, 26.6, 26.5, 26.3, 25.8, 20.5, 14.0; ESI-HRMS calcd for $(C_{26}H_{41}N_9O_3 \cdot H)+$ 528.3411, found 528.3428.

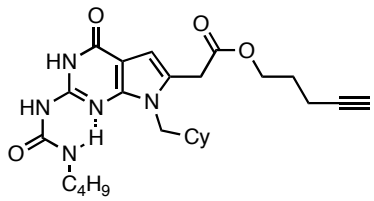

[2-(3-Butylureido)-7-cyclohexanemethyl-4-oxo-4,7-dihydro-3H-pyrrolo[2,3-d]pyrimidin-6-yl]-acetic acid 4-pentynyl ester (DeUG pentynyl ester, 21). To a solution of 210 mg (520 μmol) of **18** in 20 mL of methylene chloride was added 60.0 mg (713 μmol) of 4-pentyn-1-ol and 30 mg (103 μmol) of DPTS. The heterogeneous solution was stirred for 10 min and 150 mg (782 μmol) of EDCI was added. After 5 min, the reaction became homogeneous and the contents were heated to reflux. After 16 h, the flask was cooled to rt and the contents washed with 3 × 20 mL of water, dried over magnesium sulfate, gravity filtered and concentrated *in vacuo*. The residue was purified via column chromatography using 9:1 $CHCl_3$/MeOH as the eluent (R_f = 0.51) to afford 200 mg (91%) of **21** as a white powder: mp 139-142 °C; ^{1}H NMR (500 MHz, $CDCl_3$) δ 11.25 (br s, 1H), 9.42 (br s, 1H), 9.02 (br s, 1H), 6.87 (s, 1H), 4.23 (t, J = 6.3, 2H), 3.84 (d, J = 7.3, 2H), 3.75 (s, 2H), 3.47 (dt, J = 5.8, J = 6.3, 2H), 2.27 (dt, J = 2.4, J = 6.9,

2H), 1.98 (t, J = 2.4, 1H), 1.87 (m, 2H), 1.72 (m, 3H), 1.65 (m, 3H), 1.58 (m, 2H), 1.47 (m, 2H), 1.16 (m, 3H), 0.98 (t, J = 7.3, 3H), 0.96 (m, 2H); ^{13}C NMR (126 MHz; $CDCl_3$) δ 170.1, 159.4, 154.2, 148.7, 146.4, 127.5, 103.6, 102.5, 82.9, 69.3, 64.0, 49.4, 40.2, 39.0, 33.2, 32.2, 31.2, 27.4, 26.4, 25.9, 20.5, 15.3, 14.0; ESI-HRMS calcd for $(C_{25}H_{35}N_5O_4 \cdot H)^+$ 470.2767, found 470.2756.

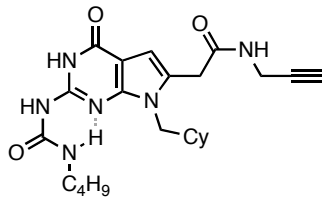

2-[2-(3-Butyl-ureido)-7-cyclohexylmethyl-4-oxo-4,7-dihydro-3*H*-pyrrolo[2,3-*d*]pyrimidin-6-yl]-*N*-prop-2-ynyl-acetamide (DeUG propargylamide, 22). To 42 mL of a 20:1 (v/v) mixture of CH_3CN/DMF was added 300 mg (0.74 mmol) of **18**, 65 µL (1.02 mmol) of propargylamine and 13 mg (0.11 mmol) of DMAP. The contents were stirred for 10 min and 180 mg (0.94 mmol) of EDCI was added. The reaction was allowed to stir at room temperature for 18 h. The contents were concentrated *in vacuo* and the residue was dissolved in 40 mL of ethyl acetate. The organic layer was washed with 3 x 40 mL portions of brine, dried over magnesium sulfate, gravity filtered and concentrated *in vacuo*. The residue was triturated with 20 mL of methylene chloride and vacuum filtered to afford 170 mg (52%) of DeUG propargylamide **22** as a light brown powder which was judged to be > 95% pure by ^{1}H NMR: mp 177-179 °C; ^{1}H NMR

($CDCl_3$) δ 11.76 (br s, 1H), 10.10 (br s, 1H), 8.53 (br s, 1H), 7.93 (br s, 1H), 6.20 (s, 1H), 3.87 (m, 2H), 3.80 (d, J = 7.6, 2H), 3.53 (s, 2H), 3.17 (m, 2H), 3.13 (t, J = 2.6, 1H), 1.71 (m, 1H), 1.62 (m, 3H), 1.45 (m, 4H), 1.33 (m, 2H), 1.10 (m, 3H), 0.94 (m, 2H), 0.90 (t, J = 7.4, 3H); ^{13}C NMR ($CDCl_3$) δ 168.55, 158.94, 154.87, 148.40, 147.83, 128.26, 101.72, 101.32, 81.03, 73.15, 38.76, 37.98, 33.71, 31.56, 30.43, 30.24, 28.74, 25.94, 25.98, 19.58, 13.67; ESI-HRMS calcd for $(C_{23}H_{32}N_6O_3 \cdot H)^+$ 441.2614, found 441.2614.

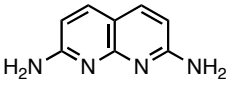

2,7-Diamino-1,8-naphthyridine (DAN, 23). A typical high pressure ammonolysis is described. To a glass pressure vessel (steel bomb) liner was added 10.94 g (49.4 mmol) of dry **28** and 10 mL of dry ethanol. The liner was fitted with a cold finger equipped with a dry nitrogen inlet. To the cold finger bleed port was attached an oil bubbler. The apparatus was purged with nitrogen for 10 min. The bleed port on the liner was sealed with teflon tape, placed in the pressure vessel and submerged in a dry ice/isopropanol bath. The cold finger was filled with dry ice/isopropanol. After 10 min, a minimal flow of anhydrous ammonia was started into the cold finger using tygon tubing. After approximately 25-30 mL of ammonia had condensed into the liner (ca. 10 min), the flow of ammonia was stopped. The teflon tape was carefully removed from the liner bleed port and the cold finger removed from the liner. The liner was stoppered with a teflon

sleeve and glass stopper. The stopper joint was wrapped with teflon tape. The pressure vessel was sealed and connected to a small mechanical rocker. The system was pressurized to 200 psi using dry nitrogen and leak checked. The program was set with following parameters: run temp = 200 °C; ramp time = 2 h; soak time = 48 h; high-temp limit = 220 °C. After 48 h, the program was stopped and the system was allowed to cool to ambient temperature before venting and purging with nitrogen. The apparatus was disassembled and the solid brown residue in the liner was suspended in 130 mL of 1:1 ethanol/H_2O. A brown orange solid was collected via vacuum filtration and washed on the filter paper with water to yield 7.17 g (91%) of **23** after drying under high vacuum: mp 268-272 °C dec; ^{1}H NMR (DMSO-d_6) δ 7.64 (d, J = 8.5, 2H), 6.50 (br s, 4H), 6.40 (d, J = 8.5, 2H); ^{13}C NMR (DMSO-d_6) δ 159.8, 150.1, 140.2, 108.6, 108.1; ESI-HRMS calcd for $(C_8H_8N_4 \cdot H)^+$ 161.0827, found 161.0819.

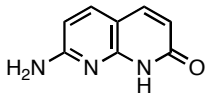

2-Amino-1,8-naphthyridine-7-one (26). To 40.0 g (367 mmol) of diaminopyridine and 60.0 g (448 mmol) of racemic malic acid, which were grounded to an intimate powder with a mortar and pestle, cooled to 0 °C in an ice water bath, was added 200 mL of concentrated sulfuric acid dropwise. The contents were stirred for 1 h using a mechanical stirrer before heating to 110 °C for 3 h. The contents were poured over ice and the pH

adjusted to 8 via careful addition of concentrated ammonium hydroxide. Vacuum filtration and washing with 3 L of water, followed by dispersing in 1.8 L of hot 10% methanol/water and a second vacuum filtration afforded 57.0 g (97%) of **26** as a pale yellow powder: mp >300 °C dec; ^{1}H NMR (DMSO-d_6) δ 11.97 (br s, 1H), 7.66 (d, J = 9.3, 1H), 7.65 (d, J = 8.5, 1H), 7.08 (br s, 2H), 6.35 (d, J = 8.5, 1H), 6.12 (d, J = 9.2, 1H); ^{13}C NMR (DMSO-d_6) δ 163.8, 160.6, 150.4, 139.8, 137.4, 114.8, 105.3, 105.0; ESI-HRMS calcd for $(C_8H_7N_3O{\cdot}H)^+$ 162.1686, found 162.1677.

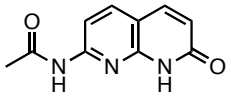

2-(Acetamido)-1,8-naphthyridine-7-one (27). To 50.0 g (310 mmol) of naphthyridone **26** was added 500 mL of of acetic anhydride. The suspension was heated to reflux for 3 h. The mixture was allowed to cool to room temperature and the resultant precipitate was collected via vacuum filtration. The solid was washed on the filter paper with 300 mL of water followed by 500 mL of diethyl ether and was dried under ambient conditions to give 55.6 g (88%) of **27** as a pale yellow powder which was used without further purification: mp >300 °C (sublimes); ^{1}H NMR (DMSO-d_6) δ 11.92 (br s, 1H), 10.54 (s, 1H), 8.01 (d, J = 8.5, 1H), 7.88 (d, J = 8.5, 1H), 7.79 (d, J = 9.2, 1H), 6.41 (d, J = 9.2, 1H), 2.10 (s, 3H); ESI-HRMS calcd for $(C_{10}H_9N_3O_2{\cdot}H)^+$ 204.0773, found 204.0771.

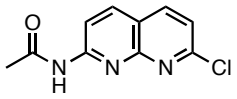

2-(Acetamido)-7-chloro-1,8-naphthyridine (28). To 20.0 g (98.4 mmol) of naphthyridone **27** was added 250 mL of of phosphorus oxychloride. The suspension was heated to 80 °C for 2 h. The mixture was allowed to cool to room temperature and excess phosphorus oxychloride was removed *in vacuo*. The residue was slurried in ice water and the pH adjusted to 8 via careful addition of concentrated ammonium hydroxide. The resultant precipitate was collected via vacuum filtration and dried by pulling ambient air over it. The solid was then purified by Soxhlet extraction for 24 h using chloroform. The extract was concentrated *in vacuo* to afford 17.3 g (79%) of **28** as a light brown powder which carried on without further purification: mp 250-253 °C; ^{1}H NMR (DMSO-d_6) δ 11.21 (br s, 1H), 8.38 (m, 3H), 7.48 (d, J = 8.5, 1H), 2.15 (s, 3H); ESI-HRMS calcd for $(C_{10}H_8N_3ClO{\cdot}H)^+$ 222.0434, found 222.0434.

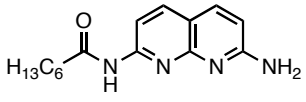

Heptanoic acid (7-amino-[1,8]naphthyridin-2-yl)-amide (30). To a stirred solution of 601 mg (1.56 mmol) of **4** in 60 mL of THF was added 71 mg (1.22 mmol) of dry sodium hydroxide pellets. The contents were heated to 80 °C for 22 h. The contents were allowed to cool to room temperature and concentrated *in vacuo*. The residue was

dissolved in 50 mL of chloroform, washed with 3 × 50 mL portions of water, dried over magnesium sulfate, gravity filtered and concentrated *in vacuo*. The residue was purified via flash chromatography using 9:1 (v/v) $CHCl_3$/MeOH as the eluent (R_f = 0.33) to afford 212 mg (51%) of **30** as an off-white powder: mp 187-188 °C; ^{1}H NMR ($CDCl_3$) δ 8.21 (d, J = 8.6, 1H, CH), 8.18 (br s, 1H, NH), 7.95 (d, J = 8.6, 1H, CH), 7.81 (d, J = 8.8, 1H, CH), 6.66 (d, J = 8.6, 1H, CH), 4.99 (br s, 2H, NH_2), 2.42 (t, J = 7.4, 2H, CH_2), 1.73 (m, 2H, CH_2), 1.38 (m, 2H, CH_2), 1.30 (m, 4H, CH_2), 0.88 (t, J = 6.4, 3H, CH_3); ^{13}C NMR ($CDCl_3$) δ 172.43, 159.99, 155.46, 153.23, 138.85, 138.03, 119.42, 115.28, 110.50, 38.17, 31.63, 28.94, 25.44, 22.60, 14.16; ESI-HRMS calcd for $(C_{15}H_{20}N_4O{\cdot}H)^+$ 273.1715, found 273.1725.

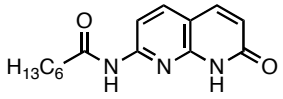

2-(Heptanoylamido)-1,8-naphthyridine-7-one (31). To a suspension of 5.3 g (32.9 mmol) of naphthyridone **26** in 150 mL of pyridine at 100 °C was added 8.0 mL of heptanoyl chloride. The solution was allowed to stir for 24 h. The contents were allowed to cool to room temperature before concentrating *in vacuo*. The residue was dissolved in 100 mL of chloroform, washed with 3 × 100 mL portions of water, 1 × 50 mL of saturated sodium bicarbonate solution, dried over magnesium sulfate, gravity filtered and concentrated *in vacuo*. The residue was triturated with 100 mL of *n*-hexane and vacuum

filtered. The product was purified via column chromatography using 9:1 (v/v) $CHCl_3$/ MeOH as the eluent (R_f = 0.70) to afford 12.1 g (87%) of **31** as a white powder: mp >300 °C dec; ^{1}H NMR ($CDCl_3$) δ 12.81 (s, 1H), 11.86 (s, 1H), 8.37 (d, J = 8.7, 1H), 7.88 (d, J = 8.7, 1H), 7.71 (d, J = 9.4, 1H), 6.59 (d, J = 9.4, 1H), 2.65 (t, J = 7.5, 2H), 1.74 (m, 2H), 1.42 (m, 2H), 1.33 (m, 4H), 0.89 (t, J = 7.0, 3H); ^{13}C NMR ($CDCl_3$) δ 174.7, 165.4, 154.4, 148.7, 139.9, 139.1, 119.8, 111.2, 110.8, 37.2, 31.8, 29.07, 25.4, 22.7, 14.2; ESI-HRMS calcd for $(C_{15}H_{19}N_3O_2 \cdot H)^+$ 274.1556, found 274.1561; Anal. calcd for $C_{15}H_{19}N_3O_2$: C, 65.91; H, 7.01; N, 15.37. Found: C, 65.99; H, 7.28; N, 15.71.

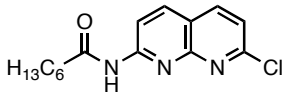

2-(Heptanolyamido)-7-chloro-1,8-naphthyridine (32). To 3.0 g (11.0 mmol) of naphthyridone **31** was added 30 mL of of phosphorus oxychloride. The suspension was heated to 80 °C for 2 h. The mixture was allowed to cool to room temperature and excess phosphorus oxychloride was removed *in vacuo*. The residue was slurried in ice water and the pH adjusted to 8 via careful addition of concentrated ammonium hydroxide. The resultant precipitate was collected via vacuum filtration and dried by pulling ambient air over it. The solid was then purified by Soxhlet extraction for 24 h using chloroform. The extract was concentrated *in vacuo* and purified via column chromatography using 9:1 (v/ v) $CHCl_3$/MeOH as the eluent (R_f = 0.73) to afford 2.75 g (85%) of **32** as an off-white

powder:: ^{1}H NMR ($CDCl_3$) δ 8.58 (d, J = 8.9, 1H), 8.51 (s, 1H), 8.19 (d, J = 8.9, 1H), 8.08 (d, J = 8.4, 1H), 7.40 (d, J = 8.4, 1H), 2.48 (t, J = 7.5, 2H), 1.75 (m, 2H), 1.38 (m, 2H), 1.31 (m, 4H), 0.89 (t, J = 6.3, 3H); MS (FD) m/z 291.2 (100).

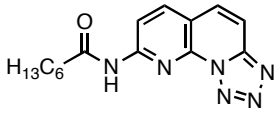

2-(Heptanolyamido)-7-azido-1,8-naphthyridine (33/34). To a solution of 0.100 g (343 μmol) of chloronaphthyridine **32** in 10 mL of DMF was added 0.120 g (1.85 mmol) of sodium azide. The contents were heated to 60 °C for 14 h. The solution was concentrated *in vacuo*. The residue was dissolved in 25 mL of chloroform and washed with 3 x 25 mL water, 5 x 25 mL of brine, dried over magnesium sulfate, gravity filtered and concentrated *in vacuo* to afford 98 mg (96%) of **33/34** as a white powder: ^{1}H NMR ($CDCl_3$) δ 8.84 (s, 1H), 8.72 (d, J = 8.8, 1H), 8.35 (d, J = 8.8, 1H), 7.95 (d, J = 0.6, 2H), 2.54 (t, J = 7.5, 2H), 1.77 (m, 2H), 1.40 (m, 2H), 1.31 (m, 4H), 0.87 (t, J = 7.0, 3H); MS (FD) m/z 298.3 (100); IR showed no azide stretch.

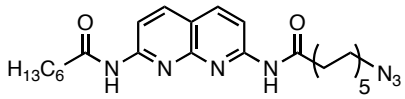

11-Azidoundecanoic acid (7-heptanoylamino-[1,8]naphthyridin-2-yl)-amide (35). To a suspension of 505 mg (1.85 mmol) of naphthyridine **30** in 27 mL of dichloromethane and 3 mL of DMF was added 510 mg (2.24 mmol) of 11-azidoundecanoic acid **36**, 70 mg of DMAP and 510 mg of EDCI. The contents were stirred at room temperature. After 18 h, the contents were concentrated *in vacuo*, dissolved in 30 mL of chloroform and washed with 3 × 50 mL portions of water and 50 mL of brine. The organic layer was dried over magnesium sulfate, gravity filtered and concentrated *in vacuo*. The residue was purified by column chromatography (9:1 chloroform/methanol, $R_f = 0.71$) to afford 787 mg (88%) of **35** as an pale yellow crystalline solid: ^{1}H NMR ($CDCl_3$) δ 10.73 (br s, 2H), 8.48 (d, J = 6.7, 2H), 7.75 (d, J = 8.7, 2H), 3.12 (t, J = 6.9, 2H), 2.43 (br m, 4H), 1.56 (br m, 4H), 1.44 (m, 2H), 1.11 (br m, 18H), 0.68 (t, J = 6.8, 3H); ^{13}C NMR ($CDCl_3$) δ 173.4, 173.3, 154.5, 154.5, 153.1, 138.5, 117.5, 113.9, 113.9, 51.2, 37.2, 31.3, 29.2, 29.2, 29.1, 29.1, 28.9, 28.7, 28.6, 26.5, 25.0, 25.0, 22.3, 13.8; MS (FD) m/z 481.4 (100); IR (cm^{-1}) 2099.

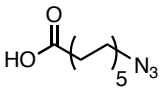

11-Azidoundecanoic acid (36). To a solution of 7.00 g (26.4 mmol) of 11-bromoundecanoic acid in 50 mL of DMF was added 2.50 g (38.5 mmol) of sodium azide and 1 mL of water. The solution was heated to 60 °C. After 12 h, the contents were concentrated *in vacuo* and the residue was dissolved in 50 mL of methylene chloride. The organic layer was washed with 3 × 50 mL of water, dried over magnesium sulfate, gravity filtered and concentrated *in vacuo* to afford 5.87 g (98%) of **36** as a pale yellow oil: ^{1}H NMR ($CDCl_3$) δ 11.15 (s, 1H), 3.24 (t, J = 7.0, 2H), 2.32 (t, J = 7.5, 2H), 1.59 (m, 4H), 1.27 (br m, 12H); ^{13}C NMR ($CDCl_3$) δ 178.6, 51.6, 34.1, 29.5, 29.4, 29.3, 29.2, 29.2, 28.9, 26.8, 24.9; MS (FD) m/z 227.2 (100); IR (cm^{-1}) 2930, 2857, 2097, 1726, 1438, 1257.

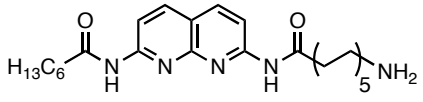

11-Aminoundecanoic acid (7-heptanoylamino-[1,8]naphthyridin-2-yl)-amide (37). To a stirred solution of 0.970 g (2.01 mmol) of 11-azidoundecanoyl DAN **35** in 50 mL of THF was added 0.530 g (2.02 mmol) of triphenylphosphine portionwise over 1 h. After 5 h, 5.0 mL of water was added. After 24 h, 100 mL of water was added and 0.894 mg (93%) of a white precipitate was collected via vacuum filtration. Trace amounts of

triphenylphosphine oxide were removed by scavenging with iodo-modified Merrifield resin according to the procedure reported by Lipshutz:[111] ^{1}H NMR ($CDCl_3$) δ 8.44 (d, J = 8.8, 1H), 8.43 (d, J = 8.8, 1H), 8.39 (s, 1H), 8.34 (s, 1H), 8.13 (d, J = 8.8, 1H), 8.12 (d, J = 8.8, 1H), 2.67 (t, J = 7.0, 2H), 2.45 (t, J = 7.5, 4H), 1.73 (m, 4H), 1.42-1.27 (m, 20H), 1.09 (s, 2H), 0.88 (t, J = 6.9, 3H); ^{13}C NMR ($CDCl_3$) δ 173.4, 173.3, 154.5, 154.5, 153.1, 138.5, 117.5, 113.9, 113.9, 51.2, 37.2, 31.3, 29.2, 29.2, 29.1, 29.1, 28.9, 28.7, 28.6, 26.5, 25.0, 25.0, 22.3, 13.8; MS (FD) m/z 455.3 (100).

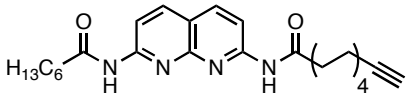

10-Undecynoic acid (7-heptanoylamino-[1,8]naphthyridin-2-yl)-amide (38). To a suspension of 750 mg (2.75 mmol) of naphthyridine **30** in 32 mL of dichloromethane and 3 mL of DMF was added 550 mg (3.02 mmol) of 10-undecynoic acid, 67 mg (0.55 mmol) of DMAP and 634 mg (3.30 mmol) of EDCI. The contents were stirred at room temperature. After 18 h, the contents were concentrated *in vacuo*, dissolved in 50 mL of chloroform and washed with 3 × 50 mL portions of water and 50 mL of brine. The organic layer was dried over magnesium sulfate, gravity filtered and concentrated *in vacuo*. The residue was purified by column chromatography (9:1 chloroform/methanol, R_f = 0.72) to afford 1.13 g (94%) of **38** as an pale yellow powder: ^{1}H NMR ($CDCl_3$) δ 9.49 (s, 2H), 8.47 (d, J = 8.8, 2H), 8.04 (d, J = 8.8, 2H), 2.33 (t, J = 7.5, 4H), 2.16 (td, J =

7.1, 2.6, 2H), 1.99 (q, J = 7.1, 2H), 1.93 (t, J = 2.6, 1H), 1.67-1.61 (m, 4H), 1.31 (t, J = 6.4, 2H), 1.20 (br m, 14H), 0.81 (t, J = 7.0, 3H); ^{13}C NMR ($CDCl_3$) δ 172.4, 160.0, 155.5, 153.2, 138.9, 138.0, 119.4, 115.3, 110.5, 84.8, 68.2, 38.2, 34.2, 31.6, 29.2, 29.1, 29.0, 28.9, 28.8, 28.5, 25.4, 24.7, 22.6, 18.5 14.2; MS (FD) m/z 436.3 (100).

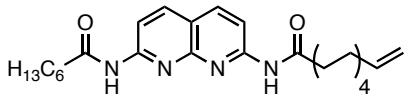

10-Undecenoic acid (7-heptanoylamino-[1,8]naphthyridin-2-yl)-amide (39). To a stirred solution of 0.380 mg (1.40 mmol) of naphthyridine **30** in 10 mL of methylene chloride was added 0.230 mL (1.65 mmol) of TEA. To this was added 0.330 mL (1.54 mmol) of 10-undecenoyl chloride (dissolved in 10 mL of methylene chloride) dropwise via addition funnel. The contents were heated to reflux for 16 h. The solution was washed with 2 × 20 mL of water and 2 × 20 mL of brine, dried over magnesium sulfate, gravity filtered and concentrated *in vacuo*. The residue was purified via column chromatography using 1:9 methanol/chloroform as the eluent (R_f = 0.72) to afford 443 mg (73%) of the product as a white powder: ^{1}H NMR ($CDCl_3$) δ 9.49 (s, 2H), 8.47 (d, J = 8.7, 2H), 8.04 (d, J = 8.8, 2H), 5.76 (ddt, J = 17.1, 10.3, 6.7, 1H), 4.95 (dd, J = 17.1, 1.9, 1H), 4.89 (dd, J = 10.2, 0.9, 1H), 2.42 (t, J = 7.6, 4H), 1.99 (q, J = 7.1, 2H), 1.67-1.61 (m, 4H), 1.31 (t, J = 6.4, 2H), 1.20 (br m, 14H), 0.81 (t, J = 7.0, 3H); ^{13}C NMR

($CDCl_3$) δ 173.0, 154.4, 153.6, 139.2, 139.1, 118.2, 114.2, 113.9, 113.4, 37.8, 33.8, 31.5, 29.4, 29.3, 29.2, 29.1, 28.9, 28.9, 25.3, 25.3, 22.5, 14.1; MS (FD) *m*/*z* 438.3 (100).

5.3.2 Synthetic Procedures for Part II

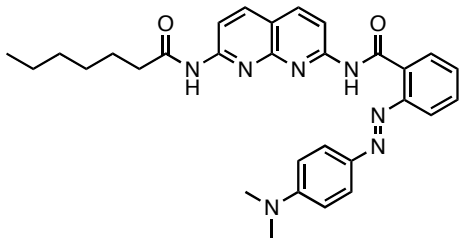

2-(4-Dimethylamino-phenylazo)-*N*-(7-heptanoylamino-[1,8]naphthyridin-2-yl)-benzamide (DAN-methyl red conjugate, 44). To a stirred solution of 0.173 g (0.64 mmol) of methyl red in 25 mL of THF was added 0.175 g (0.64 mmol) of **30** and 8 mg (65 μmol) of DMAP. After 10 min, 0.246 g (1.28 mmol) of EDCI was added. After 18 h, the contents were concentrated *in vacuo* and the residue was dissolved in 50 mL of $CHCl_3$. The organic layer was washed with 3 × 50 mL portions of water, dried over magnesium sulfate, gravity filtered and concentrated *in vacuo*. The residue was purified via flash chromatography using 9:1 (v/v) $CHCl_3$/MeOH as the eluent (R_f = 0.40) to afford 0.188 g (56%) of DAN-methyl red conjugate **44** as a red powder: ^{1}H NMR ($CDCl_3$) δ 12.65 (br s, 1H), 9.24 (br s, 1H), 8.70 (d, J = 8.6, 1H), 8.45 (dd, J = 7.8, J = 1.5, 1H), 8.40 (d, J = 8.8, 1H), 8.17 (m, 4H), 7.94 (dd, J = 8.1, J = 1.1, 1H), 7.61 (dt, J = 7.2, J = 1.7, 1H), 7.54 (dt, J = 7.9, J = 1.3, 1H), 6.75 (d, J = 9.2, 2H), 2.89 (s, 6H), 2.41 (t, J = 7.6, 2H), 1.62 (m, 2H), 1.20 (m, 6H), 0.80 (t, J = 7.0, 3H); ^{13}C NMR ($CDCl_3$) δ 172.97, 165.39, 154.93, 154.66, 153.54, 150.68, 143.56, 139.05, 138.94, 138.81, 133.02, 131.63, 129.60, 128.88, 125.14, 118.53, 116.30, 114.50, 113.73, 111.84, 40.13, 37.96, 31.62,

29.00, 25.37, 22.55 14.14; ESI-HRMS calcd for $(C_{30}H_{33}N_7O_2 \cdot H)^+$ 524.2774, found 524.2786; UV ($CHCl_3$) λ_{max}, nm: 490.8, 379.8, 361.2.

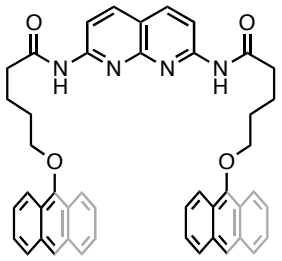

5-(9-Anthyrloxy)valeric acid (7-[5-(9-anthryloxyvaleroylamino)]-[1,8]-naphthyridinyl)-amide (pDAN, 45). To a suspension of 154 mg (0.961 mmol) of naphthyridine **23** in 14 mL of dichloromethane and 1 mL of DMF was added 600 mg (2.04 mmol) of 5-(9-anthyrloxy)valeric acid, 40 mg (0.33 mmol) of DMAP and 250 mg (1.30 mmol) of EDCI. The contents were stirred at room temperature. After 18 h, the contents were concentrated *in vacuo*, dissolved in 30 mL of chloroform and washed with 3 × 30 mL portions of water and 30 mL of brine. The organic layer was dried over magnesium sulfate, gravity filtered and concentrated *in vacuo*. The residue was purified by column chromatography (9:1 chloroform/methanol, $R_f = 0.61$) to afford 568 mg (83%) of **45** as an pale orange crystalline solid: ^{1}H NMR ($CDCl_3$) δ 9.52 (s, 2H), 8.37 (d, J = 8.8, 2H), 8.17 (m, 6H), 8.00 (d, J = 8.8, 2H), 7.96-7.92 (m, 4H), 7.43-7.39 (m, 8H), 4.06 (t, J = 6.1, 4H), 2.55 (t, J = 7.2, 4H), 1.97 (m, 8H); ^{13}C NMR ($CDCl_3$) δ 172.5, 154.4, 153.6, 151.2, 139.2, 132.5, 128.5, 125.6, 125.3, 124.7, 122.3, 122.3, 118.7, 113.9, 75.5,

37.6, 30.1, 22.1; MS (FD) *m/z* 712.3 (100), 436.2 (13); ESI-HRMS calcd for $(C_{46}H_{40}N_4O_4 \cdot H)^+$ 713.3128, found 713.3133; UV ($CHCl_3$) λ_{max}, nm: 331, 339, 347, 368, 388.

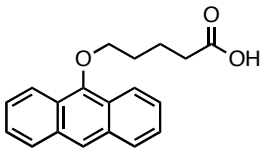

5-(9-anthryloxy)valeric acid (46). To a solution of 5.0 g (25.7 mmol) of anthrone in 250 mL of acetone (dried over 3Å molecular sieves) was added 4.3 g (31.1 mmol) of potassium carbonate and 6.2 mL (38.6 mmol) of ethyl 5-bromovalerate. The solution was heated to reflux for 24 h, allowed to cool to room temperature, gravity filtered and concentrated *in vacuo*. The residue was dissolved in 75 mL of dichloromethane, washed with 3 × 50 mL portions of water, dried over magnesium sulfate, gravity filtered, concentrated *in vacuo* and purified by column chromatography (20% ethyl acetate/ petroleum ether, R_f = 0.80) to afford 6.24 g (82%) of ethyl 5-(9-anthryloxy)valerate as a white crystalline solid: ^{1}H NMR ($CDCl_3$) δ 8.29 (d, J = 8.2, 2H, CH), 8.22 (s, 1H, CH), 8.00 (d, J = 8.2, 2H, CH), 7.48 (m, 4H, CH), 4.22 (t, J = 6.0, 2H, CH_2), 4.20 (q, J = 7.2, 2H, CH_2), 2.51 (t, J = 7.0, 2H, CH_2), 2.09 (m, 4H, CH_2), 1.30 (t, J = 7.2, 3H, CH_3); ^{13}C NMR ($CDCl_3$) δ 173.7, 151.4, 132.5, 128.6, 125.6, 125.3, 124.8, 122.5, 122.2, 75.6,

60.5, 34.3, 30.2, 22.0, 14.4; MS (FD) *m/*z 322.2 (100), 644.4 (13); Anal. calcd for $C_{21}H_{22}O_3$: C, 78.23; H, 6.88. Found: C, 78.28; H, 6.94.

To a solution of 2.51 g (7.79 mmol) of ethyl 5-(9-anthryloxy)valerate in 70 mL ethanol was added 10 mL of 0.25 M NaOH. The mixture was heated to reflux overnight (ca. 12-14 h), allowed to cool to room temperature and concentrated *in vacuo*. The residue was dissolved in 150 mL of water and the pH adjusted 3 via slow addition of concentrated hydrochloric acid. The resultant precipitate was collected via vacuum filtration, washed on the filter paper with 100 mL of water and dried under high vacuum to afford 2.10 g (91%) of **46** as a white crystalline solid: ^{1}H NMR ($CDCl_3$) δ 11.21 (br s, 1H), 8.30 (d, J = 8.2, 2H, CH), 8.20 (s, 1H, CH), 8.00 (d, J = 8.2, 2H, CH), 7.49 (m, 4H, CH), 4.19 (t, J = 6.0, 2H, CH_2), 2.55 (t, J = 7.0, 2H, CH_2), 2.13 (m, 4H, CH_2); ^{13}C NMR ($CDCl_3$) δ 179.2, 151.4, 132.5, 128.6, 125.6, 125.3, 124.8, 122.5, 122.2, 75.6, 34.3, 30.2, 22.0; MS (FD) *m/*z 294.2 (100), 588.4 (14).

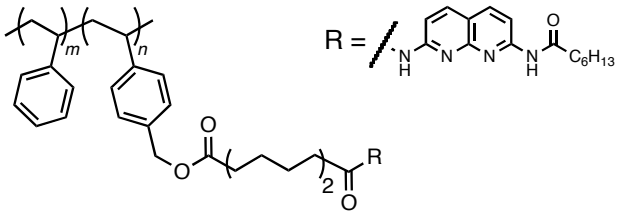

Side-chain functionalized DAN-polystyrene (DAN-PS, 51). A typical procedure is described. To a solution of 0.630 g (1.10 mmol) of DAN styrene **49** in 25 mL of DMSO

was added 1.25 mL of styrene and 100 mg (0.609 mmol) of AIBN. The flask was sealed and heated to 65 °C. After 48 h, the solvent was removed under reduced pressure. The resultant gel was dissolved in a minimal amount of chloroform and thrice precipitated into methanol and dried under high vacuum. The loading of functional monomer in the polymer was determined by ^{1}H NMR integration to be 10 mol %. SEC (DMF) M_w 52.4 kDa, M_n 22.3 kDa, PDI 2.35.

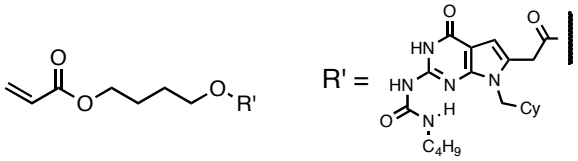

DeUG-functionalized acrylate (52). To a suspension of 1.00 g (2.48 mmol) of DeUG acetic acid **18** in 50 mL of dichloromethane was added 80 mg of DPTS (0.273 mmol) and 0.40 mL of 4-hydroxybutyl acrylate (2.89 mmol). The heterogeneous solution was stirred for 10 min and 0.570 mg (2.97 mmol) of EDCI was added. After 15 min, the mixture became homogeneous and the contents were heated to reflux. After 18 h, the flask was cooled to room temperature and the contents washed with 3 × 50 mL of water, dried over magnesium sulfate, gravity filtered and concentrated *in vacuo*. The residue was purified via column chromatography using 9:1 $CHCl_3$/MeOH as the eluent (R_f = 0.37) to afford 1.13 g (89%) of **52** as a colorless oil: ^{1}H NMR ($CDCl_3$) δ 11.26 (br s, 1H), 9.43 (br s, 1H), 9.00 (br s, 1H), 6.87 (s, 1H), 6.39 (dd, J = 17.3, 1.4, 1H), 6.10 (dd, J = 17.3, 10.4,

1H), 5.81 (dd, J = 10.4, 1.4 , 1H), 4.16 (m, 4H), 3.84 (d, J = 7.5, 2H), 3.74 (s, 2H), 3.46 (m, 2H), 1.74 (m, 8H), 1.65 (m, 4H), 1.58 (m, 2H), 1.47 (m, 3H), 1.16 (m, 3H), 0.97 (t, J = 7.4, 5H).; ^{13}C NMR ($CDCl_3$) δ 170.0, 166.3, 159.3, 154.1, 148.7, 146.4, 130.9, 128.5, 127.5, 103.6, 102.5, 65.0, 64.0, 49.3, 40.2, 39.0, 33.3, 32.3, 31.2, 26.4, 25.9, 25.4, 20.5, 14.0; MS (FD) m/z 529.4; ESI-HRMS calcd for $(C_{27}H_{39}N_5O_6 \cdot H)^+$ 529.2900, found 529.2911.

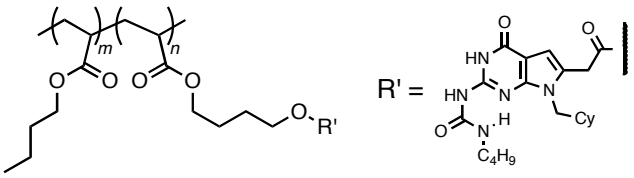

Side-chain functionalized DeUG-poly(butyl acrylate) (DeUG-PBA, 53). A typical procedure is described. To a solution of 0.490 g (0.977 mmol) of DeUG acrylate **52** in 40 mL of DMSO was added 2.25 mL of *n*-butyl acrylate and 96 mg (0.585 mmol) of AIBN. The flask was sealed and heated to 65 °C. After 24 h, the solvent was removed under reduced pressure. The crude polymer was dissolved in toluene and purified via preparative SEC (SX-1 Bio-Beads) followed by dialysis in DMF. The solvent was removed under reduced pressure and the polymer was dried under high vacuum. The loading of functional monomer in the polymer was determined by ^{1}H NMR integration to be 6 mol %. SEC (DMF) M_w 21.8 kDa, M_n 10.2 kDa, PDI 2.14.

Silica nanoparticles (54). A typical procedure for the preparation of silica particles is described.[76] The reaction was performed under a dry nitrogen atmosphere. To 200 mL of absolute ethanol was added 12 mL (300 mmol) of ammonium hydroxide. The mixture was stirred for 30 min at 30 °C and 6.8 mL (31 mmol) of tetraethyl orthosilicate was added via syringe. The mixture was allowed to stir overnight (ca. 12 h). The mixture was heated to 90 °C and allowed to stir for another hour to cure the silane surface.[110] The mixture was allowed to cool to room temperature and was split into 12 equal aliquots. The aliquots were centrifuged at 3000 rpm for 30 min. The supernatant was decanted and the particles from each aliquot were redispersed in 15 mL of absolute ethanol under sonication for 30 min. This rinsing was repeated twice more before combining the particles and drying under high vacuum for 24 h. The hydrodynamic radius of the particles was determined via DLS.

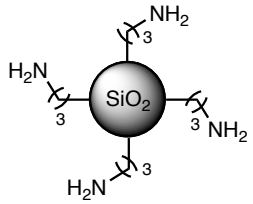

3-Aminopropyl-functionalized silica nanoparticles (55). A typical procedure for the preparation of silica particles is described.[76] The reaction was performed under a dry nitrogen atmosphere. To 200 mL of absolute ethanol was added 12 mL (300 mmol) of

ammonium hydroxide. The mixture was stirred for 30 min at 30 °C and 6.8 mL (31 mmol) of tetraethyl orthosilicate was added via syringe. The mixture was allowed to stir overnight (ca. 12 h). To this was added 0.25 mL (1.4 mmol) of 3-aminopropyl-trimethoxysilane (APTMS) via syringe and the mixture was vigorously stirred for 6 h. The mixture was heated to 90 °C and allowed to stir for another hour to cure the silane surface.[109] The mixture was allowed to cool to room temperature and was split into 12 equal aliquots. The aliquots were centrifuged at 3000 rpm for 30 min. The supernatant was decanted and the particles from each aliquot were redispersed in 15 mL of absolute ethanol under sonication for 30 min. This rinsing was repeated twice more before combining the particles and drying under high vacuum for 24 h. The particles gave a positive Kaiser amine test. The hydrodynamic radius of the particles was determined via DLS.

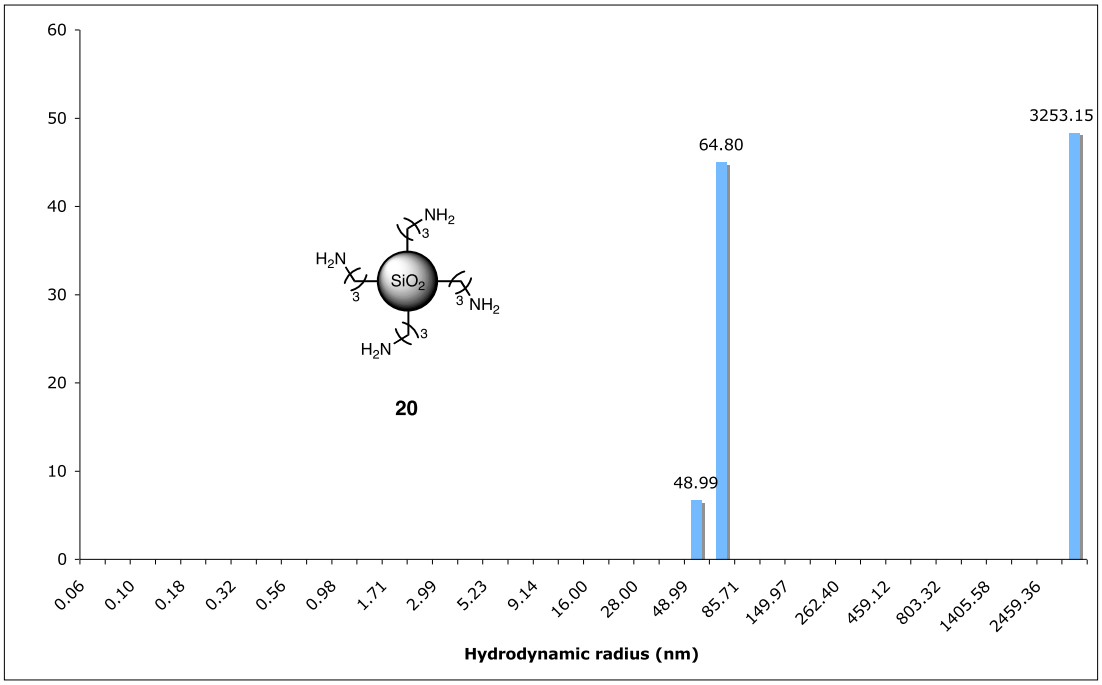

20

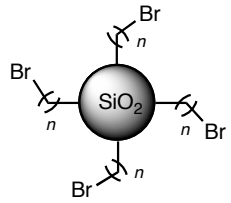

56: $n = 3$
57: $n = 11$

3-Bromopropyl- and 11-bromoundecyl-functionalized silica particles (56 and 57). A typical procedure is described. To a vigorously stirred suspension of 250 mg of silica particles in 15 mL of toluene under a dry argon atmosphere was added 150 μL (939 μmol) of 3-bromopropyltrichlorosilane or 300 μL (1.03 mmol) of 11-bromoundecyl-trichlorosilane via syringe. The contents were allowed to stir for 1 h at room temperature. The contents were centrifuged for 30 min at 3000 rpm and the supernatant was decanted. The particles were washed with 3 × 15 mL portions of toluene followed by 3 × 15 mL portions of absolute ethanol to afford an off-white powder that was dried under high vacuum for 24 h. The hydrodynamic radius of the particles was determined via DLS.

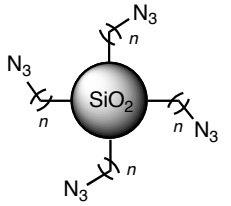

58: $n = 3$
59: $n = 11$

3-Azidopropyl- and 11-azidoundecyl-functionalized silica particles (58 and 59). A typical procedure is described. To a vigorously stirred suspension of 200 mg of the corresponding bromoalkyl-tailored silica particles (**56** or **57**) in 10 mL of DMF was

added an excess (100 mg, 1.54 mmol) of sodium azide. The solution was stirred at room temperature for 2 d. The contents were centrifuged for 30 min at 3000 rpm and the supernatant was decanted. The particles were washed with 3 × 10 mL portions of DMF, 3 × 10 mL portions of Millipore water and dried under high vacuum for 24 h to afford an off-white powder: IR (cm^{-1}) 2104.

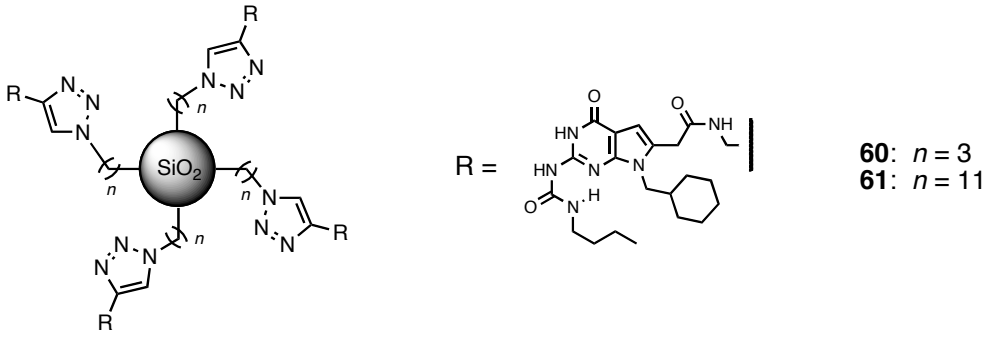

DeUG-functionalized silica particles (60 and 61). A typical procedure is described. To a stirred suspension of 50 mg of azidoalkyl-tailored silica particles in 10 mL of a 1:1 (v/v) mixture of *t*-butanol/water was added 100 mg (227 μmol) of DeUG **22**, 2.0 mg (8.01 μmol) of cupric sulfate and 4.1 mg (20.7 μmol) of sodium ascorbate. The suspension was allowed to stir overnight. The contents were centrifuged at 3000 rpm for 30 min and the supernatant was decanted. The particles were washed with 3 × 10 mL portions of Millipore water and dried under high vacuum for 12 h to yield a dull yellow powder: IR (cm^{-1}) 1660, 1620, 1545.

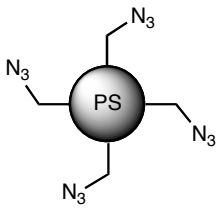

Azide-functionalized Merrifield resin (62). A typical procedure is described. To a stirred suspension of 0.503 g of Merrifield's resin (200-400 mesh, 2.25 mmol/g Cl) in 10 mL of acetone was added 0.170 g (2.61 mmol) of sodium azide. The contents were stirred at 80 C for 18 h. A pale yellow powder (0.480 g) was collected via vacuum filtration after washing with 50 mL of acetone, 150 mL of water and drying in vacuo: IR (cm^{-1}) 2101.

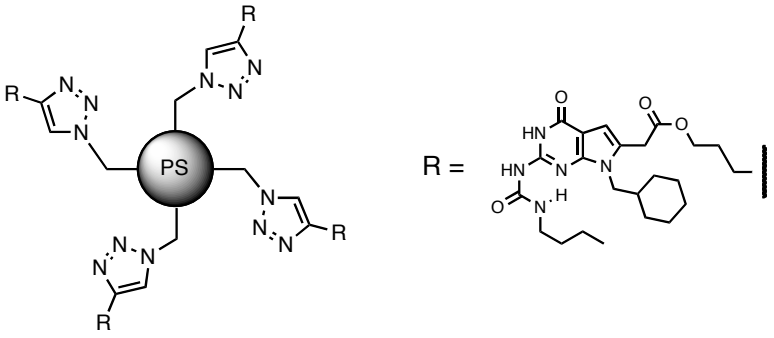

DeUG-functionalized Merrifield resin (63). A typical procedure is described. To a stirred suspension of 200 mg of azido-tailored Merrifield resin **62** in 50 mL of DMF was added 250 mg (532 μmol) of DeUG pentynyl ester **21**, 6.8 mg (27.2 μmol) of cupric sulfate and 4.1 mg (187 μmol) of sodium ascorbate. The suspension was allowed to stir

overnight. The contents were centrifuged at 3000 rpm for 30 min and the supernatant was decanted. The particles were suspended in portions of DMF (3 × 100 mL), Millipore water (3 × 100 mL) and dried under high vacuum for 12 h to yield a dull yellow powder: IR (cm^{-1}) 1660, 1620, 1545.

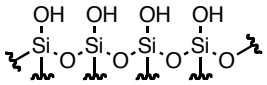

Piranha treated glass (64). To remove trace organic contaminants and to activate the surface, glass and quartz slides were rinsed with ethyl acetate (3 × 10 mL), Millipore water (3 × 10 mL) and dried at 150 °C under a stream of dry nitrogen. Sets of six slides were immersed in 100 mL of freshly prepared Piranha (3:7 30% H_2O_2/H_2SO_4, v/v) for 30 min, rinsed with Millipore water (3 × 100 mL) and dried at 150 °C under a stream of dry nitrogen. Slides were stored under dry nitrogen and used immediately after pretreatment. ***Caution:*** *Piranha reacts violently with organic compounds. Extreme care should be exercised when handling this mixture.*

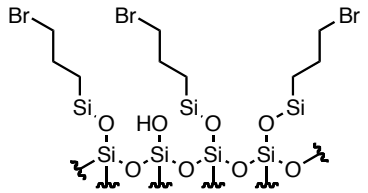

3-Bromopropyl-functionalized slides (65). A typical procedure is described. To a set of six pretreated glass or quartz slides submerged in 90 mL of dry dichloromethane was added 10.0 mL of 3-bromopropyltrichlorosilane via syringe. The solution was allowed to stand at room temperature for 1 h and the liquid was decanted. The slides were rinsed with 3 × 100 mL portions of dichloromethane, 3 × 100 mL portions of ethanol, 3 × 100 mL portions of Millipore water and dried overnight at 90 °C under a stream of dry nitrogen. The slides showed significantly reduced wettability as compared to unfunctionalized slides **64**. Samples were characterized by XPS and TOF-SIMS.

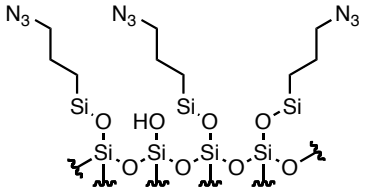

3-Azidopropyl-functionalized slides (66). A typical procedure is described. To a set of six of the corresponding 3-bromopropyl-functionalized glass or quartz slides in 100 mL of DMF was added 1.0 g of sodium azide. The solution was heated to 60 °C for 18-24 h and the solution was decanted. The slides were rinsed with 3 × 100 mL portions of DMF,

3 × 100 mL portions of Millipore water and dried for 24 h under a stream of dry nitrogen. The slides showed significantly increased wettability as compared to 3-bromopropyl-functionalized slides **65**. Samples were characterized by XPS and TOF-SIMS.

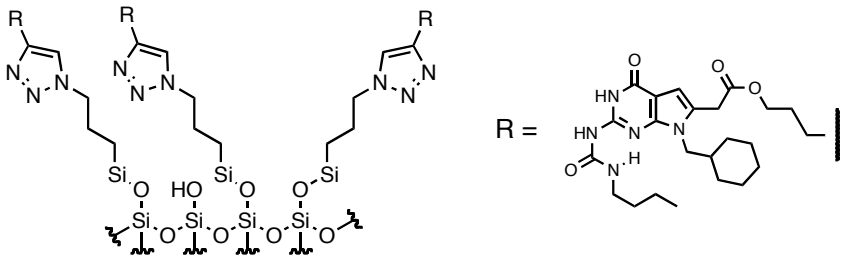

DeUG-functionalized slides (67). A typical procedure is described. To a set of six of the corresponding 3-azidopropyl-functionalized glass or quartz slides in 98 mL of DMF was added 100 mg (0.213 mmol) of DeUG pentynyl ester **21**. To this was added 3.4 mg of cupric sulfate and 17 mg of sodium ascorbate, each dissolved in 1 mL of water. The contents were heated to 60 °C for 18-24 h. The solution was decanted and the slides were washed with DMF (3 × 100 mL) and Millipore water (3 × 100 mL). The slides were rinsed with 100 mL of a 1% (v/v) aqueous solution of ammonium hydroxide to remove residual copper, followed by another rinse with Millipore water (3 × 100 mL). The slides were dried for 24 h under a stream of dry nitrogen. The slides showed significantly decreased wettability as compared to 3-azidopropyl-functionalized slides **66**. Samples were characterized by XPS and TOF-SIMS.

Piranha treated Si(111) wafers (68). To remove trace organic contaminants and to activate the surface, 1 cm × 1 cm Si(111) wafers were rinsed with ethyl acetate (3 × 10 mL), Millipore water (3 × 10 mL) and dried at 150 °C under a stream of dry nitrogen. Each wafer was immersed in 10 mL of freshly prepared Piranha (3:7 30% H_2O_2/H_2SO_4, v/v) for 30 min, rinsed with Millipore water (3 × 10 mL) and dried at 150 °C under a stream of dry nitrogen. Wafers were stored under dry nitrogen and used immediately after pretreatment. ***Caution:*** *Piranha reacts violently with organic compounds. Extreme care should be exercised when handling this mixture.*

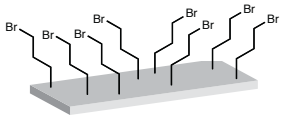

3-Bromopropyl-functionalized Si(111) wafers (69). A typical procedure is described. Each piranha-treated Si(111) wafer was submerged in 9 mL of dry dichloromethane. To this was added 1.0 mL of 3-bromopropyltrichlorosilane via syringe. The solution was allowed to stand at room temperature for 1 h and the liquid was decanted. The wafers were rinsed with 3 × 10 mL portions of dichloromethane, 3 × 10 mL portions of ethanol,

3 × 10 mL portions of Millipore water and dried overnight at 90 °C under a stream of dry nitrogen. Samples were characterized by XPS and TOF-SIMS.

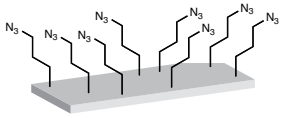

3-Azidopropyl-functionalized Si(111) wafers (70). A typical procedure is described. Each 3-bromopropyl-functionalized Si(111) wafer was placed in 10 mL of DMF. To this was added 0.10 g of sodium azide. The solution was heated to 60 °C for 18-24 h and the solution was decanted. The wafers were rinsed with 3 × 10 mL portions of DMF, 3 × 10 mL portions of Millipore water and dried for 24 h under a stream of dry nitrogen. Samples were characterized by XPS and TOF-SIMS.

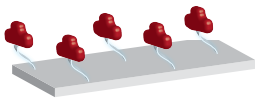

DeUG-functionalized Si(111) wafers (71). A typical procedure is described. Each of the 3-azidopropyl-functionalized Si(111) wafers was placed in 9 mL of DMF. To this was added 10 mg (0.0213 mmol) of DeUG pentynyl ester **21**. To this was added 0.50 mg of

cupric sulfate and 3.0 mg of sodium ascorbate, each dissolved in 0.5 mL of water. The contents were heated to 60 °C for 18-24 h. The solution was decanted and the wafers were washed with DMF (3 × 10 mL) and Millipore water (3 × 10 mL). The wafers were rinsed with 10 mL of a 1% (v/v) aqueous solution of ammonium hydroxide to remove residual copper, followed by another rinse with Millipore water (3 × 10 mL). The wafers were dried for 24 h under a stream of dry nitrogen. Samples were characterized by XPS and TOF-SIMS.

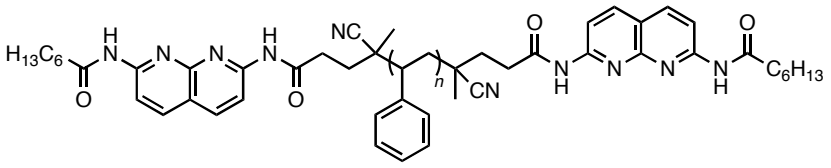

Chain-end DAN-functionalized polystyrene (73). To a solution of 53 mg (67 μmol) of **74** in 12 mL of DMSO was added 1.0 mL (8.64 mmol) of styrene. The contents were stirred and heated to 70 °C for 18 h. The flask was cooled to room temperature and the contents were concentrated *in vacuo*. The residue was dissolved in a minimum volume of methanol and the product precipitated via dropwise addition to cold (0 °C) pentane. The product was precipitated thrice more as above to afford 750 mg of **73** as an off-white powder: SEC (THF) M_w 19.8 kDa, M_n 14.6 kDa, PDI 1.36.

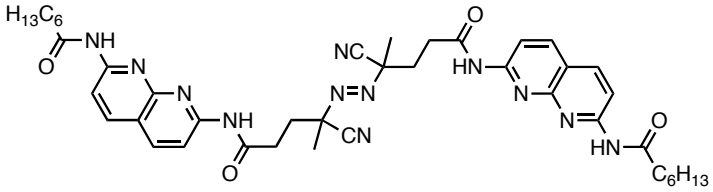

Heptanoic acid (7-{4-cyano-4-[1-cyano-3-(7-hexylamino-[1,8]naphthyridin-2-ylcarbamoyl)-1-methyl-propylazo]-4-methyl-butyrylamino}-[1,8]naphthyridin-2-yl)-amide (bisDAN ACVA, 74). To a stirred solution of 66 mg (0.24 mmol) of ACVA in 15 mL of THF was added 135 mg (0.50 mmol) of **30** and 7 mg (0.06 mmol) of DMAP. The contents were stirred for 10 min and 130 mg (0.68 mmol) of EDCI was added. The contents were allowed to stir for 20 h at room temperature. The contents were concentrated *in vacuo* and the residue was dissolved in 10 mL of chloroform, washed with 3 × 10 mL portions of water, dried over magnesium sulfate, gravity filtered and concentrated *in vacuo* to afford 168 mg (90%) of **74** as a pale yellow powder which was judged to be > 95% pure by ^{1}H NMR: mp 112-125 °C dec; ^{1}H NMR ($CDCl_3$) δ 8.44 (d, J = 8.7, 4H), 8.40 (d, J = 8.7, 4H), 6.42 (br s, 2H), 4.92 (br s, 2H), 2.81-2.23 (m, 12H), 1.71-0.99 (m, 22H), 0.77 (m, 6H); ^{13}C NMR ($CDCl_3$) δ 173.46, 154.79, 153.74, 139.13, 118.01, 114.30, 111.45, 71.77, 37.51, 32.80, 31.48, 28.87, 25.09, 23.41, 22.50, 14.05; ESI-HRMS calcd for $(C_{42}H_{52}N_{12}O_4 \cdot H)^+$ 789.4313, found 789.4294.

5.4 Analytical Methods

5.4.1 Isothermal Titration Calorimetry (ITC)

All ITC experiments were carried out using a Microcal, Inc. VP-ITC in the Microanalytical Laboratory at the University of Illinois at Urbana-Champaign. Although concentrations and experimental parameters varied from experiment to experiment, a typical ITC procedure is described. The reference cell was filled with the appropriate solvent ($CHCl_3$ or 5% DMSO/$CHCl_3$) after scrupulous rinsing and drying. $CHCl_3$ (stabilized with ethanol) was passed through a column of dry, activated basic alumina (Brockman I) and stored over 4 Å molecular sieves. DMSO was freshly distilled over CaH_2 under reduced pressure and stored over 4 Å molecular sieves. The sample cell was filled with a dilute solution of **17** (again, after rinsing and drying) and the syringe was filled with a solution of **4** at a concentration approximately 20 times that of the reference cell concentration. The titration was carried out using the following parameters: total injections, 25 to 40; injection volume, 5 μL; injection duration, 10 s; injection spacing, 180 s; cell temperature, 25 °C; and stirring speed, 300 rpm. The heat of dilution of the titrant ($CHCl_3$ or 5% DMSO/$CHCl_3$) was determined and subtracted from the data sets prior to using ORIGIN 5.0 software (Microcal, Inc.) to generate a binding curve via the single-site binding model. The fit of the binding curve reveals the association constant (K_{assoc}), enthalpy change (ΔH), entropy change (ΔS) and binding stoichiometry (n).

5.4.2 ^{1}H NMR Binding Studies

All ^{1}H NMR binding studies and van't Hoff experiments were performed under temperature control using a Varian INOVA 500NB (^{1}H, 500 MHz) spectrometer. All glassware was dried in an oven at 110 °C for at least 12 h and cooled in a vacuum dessicator prior to use. Syringes were dried in a vacuum dessicator under high vacuum for at least 12 h. $CDCl_3$ was passed through a column of dry, activated basic alumina (Brockman I) and stored over 4 Å molecular sieves. Data was fit to the appropriate non-linear equation for dilution and titration experiments.

5.4.3 Size Exclusion Chromatography (SEC)

Size exclusion chromatography (SEC) was performed using a Viscotek TDA Model 300 equipped with a Hitachi L-7250 autosampler and D-7000 interface.

5.4.4 Dynamic Light Scattering (DLS)

Dynamic light scattering (DLS) data was acquired using a Protein Solutions MSTC-800 equipped with a DynaPro 99-E-50 laser source operating at 855.1 nm. A typical procedure for gathering DLS data is described. A small amount (~ 10 mg) of the sample was dispersed in Millipore water via sonication for ca. 15 min. DLS data was acquired by taking preliminary scans and repeatedly diluting the sample until the sum-of-squares (SOS) was less than 100 for a minimum of 20 consecutive acquisitions.

5.4.5 Thermogravimetric Analysis (TGA)

All thermogravimetric analyses (TGA) were performed in the Microanalytical Laboratory at the University of Illinois at Urbana-Champaign using a Cahn Thermax 500 thermogravimetric analyzer. All samples were heated from 25 °C to 650 °C at a rate of 10 °C min^{-1} under a nitrogen atmosphere.

5.4.6 Atomic Force Microscopy (AFM)

All atomic force microscopy (AFM) was performed at the Frederick Seitz Materials Research Laboratory (FS-MRL) at the University of Illinois at Urbana-Champaign using an Asylum Research MFP-3D instrument in tapping mode with Tap30 tips.

5.4.7 Secondary Ion Mass Spectrometry (SIMS)

All secondary ion mass spectrometry (SIMS) was performed at the Frederick Seitz Materials Research Laboratory (FS-MRL) at the University of Illinois at Urbana-Champaign using a Physical Electronics PHI Trift III TOF-SIMS. In a typical experiment, data was collected in both positive and negative secondary modes for each sample.

5.4.8 X-Ray Photoelectron Spectroscopy (XPS)

All X-ray photoelectron spectroscopy (XPS) was performed at the Frederick Seitz Materials Research Laboratory (FS-MRL) at the University of Illinois at Urbana-Champaign using a Kratos Axis ULTRA instrument. In a typical experiment, a survey scan was collected prior to a quantitative scan.

5.4.9 Lap-Shear Experiments

In a typical experiment, 10 μL of a 10 mg mL^{-1} solution of the indicated polymer in dichloromethane was placed on the appropriately functionalized glass slide, followed by immediately placing another slide on top of this to create a 15 mm × 25 mm (375 mm^2) lap joint. The joints were then clamped in place and cured under dry nitrogen at ambient temperature for ca. 24 hours. The clamps were removed just prior to testing using an Instron 4400 load frame fitted with a 500 N load cell. Testing was performed at ambient conditions under displacement control (1 mm min^{-1}). Load was recorded as a function of displacement with the maximum load sustained being used in all calculations of shear strength.

References and Notes

(1) Wolf, K. L.; Frahm, F.; Harms, H. *Z.physik. Chem.* **1937**, *B36*, 237-287.

(2) Lehn, J.-M. *Supramolecular Chemistry*; VCH Press: New York, 1995.

(3) Onclin, S.; Ravoo, B. J.; Reinhoudt, D. N. *Angew. Chem. Int. Ed.* **2005**, *44*, 6282-6304.

(4) Descalzo, A. B.; Martinez-Manez, R.; Sancenon, F.; Hoffmann, K.; Rurack, K. *Angew. Chem. Int. Ed.* **2006**, *45*, 5924-5948.

(5) Love, J. C.; Estroff, L. A.; Kriebel, J. K.; Nuzzo, R. G.; Whitesides, G. M. *Chem. Rev.* **2005**, *105*, 1103-1169.

(6) Imahori, H.; Fukuzumi, S. *Adv. Func. Mater.* **2004**, *14*, 525-536.

(7) Jeffrey, G. A. *An Introduction to Hydrogen Bonding*; Oxford: New York, 1997.

(8) For reviews, see: (a) Sessler, J. L.; Jayawickramarajah, J. *Chem. Commun.* **2005**, 1939-1949. (b) Sivakova, S.; Rowan, S. J. *Chem. Soc. Rev.* **2005**, *34*, 9-21. (c) Sijbesma, R. P.; Meijer, E. W. *Chem. Commun.* **2003**, 5-16. (d) Prins, L. J.; Reinhoudt, D. N; Timmerman, P. *Angew. Chem. Int. Ed.* **2001**, *40*, 2382-2426. (e) Sherrington, D. C.; Taskinen, K. A. *Chem. Soc. Rev.* **2001**, *30*, 83-93. (f) Krische, M. J.; Lehn, J.-M. *Struc. Bond.* **2000**, *96*, 3-29. (g) Meléndez, R. E.; Carr, A. J.; Linton, B. R.; Hamilton, A. D. *Struc. Bond.* **2000**, *96*, 31-61. (h) Zimmerman, S. C.; Corbin, P. S. *Struc. Bond.* **2000**, *96*, 63-94. (i) Kato, T. *Struc. Bond.* **2000**, *96*, 95-146. (j) Lawrence, D. S.; Jiang, T.; Levett, M. *Chem. Rev.* **1995**, *95*, 2229-2260.

(9) Feldman, K. E.; Kade, M. J.; de Greef, T. F. A.; Meijer, E. W.; Kramer, E. J.; Hawker, C. J. *Macromolecules* **2008**, *41*, 4694-4700.

(10) de Greef, T. F. A.; Ercolani, G.; Ligthart, G. B. W. L.; Meijer, E. W.; Sijbesma, R. P. *J. Am. Chem Soc.* **2008,** *130*, 13755-13764.

(11) Sijbesma, R. P.; Beijer, F. H.; Brunsveld, L.; Folmer, B. J. B.; Hirshberg, J. H. K. K.; Lange, R. F. M.; Lowe, J. K. L.; Meijer, E. W. *Science* **1997**, *278*, 1601-1604.

(12) Corbin, P. S.; Zimmerman, S. C. *J. Am. Chem. Soc.* **1998**, *120*, 9710-9711.

(13) Lafitte, V. G. H.; Aliev, A. E.; Horton, P. N.; Hursthouse, M. B.; Bala, K.; Golding, P.; Hailes, H. C. *J. Am. Chem. Soc.* **2006**, *128*, 6544-6545.

(14) Wang, X.-Z.; Li, X.-Q.; Shao, X.-B.; Zhao, X.; Deng, P.; Jiang, X.-K.; Li, Z.-T.; Chen, Y.-Q. *Chem. Eur. J.* **2003**, *9*, 2904-2913.

(15) Todd, E. M.; Quinn, J. R.; Park, T.; Zimmerman, S. C. *Isr. J. Chem.* **2005**, *45*, 381-389.

(16) Park, T.; Zimmerman, S. C.; Nakashima, S. *J. Am. Chem Soc.* **2005**, *127*, 6520-6521.

(17) Park, T.; Nakashima, S.; Todd, E. J.; Zimmerman, S. C. *J. Am. Chem Soc.* **2005**, *127*, 18133-18142.

(18) Ong, H. C.; Zimmerman, S. C. *Org. Lett.* **2006**, *8*, 1589-1592.

(19) Or, more accurately, “vacuum-state”.

(20) Murray, T. J. *Synthesis and Complexation Studies of Heterocyclic Compounds with Two or Three Contiguous Hydrogen Bonding Sites,* Doctoral Thesis, University of Illinois at Urbana-Champaign, 1994.

(21) Park, T., University of Illinois at Urbana-Champaign, Urbana, IL. Personal communication.

(22) Jorgensen, W. L.; Pranata, J. *J. Am. Chem. Soc.* **1990**, *112*, 2008-2010.

(23) Appleton, W. C.; Parziale, P. A. Eur. Pat. WO9507265, 1995.

(24) Burgdorf, L. T.; Carell, T. *Chem. Eur. J.* **2002**, *8*, 293-301.

(25) Suckling, C. J.; Gibson, C. L.; La Rosa, S.; Ohta, K.; Boyle, P. H.; Leurquin, F.; Lemacon, A. *Tetrahedron* **2004**, *60*, 943-959.

(26) Gangjee, A.; Dubash, N. P.; Kisliuk, R. L. *J. Heterocycl. Chem.* **2001**, *38*, 349-54.

(27) Kuykendall, D. W.; Anderson, C. A.; Zimmerman, S. C. *Org. Lett.* **2009**, *11*, 61-64.

(28) Kolb, H. C.; Finn, M. G.; Sharpless, K. B. *Angew. Chem. Int. Ed.* **2001**, *40*, 2004-2021.

(29) Moore, J. S.; Stupp, S. I. *Macromolecules* **1990**, *23*, 65-70.

(30) Connors, K. A. *Binding Constants*; Wiley Interscience: New York, 1987.

(31) Hirose, K. *J. Inclusion Phenom. Macrocyclic Chem.* **2001**, *39*, 193-209.

(32) Quinn, J. R. *DNA Base and Base Analogue Pairing in Organic Solvents*, Doctoral Thesis, University of Illinois at Urbana-Champaign, 2005.

(33) ORTEP representations were created using ORTEP-3 for Windows, see: Farrugia, L. J. *J. Appl. Cryst* **1997**, *30*, 565.

(34) Newkome, G. R.; Garbis, S. J.; Majestic, V. K.; Fronczek, F. R.; Chiari, G. *J. Org. Chem.* **1981**, *46*, 833-839.

(35) Corbin, P. S.; Zimmerman, S. C.; Thiessen, P. A.; Hawryluk, N. A.; Murray, T. J. *J. Am. Chem. Soc.* **2001**, *123*, 10475-10488.

(36) Park, T.; Mayer, M. F.; Nakashima, S.; Zimmerman, S. C. *Synlett* **2005**, *9*, 1435-1436.

(37) Li, X.-Q.; Jiang, X.-K.; Wang, X.-Z.; Li, Z.-T. *Tetrahedron* **2004**, *60*, 2063-2069.

(38) Goswami, S.; Mukherjee, R.; Mukherjee, R.; Jana, S.; Maity, A. C.; Adak, A. K. *Molecules* **2005**, *10*, 929-936.

(39) Ligthart, G. B. W. L.; Ohkawa, H.; Sijbesma, R. P.; Meijer, E. W. *J.* Org. Chem. **2006**, 71, 375-378.

(40) Anderson, C. A.; Taylor, P. G.; Zeller, M. A.; Zimmerman, S. C. *J. Org. Chem.* **ASAP**, DOI: 10.1021/jo100476x.

(41) Tellinghuisen, J. *J. Phys. Chem. B* **2005**.

(42) For complete crystallographic structure data, see*:* Ong, H. C. *The Utility of 7-Deazaguanine: Part I. High Affinity, High Fidelity Modules for Supramolecular Chemistry*, Doctoral Thesis, University of Illinois at Urbana-Champaign, 2007.

(43) Todd, E. M.; Zimmerman, S. C. *J. Am. Chem. Soc.* **2007**, *129*, 14534-14535.

(44) Todd, E. M.; Zimmerman, S. C. *Tetrahedron* **2008**, *64*, 8558-8570.

(45) Corbin, P. S.; Zimmerman, S. C. *J. Am. Chem. Soc.* **1998**, *120*, 9710-9711.

(46) Todd, E. M. *Supramolecular Star Polymers Based on Ditopic Hydrogen-Bonding Modules*, Doctoral Thesis, University of Illinois at Urbana-Champaign, 2007.

(47) Goswami, S.; Dey, S.; Gallagher, J. F.; Lough, A. J.; Garcia-Granda, S.; Torre-Fernandez, L.; Alkorta, I.; Elguero, J. *J. Mol. Struc.* **2007**, *846*, 97-107.

(48) McKay, J. M. *The Utility of 7-Deazaguanine: Part II. Adenosine Receptors with Simultaneous Watson-Crick and Hoogsteen Binding*, Doctoral Thesis, University of Illinois at Urbana-Champaign, 2007.

(49) Isayev, A. I.; Modic, M. *Poly. Comp.* **1987**, *8*, 158-175.

(50) Armstrong, G.; Buggy M. *Mater. Sci. Eng., C* **2001**, *18*, 45-49.

(51) Armstrong, G.; Buggy M. *Polym. Int.* **2002**, *51*, 1219-1224.

(52) De Greef, T. F. A.; Smulders, M. M. J.; Wolffs, M.; Schenning, A. P. H. J.; Sijbesma, R. P.; Meijer, E. W. *Chem. Rev.* **2009**, *109*, 5687-5754.

(53) Brunsveld, L.; Folmer, B. J. B.; Meijer, E. W.; Sijbesma, R. P. *Chem. Rev.* **2001**, *101*, 4071-4097.

(54) Park, T.; Zimmerman, S. C. *J. Am. Chem. Soc.* **2006**, *128*, 13986-13987.

(55) For reviews, see: (a) George, M.; Weiss, R. G. *Acc. Chem. Res.* **2006**, *39*, 489-497. (b) Hirst, A. R.; Smith, D. K. *Chem. Eur. J.* **2005**, *11*, 5496-5508. (c) Sangeetha, N. M.; Maitra, U. *Chem. Soc. Rev.* **2005**, *34*, 821-836. (d) Estroff, L. A.; Hamilton, A. D. *Chem. Rev.* **2004**, *103*, 1201-1217. (e) van Esch, J.; Feringa, B. L. *Angew. Chem. Int. Ed.* **2000**, *39*, 2263-2354. (f) Terech, P.; Weiss, R. G. *Chem. Rev.* **1997**, *97*, 3133-3160.

(56) Flory, P. J. *Faraday Discuss.* **1974**, *57*, 7-18.

(57) Deng, W.; Yamaguchi, H.; Takashima, Y.; Harada, A. *Angew. Chem. Int. Ed.* **2007**, *46*, 5144-5147 and references therein.

(58) (a) Molard, Y.; Bassani, D. M.; Desvergne, J.-P.; Horton, P. N.; Hursthouse, M. B.; Tucker, J. H. R. *Angew. Chem. Int. Ed.* **2005**, *44*, 1072-1075. (b) Molard, Y.; Bassani, D. M.; Desvergne, J.-P.; Moran, N.; Tucker, J. H. R. *J. Org. Chem.* **2006**, *71*, 8523-8531.

(59) Chang, S.-K.; Hamilton, A. D.; *J. Am. Chem. Soc.* **1988**, *110*, 1318-1319.

(60) (a) Bouas-Laurent, H.; Castellan, A.; Desvergne, J.-P.; Lapouyadec, R. *Chem. Soc. Rev.* **2000**, *29*, 43-55 and *Chem. Soc. Rev.* **2001**, *30*, 248-263. (b) Becker, H.-D. *Chem. Rev.* **1993**, *93*, 145-172.

(61) The concentration was always kept under 5 mM to suppress intermolecular dimerization.

(62) Thermal cycloreversion was chosen as high-power 280 nm light-emitting diode arrays become prohibitively expensive. Moreover, photochemical cycloreversion results in a photostationary state of ~20% dimer (see ref. 60).

(63) Burd, C.; Weck, M. *Macromolecules* **2005**, *38*, 7225-7230.

(64) Yamauchi, K.; Lizotte, J. R.; Long, T. E. *Macromolecules* **2003**, *36*, 1083-1088.

(65) Elias, H.-G. *An Introduction to Plastics*; Wiley-VCH: Weinheim, 2003.

(66) Baron, R.; Huang, C.-H.; Bassani, D. M.; Onopriyenko, A.; Zayats, M.; Willner, I. *Angew. Chem. Int. Ed.* **2005**, *44*, 4010-4015.

(67) Gauchet, C.; Labadie, G. R.; Poulter, C. D. *J. Am. Chem. Soc.* **2006**, *128*, 9274-9275.

(68) Basabe-Desmonts, L.; Beld, J.; Zimmerman, R. S.; Hernando, J.; Mela, P.; GarciaParajo, M. F.; vanHulst, N. F.; vandenBerg, A.; Reinhoudt, D. N.; Crego-Calama, M. *J. Am. Chem. Soc.* **2004**, *126*, 7293-7299.

(69) Cui, Y.; Wei, Q.; Park, H.; Lieber, C. M. *Science* **2001**, *293*, 1289-1292.

(70) Blodgett, K. B. *J. Am. Chem. Soc.* **1934**, *56*, 495-495.

(71) Blodgett, K. B.; Langmuir, I. *Phys. Rev.* **1937**, *51*, 964-982.

(72) Decher, G. *Science* **1997**, *277*, 1232-1237.

(73) Stockton, W. B.; Rubner, M. F. *Macromolecules* **1997**, *30*, 2717-2725.

(74) Liang, Z.; Cabarcos, O. M.; Allara, D. L.; Wang, Q. *Adv. Mater.* **2004**, *16*, 823-827.

(75) Stober, W.; Fink, A.; Bohn, E. *J. Colloid Interface Sci.* **1968**, *26*, 62-69.

(76) Kim, J. H.; Chung, H. W.; Lee, T. R. *Chem. Mater.* **2006**, *18*, 4115-4120.

(77) DeGrado, W. F.; Kaiser, E. T. *J. Org. Chem.* **1980**, *45*, 1295-1300.

(78) Gruijters, B. W. T.; Broeren, M. A. C.; van Delft, F. L.; Sijbesma, R. P.; Hermkens, P. H. H.; Rutjes, F. P. J. T. *Org. Lett.* **2006**, *8*, 3163-3166.

(79) *Piranha is a strong oxidizing agent and can react violently with even trace amounts of organic compounds. Extreme care should be exercised when handling this solution.* For safe handling and disposal guidelines, see: http:// www.drs.illinois.edu/css/factsheets/PiranhaWaste.aspx.

(80) Eske, L. D.; Galipeau, D. W. *Colloids Surf., A* **1999**, *154*, 33-51.

(81) Ulman, A. *Chem. Rev.* **1996**, *96*, 1533-1554.

(82) Lummerstorfer, T.; Hoffmann, H. *J. Phys. Chem. B* **2004**, *108*, 3963-3966.

(83) Griffiths, J. *Anal. Chem.* **2008,** *80,* 7194–7197.

(84) Loh, F. C.; Tan, K. L.; Kang, E. T.; Neoh, K. G.; Pun, M. Y.*J. Vac. Sci.Technol., A* **1994**, *12*, 2705-2710.

(85) Wagner, C. D. *J. Electron Spectrosc. Relat. Phenom.* **1983**, *32*, 99-102.

(86) Liehr, M.; Thiry, P. A.; Pireaux, J. J.; Caudano, R. *Phys. Rev. B* **1986**, *33*, 5682-5697.

(87) Werner, H. W.; Warmoltz, N. *J. Vac. Sci. Technol., A* **1984**, *2*, 726-731.

(88) Wollman, E. W.; Kang, D.; Frisbie, C. D.; Lorkovic, I. M.; Wrighton, M. S. *J. Am. Chem. Soc.* **1994**, *116*, 4395-4404.

(89) Sano, M.; Wada, M.; Miyamoto, A.; Yoshimura, S. *Thin Solid Films* **1996**, *284*, 249-251.

(90) Schulze, R. K.; Boyd, D. C.; Evans, J. F.; Gladfelter, W. L. *J. Vac. Sci. Technol., A* **1990**, *8*, 2338-2343.

(91) Prakash, S; Long, T. M.; Selby, J. C.; Moore, J. S.; Shannon, M. A. *Anal. Chem.* **2007,** *79*, 1661-1667.

(92) Haensch, C.; Chiper, M.; Ulbricht, C.; Winter, A.; Hoeppener, S.; Schubert, U. S. *Langmuir* **2008**, *24*, 12981-12985.

(93) Xu, H.; Norsten, T. B.; Uzun, O.; Jeoung, E.; Rotello, V. M. *Chem. Commun.* **2005**, *41*, 5157-5159 and references therein.

(94) Fengge, G. *Materials Today* **2004**, 50-55.

(95) Vaia, R. A.; Maguire, J. F. *Chem. Mater.* **2007**, *19,* 2736-2751.

(96) Duan, H.; Wang, D.; Kurth, D. G.; Mohwald, H. *Angew. Chem. Int. Ed.* **2004**, *43,* 5639-5642.

(97) Park, S. Y.; Cho, Y. H.; Vaia, R. A. *Macromolecules* **2005**, *38,* 1729-1735.

(98) Podsiadlo, P.; Kaushik, A. K.; Arruda, E. M.; Waas, A. M.; Shim, B. S.; Xu, J.; Nandivada, H.; Pumplin, B. G.; Lahann, J.; Ramamoorthy, A.; Kotov, N. A. *Science* **2007**, *318*, 80-83.

(99) Jang, B. Z. *Advanced Polymer Composites: Principles and Applications*, ASM International: Materials Park, 1994.

(100) DiBenedetto, A. T. *Mat. Sci. Eng., A* **2001**, 74-82.

(101) Somnuk, U.; Yanumet, N.; Ellis, J. W. *Polym. Compos.* **2003**, *24*, 171-180.

(102) Lee, H.; Lee, B. P.; Messersmith, P. B. *Nature* **2007**, *448*, 338-334.

(103) Kersey, F. R.; Lee, G.; Marszalek, P.; Craig, S. L. *J. Am. Chem. Soc.* **2004**, *126*, 3038-3039.

(104) Jo, T. S.; Kim, S. H.; Shin, J.; Bae, C. *J. Am. Chem. Soc.* **2009**, *131*, 1656-1657.

(105) Shin, J.; Jensen, S. M.; Ju, J.; Lee, S.; Xue, Z.; Noh, S. K.; Bae, C. *Macromolecules* **2007**, *40*, 8600-8608.

(106) Liu, Y.; Diaz, D. D.; Accurso, A. A.; Sharpless, K. B.; Fokin, V. V.; Finn, M. G. *J. Polym. Sci., Part A: Polym. Chem.* **2007**, *45*, 5182-5189.

(107) Park, T; Zimmerman, S. C. *J. Am. Chem. Soc.* **2006**, *128*, 11582-11590.

(108) Still, W. C.; Kahn, M.; Mitra, A. *J. Org. Chem.* **1978**, *43*, 2923-2925.

(109) Lee, J. W.; Jun, S. I.; Kim, K. *Tet. Lett.* **2001**, *42*, 2709-2711.

(110) Waddell, T. G.; Leyden, D. E.; DeBello, M. T. *J. Am. Chem. Soc.* **1981**, *103*.

(111) Lipshutz, B. H.; Blomgren, P. A. *Org. Lett.* **2001**, *3*, 1869-1871.

Appendix A

X-ray Crystallographic Structure Data

A.1 Compound 17

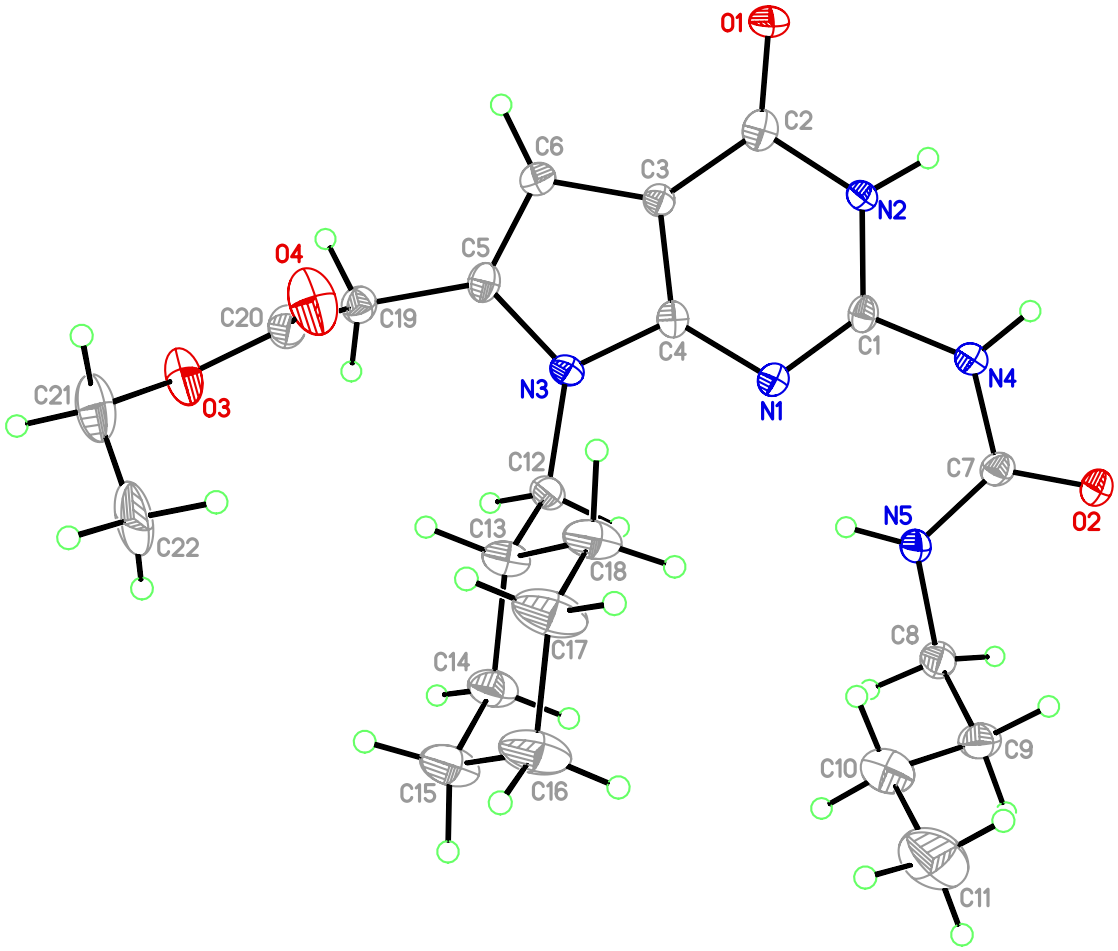

Table A.1. Crystal data and structure refinement for DeUG **17**.

Identification code	ba77bas	
Empirical formula	$C_{22}H_{33}N_5O_4$	
Formula weight	431.53	
Temperature	193(2) K	
Wavelength	0.71073 Å	
Crystal system	Orthorhombic	
Space group	P b c a	
Unit cell dimensions	a = 8.0384(7) Å	α= 90°.
	b = 16.6403(15) Å	β= 90°.
	c = 33.381(3) Å	γ = 90°.
Volume	4465.1(7) $Å^3$	
Z	8	
Density (calculated)	1.284 Mg/m^3	
Absorption coefficient	0.090 mm^{-1}	
F(000)	1856	
Crystal size	0.12 x 0.11 x 0.02 mm^3	
Theta range for data collection	2.44 to 25.38°.	
Index ranges	-9<=h<=9, -20<=k<=20, -40<=l<=40	
Reflections collected	52171	
Independent reflections	4092 [R(int) = 0.3328]	
Completeness to theta = 25.38°	99.8 %	
Absorption correction	Integration	
Max. and min. transmission	0.9982 and 0.9875	
Refinement method	Full-matrix least-squares on F^2	
Data / restraints / parameters	4092 / 272 / 366	
Goodness-of-fit on F^2	0.993	
Final R indices [I>2sigma(I)]	R1 = 0.0618, wR2 = 0.1079	
R indices (all data)	R1 = 0.1977, wR2 = 0.1533	
Largest diff. peak and hole	0.223 and -0.278 $e.Å^{-3}$	

Table A.2. Atomic coordinates ($\times 10^4$) and equivalent isotropic displacement parameters ($Å^2 \times 10^3$) for **17**. U(eq) is defined as one third of the trace of the orthogonalized U^{ij} tensor.

Atom	x	y	z	U(eq)
C(1)	4328(4)	8630(2)	376(1)	22(1)
C(2)	7033(5)	8864(2)	53(1)	25(1)
C(3)	7008(4)	9606(2)	259(1)	20(1)
C(4)	5676(4)	9760(2)	514(1)	21(1)
C(5)	7385(4)	10817(2)	539(1)	24(1)
C(6)	8069(5)	10289(2)	279(1)	26(1)
C(7)	1463(5)	8195(2)	575(1)	24(1)
C(8)	-357(5)	8982(2)	1006(1)	31(1)
C(9)	-392(5)	8588(2)	1414(1)	33(1)
C(10)	776(5)	8960(3)	1712(1)	46(1)
C(11)	778(7)	8533(3)	2119(1)	73(2)
C(12)	4751(4)	10859(2)	976(1)	26(1)
C(13)	5353(8)	10836(3)	1410(1)	33(2)
C(14)	4072(8)	11193(3)	1691(1)	39(2)
C(15)	4634(8)	11169(3)	2125(1)	50(2)
C(16)	5093(9)	10319(4)	2251(2)	55(2)
C(17)	6378(9)	9960(4)	1971(2)	57(2)
C(18)	5790(7)	9982(3)	1536(1)	43(2)
C(19)	7998(4)	11630(2)	648(1)	27(1)
C(20)	9108(5)	11678(3)	1007(1)	32(1)
C(21)	10220(20)	12589(8)	1486(4)	57(3)
C(22)	9450(40)	12273(16)	1863(3)	64(4)
N(1)	4333(3)	9279(2)	590(1)	23(1)
N(2)	5574(4)	8406(2)	118(1)	22(1)
N(3)	5895(3)	10495(2)	689(1)	22(1)
N(4)	3015(4)	8092(2)	390(1)	24(1)
N(5)	1224(4)	8846(2)	798(1)	28(1)
O(1)	8140(3)	8582(2)	-165(1)	31(1)
O(2)	396(3)	7666(2)	520(1)	30(1)
O(3)	9200(3)	12442(2)	1136(1)	45(1)
O(4)	9855(4)	11136(2)	1160(1)	53(1)

Table A.2 (cont.)

C(23)	5030(40)	10564(18)	1405(4)	39(3)
C(24)	3680(40)	10936(17)	1681(4)	41(3)
C(25)	3760(30)	10615(16)	2099(6)	48(3)
C(26)	6790(40)	10308(17)	2009(8)	50(3)
C(27)	5480(30)	10733(17)	2274(8)	50(3)
C(28)	6600(20)	10592(15)	1567(4)	40(3)
C(29)	10491(17)	12624(7)	1424(4)	55(2)
C(30)	9940(30)	12495(14)	1847(3)	64(3)

Table A.3. Bond lengths (Å) for **17**.

Bond	Length	Bond	Length	Bond	Length
C(1)-N(1)	1.295(4)	C(9)-C(10)	1.501(5)	C(14)-H(14B)	0.9900
C(1)-N(2)	1.372(4)	C(9)-H(9A)	0.9900	C(15)-C(16)	1.521(6)
C(1)-N(4)	1.385(4)	C(9)-H(9B)	0.9900	C(15)-H(15A)	0.9900
C(2)-O(1)	1.242(4)	C(10)-C(11)	1.534(6)	C(15)-H(15B)	0.9900
C(2)-N(2)	1.415(4)	C(10)-H(10A)	0.9900	C(16)-C(17)	1.516(6)
C(2)-C(3)	1.414(5)	C(10)-H(10B)	0.9900	C(16)-H(16A)	0.9900
C(3)-C(4)	1.391(5)	C(11)-H(11A)	0.9800	C(16)-H(16B)	0.9900
C(3)-C(6)	1.422(5)	C(11)-H(11B)	0.9800	C(17)-C(18)	1.528(6)
C(4)-N(3)	1.368(4)	C(11)-H(11C)	0.9800	C(17)-H(17A)	0.9900
C(4)-N(1)	1.368(4)	C(12)-N(3)	1.459(4)	C(17)-H(17B)	0.9900
C(5)-C(6)	1.352(5)	C(12)-C(13)	1.529(5)	C(18)-H(18A)	0.9900
C(5)-N(3)	1.405(4)	C(12)-C(23)	1.531(10)	C(18)-H(18B)	0.9900
C(5)-C(19)	1.484(5)	C(12)-H(12C)	0.9900	C(19)-C(20)	1.497(5)
C(6)-H(6)	0.9500	C(12)-H(12D)	0.9900	C(19)-H(19A)	0.9900
C(7)-O(2)	1.243(4)	C(12)-H(12A)	0.9922	C(19)-H(19B)	0.9900
C(7)-N(5)	1.328(5)	C(12)-H(12B)	0.9921	C(20)-O(4)	1.198(4)
C(7)-N(4)	1.401(4)	C(13)-C(14)	1.513(6)	C(20)-O(3)	1.344(5)
C(8)-N(5)	1.466(4)	C(13)-C(18)	1.522(5)	C(21)-O(3)	1.448(7)
C(8)-C(9)	1.513(5)	C(13)-H(13A)	1.0000	C(21)-C(22)	1.495(9)
C(8)-H(8A)	0.9900	C(14)-C(15)	1.520(6)	C(21)-H(21A)	0.9900
C(8)-H(8B)	0.9900	C(14)-H(14A)	0.9900	C(21)-H(21B)	0.9900

Table A.3 (cont.)

C(22)-H(22A)	0.9800	C(24)-C(25)	1.50(3)	C(27)-H(27A)	0.9900
C(22)-H(22B)	0.9800	C(24)-H(24A)	0.9900	C(27)-H(27B)	0.9900
C(22)-H(22C)	0.9800	C(24)-H(24B)	0.9900	C(28)-H(28A)	0.9900
N(2)-H(2)	0.90(2)	C(25)-C(27)	1.51(4)	C(28)-H(28B)	0.9900
N(4)-H(4)	0.89(2)	C(25)-H(25A)	0.9900	C(29)-C(30)	1.496(8)
N(5)-H(5)	0.88(2)	C(25)-H(25B)	0.9900	C(29)-H(29A)	0.9900
O(3)-C(29)	1.447(7)	C(26)-C(27)	1.55(3)	C(29)-H(29B)	0.9900
C(23)-C(28)	1.37(3)	C(26)-C(28)	1.56(3)	C(30)-H(30A)	0.9800
C(23)-C(24)	1.55(3)	C(26)-H(26A)	0.9900	C(30)-H(30B)	0.9800
C(23)-H(23A)	1.0000	C(26)-H(26B)	0.9900	C(30)-H(30C)	0.9800

Table A.4. Bond angles (°) for **17**.

Atoms	Angle	Atoms	Angle
N(1)-C(1)-N(2)	124.8(3)	N(5)-C(7)-N(4)	118.3(3)
N(1)-C(1)-N(4)	121.4(3)	N(5)-C(8)-C(9)	112.1(3)
N(2)-C(1)-N(4)	113.8(3)	N(5)-C(8)-H(8A)	109.2
O(1)-C(2)-N(2)	118.7(4)	C(9)-C(8)-H(8A)	109.2
O(1)-C(2)-C(3)	128.7(4)	N(5)-C(8)-H(8B)	109.2
N(2)-C(2)-C(3)	112.6(3)	C(9)-C(8)-H(8B)	109.2
C(4)-C(3)-C(2)	118.0(3)	H(8A)-C(8)-H(8B)	107.9
C(4)-C(3)-C(6)	106.6(3)	C(10)-C(9)-C(8)	114.0(3)
C(2)-C(3)-C(6)	135.4(4)	C(10)-C(9)-H(9A)	108.8
N(3)-C(4)-N(1)	123.1(3)	C(8)-C(9)-H(9A)	108.8
N(3)-C(4)-C(3)	109.1(3)	C(10)-C(9)-H(9B)	108.8
N(1)-C(4)-C(3)	127.8(3)	C(8)-C(9)-H(9B)	108.8
C(6)-C(5)-N(3)	109.1(3)	H(9A)-C(9)-H(9B)	107.7
C(6)-C(5)-C(19)	127.9(3)	C(9)-C(10)-C(11)	113.4(4)
N(3)-C(5)-C(19)	122.9(3)	C(9)-C(10)-H(10A)	108.9
C(5)-C(6)-C(3)	107.8(3)	C(11)-C(10)-H(10A)	108.9
C(5)-C(6)-H(6)	126.1	C(9)-C(10)-H(10B)	108.9
C(3)-C(6)-H(6)	126.1	C(11)-C(10)-H(10B)	108.9
O(2)-C(7)-N(5)	124.1(3)	H(10A)-C(10)-H(10B)	107.7
O(2)-C(7)-N(4)	117.6(4)	C(10)-C(11)-H(11A)	109.5

Table A.4 (cont.)

C(10)-C(11)-H(11B)	109.5	C(16)-C(15)-H(15B)	109.4
H(11A)-C(11)-H(11B)	109.5	H(15A)-C(15)-H(15B)	108.0
C(10)-C(11)-H(11C)	109.5	C(17)-C(16)-C(15)	111.3(4)
H(11A)-C(11)-H(11C)	109.5	C(17)-C(16)-H(16A)	109.4
H(11B)-C(11)-H(11C)	109.5	C(15)-C(16)-H(16A)	109.4
N(3)-C(12)-C(13)	114.3(3)	C(17)-C(16)-H(16B)	109.4
N(3)-C(12)-C(23)	112.9(11)	C(15)-C(16)-H(16B)	109.4
N(3)-C(12)-H(12C)	109.0	H(16A)-C(16)-H(16B)	108.0
C(23)-C(12)-H(12C)	109.0	C(16)-C(17)-C(18)	111.4(4)
N(3)-C(12)-H(12D)	109.0	C(16)-C(17)-H(17A)	109.3
C(23)-C(12)-H(12D)	109.0	C(18)-C(17)-H(17A)	109.3
H(12C)-C(12)-H(12D)	107.8	C(16)-C(17)-H(17B)	109.3
N(3)-C(12)-H(12A)	108.5	C(18)-C(17)-H(17B)	109.3
C(13)-C(12)-H(12A)	109.1	H(17A)-C(17)-H(17B)	108.0
N(3)-C(12)-H(12B)	108.9	C(13)-C(18)-C(17)	110.8(4)
C(13)-C(12)-H(12B)	108.2	C(13)-C(18)-H(18A)	109.5
C(23)-C(12)-H(12B)	124.5	C(17)-C(18)-H(18A)	109.5
H(12A)-C(12)-H(12B)	107.6	C(13)-C(18)-H(18B)	109.5
C(14)-C(13)-C(18)	110.7(4)	C(17)-C(18)-H(18B)	109.5
C(14)-C(13)-C(12)	111.2(4)	H(18A)-C(18)-H(18B)	108.1
C(18)-C(13)-C(12)	111.0(4)	C(5)-C(19)-C(20)	116.2(3)
C(14)-C(13)-H(13A)	107.9	C(5)-C(19)-H(19A)	108.2
C(18)-C(13)-H(13A)	107.9	C(20)-C(19)-H(19A)	108.2
C(12)-C(13)-H(13A)	107.9	C(5)-C(19)-H(19B)	108.2
C(13)-C(14)-C(15)	112.2(4)	C(20)-C(19)-H(19B)	108.2
C(13)-C(14)-H(14A)	109.2	H(19A)-C(19)-H(19B)	107.4
C(15)-C(14)-H(14A)	109.2	O(4)-C(20)-O(3)	123.2(4)
C(13)-C(14)-H(14B)	109.2	O(4)-C(20)-C(19)	126.9(4)
C(15)-C(14)-H(14B)	109.2	O(3)-C(20)-C(19)	109.8(4)
H(14A)-C(14)-H(14B)	107.9	O(3)-C(21)-C(22)	112.9(7)
C(14)-C(15)-C(16)	111.0(4)	O(3)-C(21)-H(21A)	109.0
C(14)-C(15)-H(15A)	109.4	C(22)-C(21)-H(21A)	109.0
C(16)-C(15)-H(15A)	109.4	O(3)-C(21)-H(21B)	109.0
C(14)-C(15)-H(15B)	109.4	C(22)-C(21)-H(21B)	109.0

Table A.4 (cont.)

H(21A)-C(21)-H(21B)	107.8	H(25A)-C(25)-H(25B)	108.1
C(1)-N(1)-C(4)	112.9(3)	C(27)-C(26)-C(28)	110(2)
C(1)-N(2)-C(2)	123.7(3)	C(27)-C(26)-H(26A)	109.8
C(1)-N(2)-H(2)	122(2)	C(28)-C(26)-H(26A)	109.7
C(2)-N(2)-H(2)	114(2)	C(27)-C(26)-H(26B)	109.7
C(4)-N(3)-C(5)	107.4(3)	C(28)-C(26)-H(26B)	109.7
C(4)-N(3)-C(12)	124.8(3)	H(26A)-C(26)-H(26B)	108.2
C(5)-N(3)-C(12)	127.8(3)	C(25)-C(27)-C(26)	110(2)
C(1)-N(4)-C(7)	128.0(3)	C(25)-C(27)-H(27A)	109.7
C(1)-N(4)-H(4)	121(2)	C(26)-C(27)-H(27A)	109.7
C(7)-N(4)-H(4)	110(2)	C(25)-C(27)-H(27B)	109.7
C(7)-N(5)-C(8)	121.2(3)	C(26)-C(27)-H(27B)	109.7
C(7)-N(5)-H(5)	120(2)	H(27A)-C(27)-H(27B)	108.2
C(8)-N(5)-H(5)	119(2)	C(23)-C(28)-C(26)	117(2)
C(20)-O(3)-C(29)	116.7(6)	C(23)-C(28)-H(28A)	108.1
C(20)-O(3)-C(21)	116.7(6)	C(26)-C(28)-H(28A)	108.1
C(28)-C(23)-C(12)	119.4(19)	C(23)-C(28)-H(28B)	108.1
C(28)-C(23)-C(24)	113(2)	C(26)-C(28)-H(28B)	108.1
C(12)-C(23)-C(24)	108.9(16)	H(28A)-C(28)-H(28B)	107.3
C(28)-C(23)-H(23A)	104.5	O(3)-C(29)-C(30)	112.6(7)
C(12)-C(23)-H(23A)	104.5	O(3)-C(29)-H(29A)	109.1
C(24)-C(23)-H(23A)	104.5	C(30)-C(29)-H(29A)	109.1
C(25)-C(24)-C(23)	112(2)	O(3)-C(29)-H(29B)	109.1
C(25)-C(24)-H(24A)	109.1	C(30)-C(29)-H(29B)	109.1
C(23)-C(24)-H(24A)	109.1	H(29A)-C(29)-H(29B)	107.8
C(25)-C(24)-H(24B)	109.1	C(29)-C(30)-H(30A)	109.5
C(23)-C(24)-H(24B)	109.1	C(29)-C(30)-H(30B)	109.5
H(24A)-C(24)-H(24B)	107.9	H(30A)-C(30)-H(30B)	109.5
C(24)-C(25)-C(27)	111(2)	C(29)-C(30)-H(30C)	109.5
C(24)-C(25)-H(25A)	109.5	H(30A)-C(30)-H(30C)	109.5
C(27)-C(25)-H(25A)	109.5	H(30B)-C(30)-H(30C)	109.5
C(24)-C(25)-H(25B)	109.5		
C(27)-C(25)-H(25B)	109.5		

Table A.5. Anisotropic displacement parameters ($Å^2 \times 10^3$) for **17**. The anisotropic displacement factor takes the form: $-2\pi[h^2a^{*2}U^{11} + ... + 2\ h\ k\ a^*\ b^*\ U^{12}]$.

Atoms	U^{11}	U^{22}	U^{33}	U^{23}	U^{13}	U^{12}
C(1)	23(2)	22(2)	21(2)	2(2)	-5(2)	-4(2)
C(2)	27(2)	24(2)	25(2)	7(2)	-6(2)	0(2)
C(3)	19(2)	18(2)	23(2)	1(2)	-1(2)	2(2)
C(4)	23(2)	19(2)	21(2)	3(2)	-5(2)	0(2)
C(5)	25(2)	21(2)	27(3)	4(2)	-4(2)	-2(2)
C(6)	22(2)	27(2)	29(3)	-1(2)	4(2)	-1(2)
C(7)	27(2)	25(2)	21(2)	4(2)	2(2)	-1(2)
C(8)	26(2)	26(2)	40(3)	-2(2)	4(2)	3(2)
C(9)	32(2)	36(3)	32(3)	0(2)	7(2)	3(2)
C(10)	47(3)	53(3)	39(3)	-7(3)	-1(2)	8(2)
C(11)	105(5)	75(4)	39(3)	-1(3)	-12(3)	12(4)
C(12)	25(2)	26(2)	26(2)	-6(2)	0(2)	1(2)
C(13)	35(3)	36(4)	27(3)	-1(2)	4(2)	9(3)
C(14)	48(4)	35(4)	35(3)	0(3)	11(2)	11(3)
C(15)	66(4)	50(4)	34(3)	-5(3)	11(3)	13(3)
C(16)	76(4)	59(4)	30(3)	5(3)	10(3)	27(4)
C(17)	78(4)	64(4)	29(3)	2(3)	3(3)	31(4)
C(18)	56(3)	43(3)	31(3)	3(3)	11(3)	17(3)
C(19)	27(2)	24(2)	29(3)	2(2)	1(2)	-1(2)
C(20)	29(3)	29(3)	39(3)	-1(2)	-2(2)	-1(2)
C(21)	59(5)	49(5)	62(4)	-11(4)	-26(4)	-12(4)
C(22)	74(8)	64(7)	55(5)	-18(5)	-32(5)	-25(6)
N(1)	22(2)	23(2)	25(2)	-1(2)	2(2)	-3(2)
N(2)	20(2)	21(2)	23(2)	-6(2)	3(2)	1(2)
N(3)	25(2)	24(2)	17(2)	-3(2)	1(2)	0(2)
N(4)	25(2)	21(2)	28(2)	-2(2)	3(2)	-1(2)
N(5)	24(2)	27(2)	34(2)	-10(2)	5(2)	-6(2)
O(1)	24(2)	32(2)	37(2)	-7(1)	8(1)	3(1)
O(2)	26(2)	28(2)	37(2)	-4(1)	4(1)	-7(1)
O(3)	47(2)	29(2)	58(2)	-10(2)	-17(2)	-1(2)
O(4)	58(2)	36(2)	63(2)	-2(2)	-26(2)	7(2)
C(23)	48(5)	40(5)	28(4)	-2(5)	9(4)	16(5)

Table A.5 (cont.)

C(24)	51(5)	40(6)	32(5)	-2(5)	9(5)	17(5)
C(25)	63(5)	49(5)	32(4)	0(5)	13(4)	15(5)
C(26)	67(5)	55(6)	30(5)	0(5)	4(5)	22(5)
C(27)	67(5)	52(6)	30(5)	1(6)	7(4)	17(6)
C(28)	50(5)	43(6)	28(5)	-2(5)	6(5)	16(5)
C(29)	55(5)	47(4)	62(4)	-10(4)	-27(4)	-8(4)
C(30)	65(7)	64(6)	63(4)	-11(5)	-24(4)	-25(5)

Table A.6. Hydrogen coordinates ($\times 10^4$) and isotropic displacement parameters ($Å^2 \times 10^3$) for **17**.

Atom	x	y	z	U(eq)
H(6)	9079	10361	136	31
H(8A)	-1278	8766	841	37
H(8B)	-536	9567	1037	37
H(9A)	-1538	8618	1521	40
H(9B)	-105	8013	1384	40
H(10A)	461	9530	1752	55
H(10B)	1917	8950	1601	55
H(11A)	1564	8802	2299	109
H(11B)	1111	7972	2083	109
H(11C)	-341	8554	2235	109
H(12C)	3594	10735	895	31
H(12D)	4888	11450	968	31
H(12A)	3664	10579	957	31
H(12B)	4569	11429	900	31
H(13A)	6385	11169	1429	39
H(14A)	3016	10891	1664	47
H(14B)	3856	11757	1612	47
H(15A)	3729	11371	2299	60
H(15B)	5610	11525	2160	60
H(16A)	5540	10327	2527	66
H(16B)	4082	9979	2250	66

Table A.6 (cont.)

H(17A)	6598	9396	2050	69
H(17B)	7433	10263	1995	69
H(18A)	6680	9772	1359	52
H(18B)	4802	9633	1505	52
H(19A)	7022	11981	695	32
H(19B)	8609	11852	415	32
H(21A)	10396	13175	1514	68
H(21B)	11318	12334	1447	68
H(22A)	10242	12336	2085	96
H(22B)	9187	11702	1829	96
H(22C)	8435	12573	1922	96
H(2)	5460(40)	7993(17)	-55(9)	26
H(4)	3130(40)	7584(15)	308(10)	29
H(5)	2030(40)	9197(19)	824(11)	34
H(23A)	4753	9979	1396	46
H(24A)	3823	11527	1687	49
H(24B)	2567	10821	1567	49
H(25A)	3481	10035	2098	58
H(25B)	2929	10896	2268	58
H(26A)	6635	9719	2025	61
H(26B)	7920	10437	2107	61
H(27A)	5516	10510	2549	59
H(27B)	5733	11314	2290	59
H(28A)	7003	11153	1549	49
H(28B)	7340	10259	1398	49
H(29A)	10838	13191	1391	65
H(29B)	11470	12280	1370	65
H(30A)	10820	12666	2031	96
H(30B)	9699	11923	1889	96
H(30C)	8930	12810	1898	96

Table A.7. Torsion angles (°) for **17**.

Atoms	Angle	Atoms	Angle
O(1)-C(2)-C(3)-C(4)	-174.7(4)	C(3)-C(4)-N(1)-C(1)	-3.6(5)
N(2)-C(2)-C(3)-C(4)	4.9(5)	N(1)-C(1)-N(2)-C(2)	0.0(5)
O(1)-C(2)-C(3)-C(6)	4.9(7)	N(4)-C(1)-N(2)-C(2)	179.7(3)
N(2)-C(2)-C(3)-C(6)	-175.6(4)	O(1)-C(2)-N(2)-C(1)	174.9(3)
C(2)-C(3)-C(4)-N(3)	178.9(3)	C(3)-C(2)-N(2)-C(1)	-4.7(5)
C(6)-C(3)-C(4)-N(3)	-0.8(4)	N(1)-C(4)-N(3)-C(5)	-179.4(3)
C(2)-C(3)-C(4)-N(1)	-1.0(6)	C(3)-C(4)-N(3)-C(5)	0.7(4)
C(6)-C(3)-C(4)-N(1)	179.3(3)	N(1)-C(4)-N(3)-C(12)	0.2(5)
N(3)-C(5)-C(6)-C(3)	-0.1(4)	C(3)-C(4)-N(3)-C(12)	-179.8(3)
C(19)-C(5)-C(6)-C(3)	-177.4(4)	C(6)-C(5)-N(3)-C(4)	-0.3(4)
C(4)-C(3)-C(6)-C(5)	0.5(4)	C(19)-C(5)-N(3)-C(4)	177.1(3)
C(2)-C(3)-C(6)-C(5)	-179.1(4)	C(6)-C(5)-N(3)-C(12)	-179.9(3)
N(5)-C(8)-C(9)-C(10)	68.0(4)	C(19)-C(5)-N(3)-C(12)	-2.4(6)
C(8)-C(9)-C(10)-C(11)	-177.7(4)	C(13)-C(12)-N(3)-C(4)	104.5(4)
N(3)-C(12)-C(13)-C(14)	-177.7(4)	C(23)-C(12)-N(3)-C(4)	83.2(13)
C(23)-C(12)-C(13)-C(14)	-88(4)	C(13)-C(12)-N(3)-C(5)	-76.0(5)
N(3)-C(12)-C(13)-C(18)	-54.0(6)	C(23)-C(12)-N(3)-C(5)	-97.4(13)
C(23)-C(12)-C(13)-C(18)	36(3)	N(1)-C(1)-N(4)-C(7)	9.9(6)
C(18)-C(13)-C(14)-C(15)	55.6(6)	N(2)-C(1)-N(4)-C(7)	-169.9(3)
C(12)-C(13)-C(14)-C(15)	179.5(4)	O(2)-C(7)-N(4)-C(1)	173.3(4)
C(13)-C(14)-C(15)-C(16)	-55.0(7)	N(5)-C(7)-N(4)-C(1)	-7.0(6)
C(14)-C(15)-C(16)-C(17)	54.5(8)	O(2)-C(7)-N(5)-C(8)	1.0(6)
C(15)-C(16)-C(17)-C(18)	-55.5(8)	N(4)-C(7)-N(5)-C(8)	-178.7(3)
C(14)-C(13)-C(18)-C(17)	-55.6(7)	C(9)-C(8)-N(5)-C(7)	87.1(4)
C(12)-C(13)-C(18)-C(17)	-179.6(5)	O(4)-C(20)-O(3)-C(29)	11.4(9)
C(16)-C(17)-C(18)-C(13)	56.0(7)	C(19)-C(20)-O(3)-C(29)	-167.0(8)
C(6)-C(5)-C(19)-C(20)	-92.8(5)	O(4)-C(20)-O(3)-C(21)	-2.3(12)
N(3)-C(5)-C(19)-C(20)	90.2(4)	C(19)-C(20)-O(3)-C(21)	179.3(10)
C(5)-C(19)-C(20)-O(4)	18.4(6)	C(22)-C(21)-O(3)-C(20)	-71.5(16)
C(5)-C(19)-C(20)-O(3)	-163.3(3)	C(22)-C(21)-O(3)-C(29)	-165(5)
N(2)-C(1)-N(1)-C(4)	4.1(5)	N(3)-C(12)-C(23)-C(28)	52(3)
N(4)-C(1)-N(1)-C(4)	-175.6(3)	C(13)-C(12)-C(23)-C(28)	-47(3)
N(3)-C(4)-N(1)-C(1)	176.4(3)	N(3)-C(12)-C(23)-C(24)	-175.9(16)

Table A.7 (cont.)

C(13)-C(12)-C(23)-C(24)	86(4)	C(12)-C(23)-C(28)-C(26)	178(2)
C(28)-C(23)-C(24)-C(25)	-50(3)	C(24)-C(23)-C(28)-C(26)	48(3)
C(12)-C(23)-C(24)-C(25)	174(2)	C(27)-C(26)-C(28)-C(23)	-50(3)
C(23)-C(24)-C(25)-C(27)	55(3)	C(20)-O(3)-C(29)-C(30)	-88.4(13)
C(24)-C(25)-C(27)-C(26)	-58(3)	C(21)-O(3)-C(29)-C(30)	5(4)
C(28)-C(26)-C(27)-C(25)	53(3)		

Table A.8. Hydrogen Bonds (Å and °) for **17**.

D-H...A	d(D-H)	d(H...A)	d(D...A)	∠(DHA)
N(2)-H(2)...O(2)#1	0.90(2)	1.90(2)	2.780(4)	165(3)
N(4)-H(4)...O(1)#2	0.89(2)	2.00(2)	2.888(4)	173(3)
N(5)-H(5)...N(1)	0.88(2)	2.02(3)	2.692(4)	133(3)

Symmetry transformations used to generate equivalent atoms: #1 x + 1/2, -y + 3/2, -z; #2 x - 1/2, -y + 3/2, -z.

A.2 Compound 31

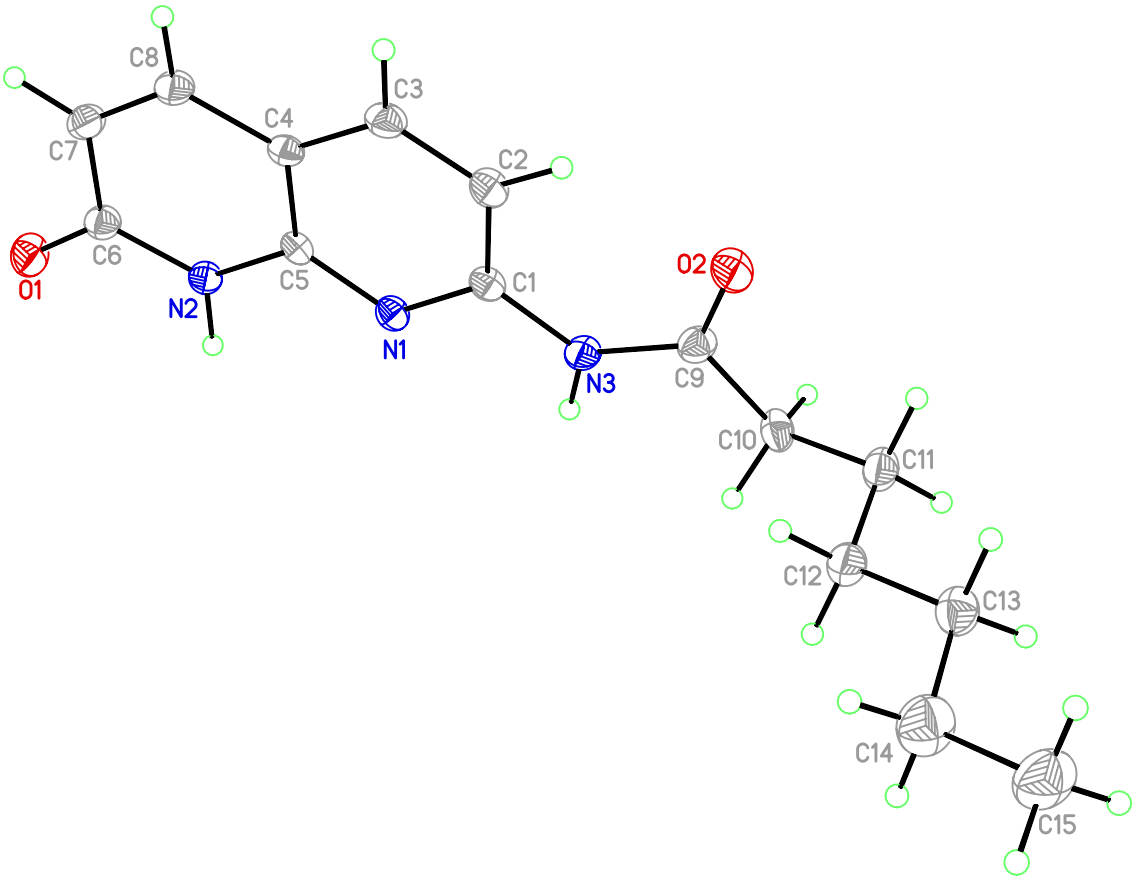

Table A.9. Crystal data and structure refinement for **31**.

Identification code	ba25cas	
Empirical formula	$C_{15}H_{19}N_3O_2$	
Formula weight	273.33	
Temperature	193(2) K	
Wavelength	0.71073 Å	
Crystal system	Triclinic	
Space group	P-1	
Unit cell dimensions	a = 5.1670(10) Å	α= 100.296(9)°.
	b = 8.8934(17) Å	β= 90.218(9)°.
	c = 15.560(3) Å	γ = 99.571(10)°.
Volume	693.3(2) $Å^3$	
Z	2	
Density (calculated)	1.309 Mg/m^3	
Absorption coefficient	0.089 mm^{-1}	
F(000)	292	
Crystal size	0.38 x 0.15 x 0.04 mm^3	
Theta range for data collection	2.36 to 25.34°.	
Index ranges	-6<=h<=6, -10<=k<=10, -18<=l<=18	
Reflections collected	8201	
Independent reflections	2537 [R(int) = 0.1204]	
Completeness to theta = 25.34°	99.5 %	
Absorption correction	Integration	
Max. and min. transmission	0.9984 and 0.9848	
Refinement method	Full-matrix least-squares on F^2	
Data / restraints / parameters	2537 / 2 / 188	
Goodness-of-fit on F^2	0.921	
Final R indices [I>2sigma(I)]	R1 = 0.0572, wR2 = 0.0933	
R indices (all data)	R1 = 0.2009, wR2 = 0.1308	
Largest diff. peak and hole	0.227 and -0.248 $e.Å^{-3}$	

Table A.10. Atomic coordinates ($\times 10^4$) and equivalent isotropic displacement parameters ($Å^2 \times 10^3$) for **31**. U(eq) is defined as one third of the trace of the orthogonalized U^{ij} tensor.

Atom	x	y	z	U(eq)
C(1)	4570(7)	2676(4)	9482(2)	23(1)
C(2)	7005(7)	3444(5)	9861(2)	29(1)
C(3)	7782(7)	3152(4)	10646(2)	29(1)
C(4)	6180(7)	2115(4)	11059(2)	22(1)
C(5)	3782(7)	1387(4)	10633(3)	22(1)
C(6)	2658(7)	-66(5)	11804(2)	27(1)
C(7)	5124(7)	701(5)	12248(2)	29(1)
C(8)	6775(7)	1723(4)	11878(2)	28(1)
C(9)	4695(8)	3910(5)	8164(2)	29(1)
C(10)	3015(7)	3910(4)	7369(2)	30(1)
C(11)	4646(7)	4255(5)	6600(2)	33(1)
C(12)	5803(8)	2874(5)	6154(2)	36(1)
C(13)	7497(7)	3187(5)	5387(2)	37(1)
C(14)	8431(9)	1768(6)	4893(3)	56(1)
C(15)	10236(8)	2071(6)	4144(3)	59(2)
N(1)	2965(5)	1633(3)	9855(2)	24(1)
N(2)	2132(6)	330(4)	11021(2)	25(1)
N(3)	3588(6)	2903(4)	8695(2)	26(1)
O(1)	1077(5)	-1031(3)	12103(2)	37(1)
O(2)	6826(5)	4743(3)	8326(2)	37(1)

Table A.11. Bond lengths (Å) for **31**.

Bond	Length	Bond	Length
C(1)-N(1)	1.351(4)	C(10)-C(11)	1.513(4)
C(1)-N(3)	1.385(4)	C(10)-H(10A)	0.9900
C(1)-C(2)	1.401(5)	C(10)-H(10B)	0.9900
C(2)-C(3)	1.366(5)	C(11)-C(12)	1.513(5)
C(2)-H(2)	0.9500	C(11)-H(11A)	0.9900
C(3)-C(4)	1.383(5)	C(11)-H(11B)	0.9900
C(3)-H(3)	0.9500	C(12)-C(13)	1.522(4)
C(4)-C(5)	1.403(5)	C(12)-H(12A)	0.9900
C(4)-C(8)	1.425(5)	C(12)-H(12B)	0.9900
C(5)-N(1)	1.346(4)	C(13)-C(14)	1.508(5)
C(5)-N(2)	1.384(4)	C(13)-H(13A)	0.9900
C(6)-O(1)	1.238(4)	C(13)-H(13B)	0.9900
C(6)-N(2)	1.366(4)	C(14)-C(15)	1.529(5)
C(6)-C(7)	1.450(5)	C(14)-H(14A)	0.9900
C(7)-C(8)	1.349(5)	C(14)-H(14B)	0.9900
C(7)-H(7)	0.9500	C(15)-H(15A)	0.9800
C(8)-H(8)	0.9500	C(15)-H(15B)	0.9800
C(9)-O(2)	1.218(4)	C(15)-H(15C)	0.9800
C(9)-N(3)	1.381(4)	N(2)-H(2A)	0.93(2)
C(9)-C(10)	1.509(5)	N(3)-H(3A)	0.89(2)

Table A.12. Bond angles (°) for **31**.

Atoms	Angle	Atoms	Angle
N(1)-C(1)-N(3)	113.8(3)	C(10)-C(11)-C(12)	112.6(3)
N(1)-C(1)-C(2)	122.7(4)	C(10)-C(11)-H(11A)	109.1
N(3)-C(1)-C(2)	123.5(3)	C(12)-C(11)-H(11A)	109.1
C(3)-C(2)-C(1)	119.0(3)	C(10)-C(11)-H(11B)	109.1
C(3)-C(2)-H(2)	120.5	C(12)-C(11)-H(11B)	109.1
C(1)-C(2)-H(2)	120.5	H(11A)-C(11)-H(11B)	107.8
C(2)-C(3)-C(4)	120.3(4)	C(11)-C(12)-C(13)	114.1(3)
C(2)-C(3)-H(3)	119.9	C(11)-C(12)-H(12A)	108.7
C(4)-C(3)-H(3)	119.9	C(13)-C(12)-H(12A)	108.7
C(3)-C(4)-C(5)	117.1(4)	C(11)-C(12)-H(12B)	108.7
C(3)-C(4)-C(8)	125.3(3)	C(13)-C(12)-H(12B)	108.7
C(5)-C(4)-C(8)	117.6(3)	H(12A)-C(12)-H(12B)	107.6
N(1)-C(5)-N(2)	116.8(3)	C(14)-C(13)-C(12)	113.7(3)
N(1)-C(5)-C(4)	124.3(3)	C(14)-C(13)-H(13A)	108.8
N(2)-C(5)-C(4)	118.9(4)	C(12)-C(13)-H(13A)	108.8
O(1)-C(6)-N(2)	120.5(3)	C(14)-C(13)-H(13B)	108.8
O(1)-C(6)-C(7)	123.1(4)	C(12)-C(13)-H(13B)	108.8
N(2)-C(6)-C(7)	116.4(3)	H(13A)-C(13)-H(13B)	107.7
C(8)-C(7)-C(6)	120.0(4)	C(13)-C(14)-C(15)	114.5(4)
C(8)-C(7)-H(7)	120.0	C(13)-C(14)-H(14A)	108.6
C(6)-C(7)-H(7)	120.0	C(15)-C(14)-H(14A)	108.6
C(7)-C(8)-C(4)	122.4(4)	C(13)-C(14)-H(14B)	108.6
C(7)-C(8)-H(8)	118.8	C(15)-C(14)-H(14B)	108.6
C(4)-C(8)-H(8)	118.8	H(14A)-C(14)-H(14B)	107.6
O(2)-C(9)-N(3)	123.3(3)	C(14)-C(15)-H(15A)	109.5
O(2)-C(9)-C(10)	122.6(3)	C(14)-C(15)-H(15B)	109.5
N(3)-C(9)-C(10)	114.1(3)	H(15A)-C(15)-H(15B)	109.5
C(9)-C(10)-C(11)	112.2(3)	C(14)-C(15)-H(15C)	109.5
C(9)-C(10)-H(10A)	109.2	H(15A)-C(15)-H(15C)	109.5
C(11)-C(10)-H(10A)	109.2	H(15B)-C(15)-H(15C)	109.5
C(9)-C(10)-H(10B)	109.2	C(5)-N(1)-C(1)	116.7(3)
C(11)-C(10)-H(10B)	109.2	C(6)-N(2)-C(5)	124.6(3)
H(10A)-C(10)-H(10B)	107.9	C(6)-N(2)-H(2A)	119(2)

Table A.12 (cont.)

C(5)-N(2)-H(2A)	116(2)	C(9)-N(3)-H(3A)	116(2)
C(9)-N(3)-C(1)	128.3(3)	C(1)-N(3)-H(3A)	116(2)

Table A.13. Anisotropic displacement parameters ($Å^2 \times 10^3$) for **31**. The anisotropic displacement factor takes the form: $-2\pi[h^2a^{*2}U^{11} + ... + 2\ h\ k\ a^*\ b^*\ U^{12}]$.

Atoms	U^{11}	U^{22}	U^{33}	U^{23}	U^{13}	U^{12}
C(1)	20(2)	22(2)	26(2)	3(2)	4(2)	2(2)
C(2)	21(2)	29(3)	33(3)	9(2)	2(2)	-6(2)
C(3)	25(2)	26(3)	32(3)	2(2)	-3(2)	-2(2)
C(4)	19(2)	20(2)	25(2)	1(2)	-1(2)	1(2)
C(5)	23(2)	16(2)	26(2)	4(2)	2(2)	3(2)
C(6)	24(2)	27(3)	27(3)	4(2)	-2(2)	2(2)
C(7)	30(2)	31(3)	24(2)	5(2)	-3(2)	0(2)
C(8)	22(2)	29(3)	30(2)	5(2)	-6(2)	-3(2)
C(9)	27(2)	33(3)	25(2)	4(2)	1(2)	1(2)
C(10)	26(2)	29(3)	36(3)	14(2)	0(2)	1(2)
C(11)	34(2)	35(3)	29(2)	12(2)	2(2)	2(2)
C(12)	40(3)	36(3)	30(2)	9(2)	0(2)	-1(2)
C(13)	35(3)	39(3)	37(3)	11(2)	2(2)	4(2)
C(14)	55(3)	61(4)	53(3)	12(3)	15(3)	15(3)
C(15)	56(3)	69(4)	47(3)	6(3)	14(2)	6(3)
N(1)	22(2)	22(2)	26(2)	6(2)	3(2)	1(2)
N(2)	21(2)	24(2)	28(2)	7(2)	-6(2)	-5(2)
N(3)	19(2)	30(2)	25(2)	6(2)	-4(2)	-5(2)
O(1)	31(2)	40(2)	39(2)	18(2)	-1(1)	-7(2)
O(2)	26(2)	39(2)	41(2)	13(1)	-3(1)	-10(2)

Table A.14. Hydrogen coordinates ($\times 10^4$) and isotropic displacement parameters ($Å^2 \times 10^3$) for **31**.

Atom	x	y	z	U(eq)
H(2)	8099	4158	9576	34
H(3)	9432	3663	10909	34
H(7)	5577	483	12800	35
H(8)	8395	2200	12175	34
H(10A)	1862	4698	7514	36
H(10B)	1880	2884	7204	36
H(11A)	6088	5130	6805	39
H(11B)	3533	4577	6171	39
H(12A)	4352	2006	5944	43
H(12B)	6880	2540	6589	43
H(13A)	6476	3617	4978	44
H(13B)	9045	3982	5606	44
H(14A)	6879	992	4653	67
H(14B)	9376	1311	5309	67
H(15A)	10719	1092	3849	88
H(15B)	11826	2796	4378	88
H(15C)	9321	2519	3726	88
H(2A)	720(50)	-250(40)	10673(19)	37
H(3A)	2070(50)	2310(40)	8500(20)	38

Table A.15. Torsion angles (°) for **31**.

Atoms	Angle	Atoms	Angle
N(1)-C(1)-C(2)-C(3)	-1.1(6)	C(9)-C(10)-C(11)-C(12)	77.0(4)
N(3)-C(1)-C(2)-C(3)	179.3(4)	C(10)-C(11)-C(12)-C(13)	-179.0(3)
C(1)-C(2)-C(3)-C(4)	-0.2(6)	C(11)-C(12)-C(13)-C(14)	-174.5(4)
C(2)-C(3)-C(4)-C(5)	0.6(5)	C(12)-C(13)-C(14)-C(15)	-177.4(4)
C(2)-C(3)-C(4)-C(8)	-179.7(4)	N(2)-C(5)-N(1)-C(1)	179.4(3)
C(3)-C(4)-C(5)-N(1)	0.2(5)	C(4)-C(5)-N(1)-C(1)	-1.4(5)
C(8)-C(4)-C(5)-N(1)	-179.5(4)	N(3)-C(1)-N(1)-C(5)	-178.5(3)
C(3)-C(4)-C(5)-N(2)	179.4(3)	C(2)-C(1)-N(1)-C(5)	1.8(5)
C(8)-C(4)-C(5)-N(2)	-0.3(5)	O(1)-C(6)-N(2)-C(5)	-179.6(4)
O(1)-C(6)-C(7)-C(8)	179.0(4)	C(7)-C(6)-N(2)-C(5)	0.5(5)
N(2)-C(6)-C(7)-C(8)	-1.1(6)	N(1)-C(5)-N(2)-C(6)	179.5(4)
C(6)-C(7)-C(8)-C(4)	1.1(6)	C(4)-C(5)-N(2)-C(6)	0.2(5)
C(3)-C(4)-C(8)-C(7)	180.0(4)	O(2)-C(9)-N(3)-C(1)	2.0(6)
C(5)-C(4)-C(8)-C(7)	-0.4(5)	C(10)-C(9)-N(3)-C(1)	-177.2(4)
O(2)-C(9)-C(10)-C(11)	32.1(5)	N(1)-C(1)-N(3)-C(9)	178.0(4)
N(3)-C(9)-C(10)-C(11)	-148.7(3)	C(2)-C(1)-N(3)-C(9)	-2.3(6)

Table A.16. Hydrogen Bonds (Å and °) for **31**.

D-H...A	d(D-H)	d(H...A)	d(D...A)	∠(DHA)
N(2)-H(2A)...N(1)#1	0.93(2)	2.16(2)	3.072(4)	167(3)
N(3)-H(3A)...O(1)#1	0.89(2)	1.95(2)	2.833(4)	171(3)

Symmetry transformations used to generate equivalent atoms: #1 -x, -y, -z + 2.

A.3 Compound 41

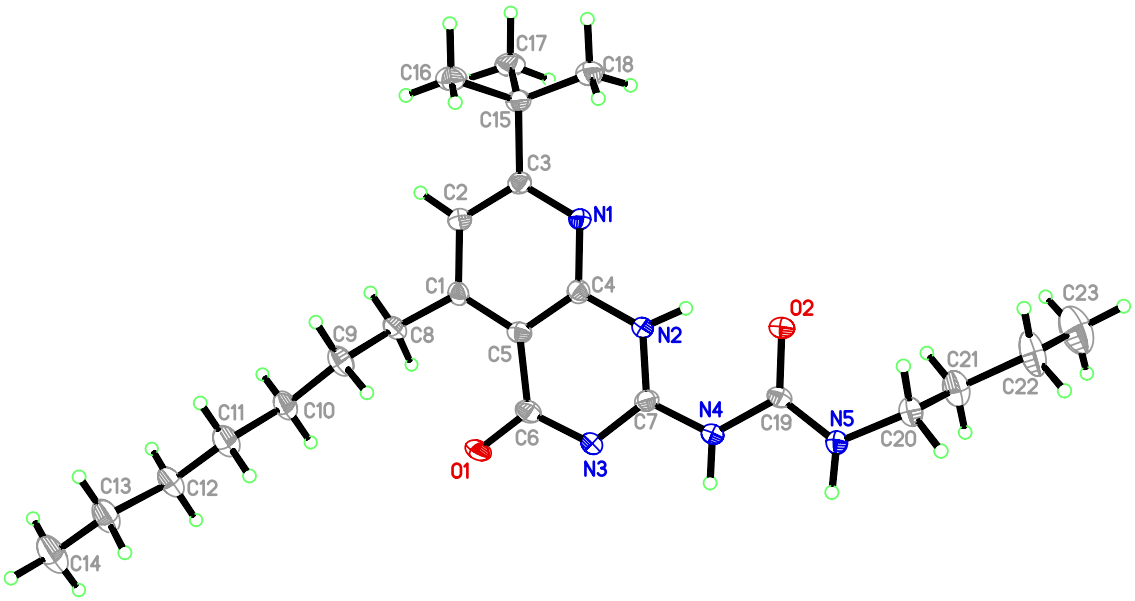

Table A.17. Crystal data and structure refinement for **41**.

Identification code	ba58bas	
Empirical formula	$C_{23}H_{37}N_5O_2$	
Formula weight	415.58	
Temperature	193(2) K	
Wavelength	0.71073 Å	
Crystal system	Monoclinic	
Space group	P 21/c	
Unit cell dimensions	a = 13.838(5) Å	α= 90°.
	b = 6.352(2) Å	β= 92.933(17)°.
	c = 27.274(9) Å	γ = 90°.
Volume	2394.2(14) $Å^3$	
Z	4	
Density (calculated)	1.153 Mg/m^3	
Absorption coefficient	0.075 mm^{-1}	
F(000)	904	
Crystal size	0.44 x 0.02 x 0.02 mm^3	
Theta range for data collection	1.50 to 25.30°.	
Index ranges	-16<=h<=16, -5<=k<=7, -32<=l<=32	
Reflections collected	26475	
Independent reflections	4295 [R(int) = 0.4126]	
Completeness to theta = 25.30°	98.2 %	
Absorption correction	Integration	
Max. and min. transmission	0.9986 and 0.9927	
Refinement method	Full-matrix least-squares on F^2	
Data / restraints / parameters	4295 / 262 / 286	
Goodness-of-fit on F^2	0.885	
Final R indices [I>2sigma(I)]	R1 = 0.0898, wR2 = 0.1038	
R indices (all data)	R1 = 0.3099, wR2 = 0.1641	
Extinction coefficient	0.0064(7)	
Largest diff. peak and hole	0.210 and -0.239 $e.Å^{-3}$	

Table A.18. Atomic coordinates ($\times 10^4$) and equivalent isotropic displacement parameters ($Å^2 \times 10^3$) for **41**. U(eq) is defined as one third of the trace of the orthogonalized U^{ij} tensor.

Atom	x	y	z	U(eq)
C(1)	8522(4)	12375(8)	-895(2)	26(1)
C(2)	7602(4)	13271(9)	-948(2)	31(1)
C(3)	6782(4)	12302(9)	-744(2)	27(1)
C(4)	7779(4)	9775(8)	-401(2)	27(1)
C(5)	8611(4)	10479(9)	-622(2)	28(1)
C(6)	9505(4)	9217(9)	-537(2)	30(1)
C(7)	8671(4)	6904(9)	-54(2)	28(1)
C(8)	9363(3)	13443(8)	-1127(2)	31(1)
C(9)	9610(3)	12448(9)	-1619(2)	38(2)
C(10)	10567(4)	13325(9)	-1796(2)	39(2)
C(11)	10847(4)	12423(9)	-2288(2)	44(2)
C(12)	11781(4)	13367(9)	-2471(2)	42(2)
C(13)	12027(4)	12554(9)	-2978(2)	50(2)
C(14)	12953(4)	13570(10)	-3153(2)	64(2)
C(15)	5775(4)	13200(9)	-837(2)	28(1)
C(16)	5538(4)	13276(9)	-1399(2)	39(2)
C(17)	5711(4)	15445(8)	-628(2)	38(2)
C(18)	5026(3)	11813(9)	-598(2)	39(2)
C(19)	7878(4)	4319(9)	479(2)	28(1)
C(20)	7270(4)	1443(9)	952(2)	37(2)
C(21)	7171(4)	2239(10)	1473(2)	52(2)
C(22)	6326(4)	1146(11)	1713(2)	67(2)
C(23)	6190(5)	1925(11)	2236(2)	86(2)
N(1)	6890(3)	10615(7)	-458(1)	27(1)
N(2)	7841(3)	7987(7)	-112(2)	29(1)
N(3)	9488(3)	7407(7)	-263(1)	27(1)
N(4)	8677(3)	5120(7)	229(2)	29(1)
N(5)	8038(3)	2485(7)	699(2)	33(1)
O(1)	10273(2)	9731(6)	-730(1)	42(1)
O(2)	7102(2)	5322(6)	477(1)	37(1)

Table A.19. Bond lengths (Å) for **41**.

Bond	Length	Bond	Length
C(1)-C(2)	1.395(6)	C(13)-H(13B)	0.9900
C(1)-C(5)	1.418(7)	C(14)-H(14A)	0.9800
C(1)-C(8)	1.514(6)	C(14)-H(14B)	0.9800
C(2)-C(3)	1.428(6)	C(14)-H(14C)	0.9800
C(2)-H(2A)	0.9500	C(15)-C(18)	1.531(6)
C(3)-N(1)	1.329(6)	C(15)-C(17)	1.539(7)
C(3)-C(15)	1.515(7)	C(15)-C(16)	1.553(6)
C(4)-N(1)	1.343(6)	C(16)-H(16A)	0.9800
C(4)-N(2)	1.383(6)	C(16)-H(16B)	0.9800
C(4)-C(5)	1.400(6)	C(16)-H(16C)	0.9800
C(5)-C(6)	1.482(7)	C(17)-H(17A)	0.9800
C(6)-O(1)	1.253(5)	C(17)-H(17B)	0.9800
C(6)-N(3)	1.371(6)	C(17)-H(17C)	0.9800
C(7)-N(3)	1.332(6)	C(18)-H(18A)	0.9800
C(7)-N(2)	1.341(6)	C(18)-H(18B)	0.9800
C(7)-N(4)	1.370(6)	C(18)-H(18C)	0.9800
C(8)-C(9)	1.537(6)	C(19)-O(2)	1.248(5)
C(8)-H(8A)	0.9900	C(19)-N(5)	1.324(6)
C(8)-H(8B)	0.9900	C(19)-N(4)	1.422(6)
C(9)-C(10)	1.537(6)	C(20)-N(5)	1.457(6)
C(9)-H(9A)	0.9900	C(20)-C(21)	1.521(6)
C(9)-H(9B)	0.9900	C(20)-H(20A)	0.9900
C(10)-C(11)	1.526(6)	C(20)-H(20B)	0.9900
C(10)-H(10A)	0.9900	C(21)-C(22)	1.535(6)
C(10)-H(10B)	0.9900	C(21)-H(21A)	0.9900
C(11)-C(12)	1.532(6)	C(21)-H(21B)	0.9900
C(11)-H(11A)	0.9900	C(22)-C(23)	1.530(7)
C(11)-H(11B)	0.9900	C(22)-H(22A)	0.9900
C(12)-C(13)	1.532(6)	C(22)-H(22B)	0.9900
C(12)-H(12A)	0.9900	C(23)-H(23A)	0.9800
C(12)-H(12B)	0.9900	C(23)-H(23B)	0.9800
C(13)-C(14)	1.532(6)	C(23)-H(23C)	0.9800
C(13)-H(13A)	0.9900	N(2)-H(2)	0.88(2)

Table A.19 (cont.)

N(4)-H(4)	0.89(3)	N(5)-H(5)	0.91(3)

Table A.20. Bond angles (°) for **41**.

Atoms	Angle	Atoms	Angle
C(2)-C(1)-C(5)	117.1(5)	C(10)-C(9)-H(9A)	109.4
C(2)-C(1)-C(8)	119.4(5)	C(8)-C(9)-H(9B)	109.4
C(5)-C(1)-C(8)	123.5(5)	C(10)-C(9)-H(9B)	109.4
C(1)-C(2)-C(3)	121.5(5)	H(9A)-C(9)-H(9B)	108.0
C(1)-C(2)-H(2A)	119.2	C(11)-C(10)-C(9)	113.7(4)
C(3)-C(2)-H(2A)	119.2	C(11)-C(10)-H(10A)	108.8
N(1)-C(3)-C(2)	120.6(5)	C(9)-C(10)-H(10A)	108.8
N(1)-C(3)-C(15)	118.4(5)	C(11)-C(10)-H(10B)	108.8
C(2)-C(3)-C(15)	121.0(5)	C(9)-C(10)-H(10B)	108.8
N(1)-C(4)-N(2)	114.9(5)	H(10A)-C(10)-H(10B)	107.7
N(1)-C(4)-C(5)	126.3(5)	C(10)-C(11)-C(12)	113.3(4)
N(2)-C(4)-C(5)	118.7(5)	C(10)-C(11)-H(11A)	108.9
C(4)-C(5)-C(1)	116.5(5)	C(12)-C(11)-H(11A)	108.9
C(4)-C(5)-C(6)	117.2(5)	C(10)-C(11)-H(11B)	108.9
C(1)-C(5)-C(6)	126.3(5)	C(12)-C(11)-H(11B)	108.9
O(1)-C(6)-N(3)	119.0(5)	H(11A)-C(11)-H(11B)	107.7
O(1)-C(6)-C(5)	120.8(5)	C(11)-C(12)-C(13)	113.1(5)
N(3)-C(6)-C(5)	120.2(5)	C(11)-C(12)-H(12A)	108.9
N(3)-C(7)-N(2)	124.5(5)	C(13)-C(12)-H(12A)	108.9
N(3)-C(7)-N(4)	117.3(5)	C(11)-C(12)-H(12B)	108.9
N(2)-C(7)-N(4)	118.1(5)	C(13)-C(12)-H(12B)	108.9
C(1)-C(8)-C(9)	113.0(4)	H(12A)-C(12)-H(12B)	107.8
C(1)-C(8)-H(8A)	109.0	C(12)-C(13)-C(14)	111.5(5)
C(9)-C(8)-H(8A)	109.0	C(12)-C(13)-H(13A)	109.3
C(1)-C(8)-H(8B)	109.0	C(14)-C(13)-H(13A)	109.3
C(9)-C(8)-H(8B)	109.0	C(12)-C(13)-H(13B)	109.3
H(8A)-C(8)-H(8B)	107.8	C(14)-C(13)-H(13B)	109.3
C(8)-C(9)-C(10)	111.0(4)	H(13A)-C(13)-H(13B)	108.0
C(8)-C(9)-H(9A)	109.4	C(13)-C(14)-H(14A)	109.5

Table A.20 (cont.)

C(13)-C(14)-H(14B)	109.5	C(21)-C(20)-H(20A)	108.9
H(14A)-C(14)-H(14B)	109.5	N(5)-C(20)-H(20B)	108.9
C(13)-C(14)-H(14C)	109.5	C(21)-C(20)-H(20B)	108.9
H(14A)-C(14)-H(14C)	109.5	H(20A)-C(20)-H(20B)	107.7
H(14B)-C(14)-H(14C)	109.5	C(20)-C(21)-C(22)	110.8(5)
C(3)-C(15)-C(18)	110.4(4)	C(20)-C(21)-H(21A)	109.5
C(3)-C(15)-C(17)	110.9(5)	C(22)-C(21)-H(21A)	109.5
C(18)-C(15)-C(17)	108.8(4)	C(20)-C(21)-H(21B)	109.5
C(3)-C(15)-C(16)	108.8(4)	C(22)-C(21)-H(21B)	109.5
C(18)-C(15)-C(16)	109.0(4)	H(21A)-C(21)-H(21B)	108.1
C(17)-C(15)-C(16)	108.9(4)	C(23)-C(22)-C(21)	112.6(5)
C(15)-C(16)-H(16A)	109.5	C(23)-C(22)-H(22A)	109.1
C(15)-C(16)-H(16B)	109.5	C(21)-C(22)-H(22A)	109.1
H(16A)-C(16)-H(16B)	109.5	C(23)-C(22)-H(22B)	109.1
C(15)-C(16)-H(16C)	109.5	C(21)-C(22)-H(22B)	109.1
H(16A)-C(16)-H(16C)	109.5	H(22A)-C(22)-H(22B)	107.8
H(16B)-C(16)-H(16C)	109.5	C(22)-C(23)-H(23A)	109.5
C(15)-C(17)-H(17A)	109.5	C(22)-C(23)-H(23B)	109.5
C(15)-C(17)-H(17B)	109.5	H(23A)-C(23)-H(23B)	109.5
H(17A)-C(17)-H(17B)	109.5	C(22)-C(23)-H(23C)	109.5
C(15)-C(17)-H(17C)	109.5	H(23A)-C(23)-H(23C)	109.5
H(17A)-C(17)-H(17C)	109.5	H(23B)-C(23)-H(23C)	109.5
H(17B)-C(17)-H(17C)	109.5	C(3)-N(1)-C(4)	117.5(4)
C(15)-C(18)-H(18A)	109.5	C(7)-N(2)-C(4)	121.1(4)
C(15)-C(18)-H(18B)	109.5	C(7)-N(2)-H(2)	111(3)
H(18A)-C(18)-H(18B)	109.5	C(4)-N(2)-H(2)	128(3)
C(15)-C(18)-H(18C)	109.5	C(7)-N(3)-C(6)	118.2(5)
H(18A)-C(18)-H(18C)	109.5	C(7)-N(4)-C(19)	125.7(5)
H(18B)-C(18)-H(18C)	109.5	C(7)-N(4)-H(4)	113(3)
O(2)-C(19)-N(5)	125.1(5)	C(19)-N(4)-H(4)	121(3)
O(2)-C(19)-N(4)	120.3(5)	C(19)-N(5)-C(20)	120.4(5)
N(5)-C(19)-N(4)	114.6(5)	C(19)-N(5)-H(5)	119(3)
N(5)-C(20)-C(21)	113.3(4)	C(20)-N(5)-H(5)	120(3)
N(5)-C(20)-H(20A)	108.9		

Table A.21. Anisotropic displacement parameters ($Å^2 \times 10^3$) for **41**. The anisotropic displacement factor takes the form: $-2\pi[h^2a^{*2}U^{11} + ... + 2\ h\ k\ a^*\ b^*\ U^{12}]$.

Atoms	U^{11}	U^{22}	U^{33}	U^{23}	U^{13}	U^{12}
C(1)	28(3)	29(3)	20(3)	-2(2)	4(2)	0(2)
C(2)	31(3)	30(3)	33(3)	4(3)	6(3)	6(3)
C(3)	30(3)	27(3)	24(3)	-1(2)	1(2)	6(2)
C(4)	30(3)	26(3)	25(3)	0(2)	3(2)	2(2)
C(5)	26(3)	28(3)	29(3)	-3(2)	3(2)	4(2)
C(6)	29(3)	28(3)	32(3)	-7(2)	6(3)	2(2)
C(7)	28(3)	28(3)	27(3)	1(2)	1(2)	7(2)
C(8)	27(3)	33(3)	34(3)	-2(3)	11(2)	0(3)
C(9)	37(3)	40(4)	39(3)	-5(3)	12(3)	-9(3)
C(10)	42(3)	36(3)	40(3)	1(3)	17(3)	-5(3)
C(11)	47(4)	42(4)	43(3)	-3(3)	16(3)	-5(3)
C(12)	42(3)	45(4)	40(3)	-7(3)	19(3)	-5(3)
C(13)	60(4)	47(4)	44(3)	-5(3)	23(3)	-1(3)
C(14)	75(5)	56(5)	65(4)	-6(4)	41(4)	-9(4)
C(15)	26(3)	30(3)	29(3)	0(2)	0(2)	4(2)
C(16)	31(3)	52(4)	36(3)	-4(3)	-4(3)	9(3)
C(17)	38(4)	26(3)	49(3)	-5(3)	5(3)	10(3)
C(18)	34(3)	33(4)	49(3)	5(3)	7(3)	8(3)
C(19)	26(3)	29(3)	29(3)	-2(3)	7(2)	6(3)
C(20)	35(3)	37(4)	41(3)	7(3)	9(3)	-4(3)
C(21)	57(4)	57(4)	43(3)	3(3)	15(3)	-8(3)
C(22)	73(4)	82(5)	48(3)	5(4)	25(3)	-26(4)
C(23)	88(5)	115(6)	57(4)	-1(4)	24(4)	-25(5)
N(1)	27(2)	30(3)	25(2)	3(2)	4(2)	7(2)
N(2)	23(3)	31(3)	32(3)	9(2)	8(2)	5(2)
N(3)	24(2)	31(3)	27(2)	2(2)	7(2)	3(2)
N(4)	25(3)	30(3)	31(3)	5(2)	9(2)	7(2)
N(5)	31(3)	27(3)	42(3)	11(2)	14(2)	4(2)
O(1)	25(2)	42(3)	61(2)	14(2)	19(2)	8(2)
O(2)	28(2)	37(3)	47(2)	11(2)	11(2)	11(2)

Table A.22. Hydrogen coordinates ($\times 10^4$) and isotropic displacement parameters ($Å^2 \times 10^3$) for **41**.

Atom	x	y	z	U(eq)
H(2A)	7519	14556	-1124	38
H(8A)	9939	13368	-897	37
H(8B)	9205	14948	-1181	37
H(9A)	9082	12742	-1868	46
H(9B)	9664	10902	-1580	46
H(10A)	10512	14874	-1826	46
H(10B)	11091	13016	-1545	46
H(11A)	10313	12683	-2536	52
H(11B)	10927	10880	-2255	52
H(12A)	12322	13031	-2232	50
H(12B)	11715	14918	-2485	50
H(13A)	11483	12865	-3217	60
H(13B)	12112	11007	-2964	60
H(14A)	13105	12973	-3471	96
H(14B)	13489	13295	-2913	96
H(14C)	12857	15093	-3186	96
H(16A)	5571	11851	-1535	59
H(16B)	6008	14181	-1554	59
H(16C)	4885	13844	-1463	59
H(17A)	5880	15420	-275	56
H(17B)	5050	15978	-684	56
H(17C)	6162	16365	-792	56
H(18A)	5151	11817	-241	58
H(18B)	5074	10370	-722	58
H(18C)	4376	12363	-678	58
H(20A)	7401	-89	963	45
H(20B)	6649	1659	763	45
H(21A)	7060	3779	1467	62
H(21B)	7778	1965	1670	62
H(22A)	5723	1401	1511	80
H(22B)	6444	-391	1721	80
H(23A)	5627	1228	2368	129

Table A.22 (cont.)

H(23B)	6087	3451	2232	129
H(23C)	6769	1593	2444	129
H(2)	7390(30)	7440(70)	67(15)	43
H(4)	9230(20)	4420(70)	228(16)	43
H(5)	8650(20)	1950(80)	718(17)	49

Table A.23. Torsion angles (°) for **41**.

Atoms	Angle	Atoms	Angle
C(5)-C(1)-C(2)-C(3)	-1.2(7)	C(2)-C(3)-C(15)-C(18)	177.4(5)
C(8)-C(1)-C(2)-C(3)	178.8(4)	N(1)-C(3)-C(15)-C(17)	116.5(5)
C(1)-C(2)-C(3)-N(1)	6.4(7)	C(2)-C(3)-C(15)-C(17)	-61.9(6)
C(1)-C(2)-C(3)-C(15)	-175.3(5)	N(1)-C(3)-C(15)-C(16)	-123.8(5)
N(1)-C(4)-C(5)-C(1)	6.2(7)	C(2)-C(3)-C(15)-C(16)	57.8(6)
N(2)-C(4)-C(5)-C(1)	-177.0(5)	N(5)-C(20)-C(21)-C(22)	177.8(5)
N(1)-C(4)-C(5)-C(6)	-175.5(5)	C(20)-C(21)-C(22)-C(23)	-179.2(5)
N(2)-C(4)-C(5)-C(6)	1.2(7)	C(2)-C(3)-N(1)-C(4)	-5.0(7)
C(2)-C(1)-C(5)-C(4)	-4.6(7)	C(15)-C(3)-N(1)-C(4)	176.6(4)
C(8)-C(1)-C(5)-C(4)	175.5(5)	N(2)-C(4)-N(1)-C(3)	-178.1(4)
C(2)-C(1)-C(5)-C(6)	177.4(5)	C(5)-C(4)-N(1)-C(3)	-1.3(7)
C(8)-C(1)-C(5)-C(6)	-2.5(8)	N(3)-C(7)-N(2)-C(4)	-0.6(8)
C(4)-C(5)-C(6)-O(1)	178.7(5)	N(4)-C(7)-N(2)-C(4)	-178.6(5)
C(1)-C(5)-C(6)-O(1)	-3.2(8)	N(1)-C(4)-N(2)-C(7)	175.2(5)
C(4)-C(5)-C(6)-N(3)	1.9(7)	C(5)-C(4)-N(2)-C(7)	-1.9(7)
C(1)-C(5)-C(6)-N(3)	180.0(5)	N(2)-C(7)-N(3)-C(6)	3.7(7)
C(2)-C(1)-C(8)-C(9)	-99.2(6)	N(4)-C(7)-N(3)-C(6)	-178.3(5)
C(5)-C(1)-C(8)-C(9)	80.7(6)	O(1)-C(6)-N(3)-C(7)	178.8(5)
C(1)-C(8)-C(9)-C(10)	-170.3(5)	C(5)-C(6)-N(3)-C(7)	-4.3(7)
C(8)-C(9)-C(10)-C(11)	-179.1(5)	N(3)-C(7)-N(4)-C(19)	-179.6(5)
C(9)-C(10)-C(11)-C(12)	177.8(5)	N(2)-C(7)-N(4)-C(19)	-1.4(8)
C(10)-C(11)-C(12)-C(13)	-176.6(5)	O(2)-C(19)-N(4)-C(7)	-4.4(8)
C(11)-C(12)-C(13)-C(14)	178.8(5)	N(5)-C(19)-N(4)-C(7)	175.2(5)
N(1)-C(3)-C(15)-C(18)	-4.2(6)	O(2)-C(19)-N(5)-C(20)	2.0(8)

Table A.23 (cont.)

N(4)-C(19)-N(5)-C(20)	-177.6(4)	C(21)-C(20)-N(5)-C(19)	-83.5(6)

Table A.24. Hydrogen Bonds (Å and °) for **41**.

D-H...A	d(D-H)	d(H...A)	d(D...A)	∠(DHA)
N(2)-H(2)...O(2)	0.88(2)	1.80(3)	2.580(5)	145(5)
N(4)-H(4)...N(3)#1	0.89(3)	2.12(3)	3.002(6)	176(4)
N(5)-H(5)...O(1)#1	0.91(3)	1.84(3)	2.726(5)	166(5)

Symmetry transformations used to generate equivalent atoms: #1 -x + 2, -y + 1, -z.

Appendix B

Nonlinear Regression Plots for van't Hoff Analysis

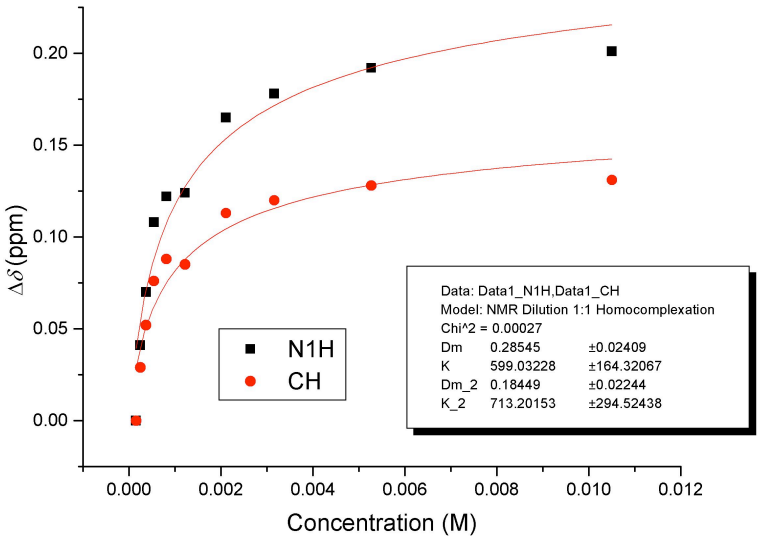

Figure B.1. DeUG **17** dilution study at 5 °C in $CDCl_3$.

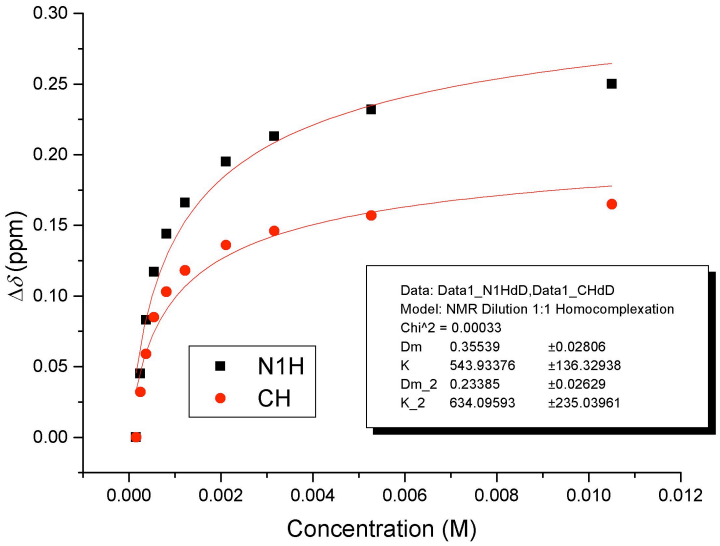

Figure B.2. DeUG **17** dilution study at 17 °C in $CDCl_3$.

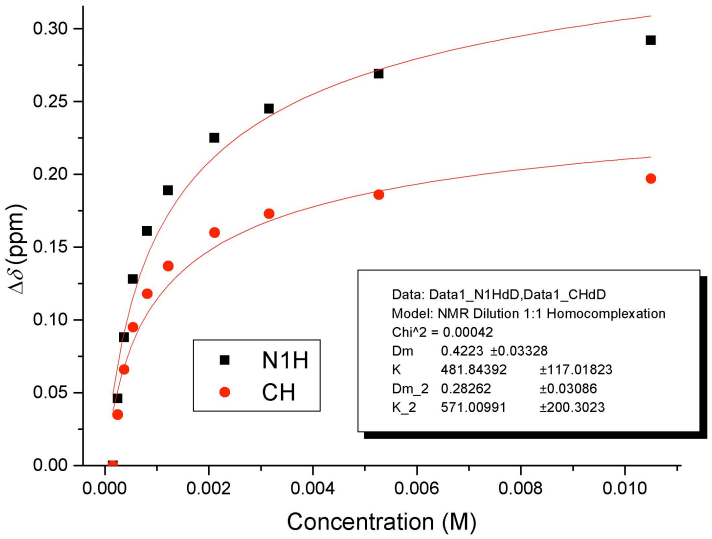

Figure B.3. DeUG **17** dilution study at 29 °C in $CDCl_3$.

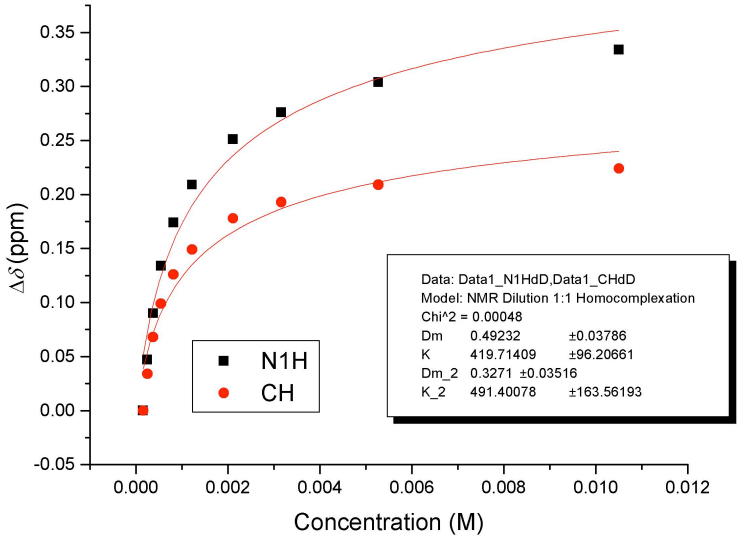

Figure B.4. DeUG 17 dilution study at 41 °C in $CDCl_3$.

Author's Biography

Darrell W. Kuykendall was born and raised in Orange County, California. He received his baccalaureate degree in Chemistry from California State University, Bakersfield in June of 2003. During his undergraduate studies, Darrell studied reactive intermediates in the Criegee mechanism of ozonolysis using cryogenic argon matrix isolation techniques under Professor Carl Kemnitz. Before obtaining his baccalaureate degree, Darrell was in the United States Air Force and worked in refinery operations at the Mobil Oil Corporation.

Darrell came to the University of Illinois in the fall of 2004 and joined Steven C. Zimmerman's research group. While at the University of Illinois, Darrell focused on the design, synthesis and materials applications of high-affinity, high-fidelity quadruply hydrogen bonding modules. Darrell also taught Chemistry 233 during his last year of graduate studies at Illinois. He will receive his Ph.D. in August of 2010 and has accepted a tenure-track position at Eastern Oklahoma State College.

Publications:

Darrell W. Kuykendall, Cyrus A. Anderson and Steven C. Zimmerman, "Hydrogen-Bonded DeUG·DAN Heterocomplex: Structure and Stability and a Scalable Synthesis of DeUG with Reactive Functionality" *Org. Lett.* **2009**, *11*, 61-64.

Darrell W. Kuykendall and Steven C. Zimmerman, "Nanoparticles - A Very Versatile Nanocapsule" *Nature Nano.* **2007**, *2*, 201-202.

Taiho Park, Steven C. Zimmerman, Hugo C. Ong, Eric M. Todd, Darrell W. Kuykendall and J. Kwansima Quansah, "Supramolecular Polymers Formed by Interaction of Hydrogen Bonding" *PMSE Preprints* **2007**, *96*, 138-139